

Structure-Function Studies of the Cul3/Rbx1:Keap1 E3 Ubiquitin Ligase Complex

BY

EVAN SMALL
B.S., University of Central Florida, 2005

THESIS

Submitted as partial fulfillment of the requirements for the degree of Doctor of Philosophy in
Biochemistry and Molecular Genetics in the Graduate College of the University of Illinois at
Chicago, 2012

Chicago, Illinois

Defense Committee:

Peter G.W. Gettins, Chair
Andrew D. Mesecar, Advisor, Purdue University
Yee-Kin Ho
Pradip Raychaudhuri
Karl Volz, Microbiology and Immunology

This work is dedicated to my parents, Daniel and Janis, for all their love and gracious support through the years. My father's example instills in me a hard work ethic and always shows me that the fruit of life is worth the climb to get it. His love of medicine and research was infectious growing up and after seeing the way he interacts with patients, it's no wonder I ended up following in his footsteps and applying to medical school. If I got the left side of my brain from my father, then I got the right brain of my mother. Most of the memories I have of my childhood interactions with her are a mix of science and art. She made it fun, exciting, and occasionally a requirement when I stayed home sick from school; what other 9-year old was memorizing the periodic table of elements? My parents gave me confidence, ability, and an environment to use them in and for that I think they are the best parents in the world.

Acknowledgements

I joined the Mesecar lab in 2005 as a rotation student two years before officially joining as a graduate student. The lab was a great place to work with so many fun, smart people there and I soon found myself coming to lab during lunch in medical school or using my desk and bookcase in lab instead of the ones provided for medical students in the student center. Over the next five years many people gave me useful advice, helped me out with experiments, supplied me with reagents, showed interest in my life, or were just friendly enough for me to remember then on this list.

Yahira Baez
Dr. Barbara Calamini
Rebeca Calderon
Dr. George Chlipala
Dr. Jill Dombrauckas
Dr. Michael Federle
Dr. Chris Fleming
Nicole Freedman
Dr. Vadim Gaponenko
Kelly Gay
Dr. Valerie Grum-Tokars
Dr. Renda Hawwa

Katie Jermihov
Gary Klein
Dr. Soni Larsen
Dr. Alexander Mankin
Dr. Melissa May
Dr. Patrick Miller
Dr. Bernie Santarsiero
Dr. Valerie Sershon
Dr. Megan Sturdy
Dr. Sasi Taneja
Dr. Yang Tian

Dr. Andrew Mesecar forever has my gratitude for bringing me into his lab and fostering my growth as a scientist. He is an exceptional researcher, a great boss, and a fun person to be around. He is an excellent judge of character and he personalizes his advising tactics based on his students' personalities. For me, he was very hands-off, which worked well with my style. He was always there when I needed advice and direction, but he never hovered or micromanaged. I could not have completed this work without him (and his funding) and I am very thankful that Dr. Thomas Selby told me to look Andy up when I moved here to Chicago from Florida back in 2005.

Dr. Aimee Egger was the most influential person related to my thesis project. She and I were both studying the same system using two very different approaches, so we were constantly bouncing new ideas off one another (occasionally a few would stick). She is a very meticulous scientist who has creative ideas and whose work forms the basis for a significant portion of this thesis. I could not have accomplished this without her

Dr. Kiira Ratia is one of my main scientific role models. She is masterful in everything that she does and has rightfully earned the moniker "Gold Standard" for good reason. This makes her a marvelous scientist and for those habits that have thankfully rubbed off on me, I am forever grateful. You can tell when something was created by her because it has a particular style to it. From the bottles on the shelves, to the pictures on the walls, to her incredibly artistic group meeting presentations, she had a style that made lab a unique place to spend time.

Dr. Scott Pegan is another person who made my graduate years a more enjoyable and rewarding experience. I regularly benefitted from his expertise on work and life. I will miss our golf outings and poker nights. Glenn Capodagli trained me on a few techniques when I first joined lab and also helped purify the Nrf2 and some of the Keap1 mutants used in my

Acknowledgements (continued)

experiments. We shared a number of common interests and soon became good friends. Both he and Dr. Pegan have moved on to University of Denver where they will no doubt be successful.

Thomas Wubben, like Scott and Glenn, made lab a great place to work. We sat back-to-back for two years, discussing (and sometimes mildly arguing about) topics in our work and personal lives. Unlike Scott and Glenn, however, Thomas is in the Medical Scientist Training Program with me, so he also made all the MSTP functions more enjoyable too. He is an incredibly driven and intelligent person, with interesting stories and opinions, and I am thankful for the friendship we have.

I really want to thank Dr. Christine Schar for her help with my project. She spent a lot of time discussing ultracentrifugation with me while she was here at UIC and even after she moved away to Denmark. I would not have been able to complete the later AUC experiments after she left, without the foundation of experimental design, collection, and analysis knowledge she helped me to learn in the earlier experiments.

Dr. Borries Demeler continues to open my eyes to ultracentrifugation's potential and power. His workshop in San Antonio at UTHSCSA (apparently pronounced "*You-Tesk-Ah*") was phenomenal and incredibly helpful to my research. He is a brilliant and progressive scientist, while also remaining quite an interesting character outside of lab.

Dr. Gary Ramsay helped with the surface plasmon resonance experiments. His jovial attitude rubs off easily and he was very generous with supplies and reagents for the Biacore T100 machine. Chenqi Hu, a graduate student from the Van Breeman lab was very helpful during our collaboration on the mass spectrometry experiments.

Dr. Liang Guo and Dr. Sönke Seifert were crucial to the execution of the SAXS portion of this work. They were both extremely helpful during the experiments and did not seem too bothered when I pestered them with a million questions afterwards. They were incredibly generous with beamtime and Sonke even called me a few times when he had spare time since he knew I needed it.

Dr. Brenda Schulman at St. Jude's generously donated reagents and a few of the purified proteins used in the development of the *in vitro* ubiquitination assay described in this dissertation.

I would like to thank my committee members, Drs. Peter Gettins, Karl Volz, Yee-kin Ho, and Pradip Raychaudhuri. Their insightful critiques of my work over the years have pushed me to excel and helped me to see the forest for the trees, when it comes to my research.

Last, but certainly not least, my wonderful wife, Dr. Molly Small, has been supporting through this process and encouraging me to remain focused and driven, while also enjoying myself in the process. She is an incredibly loving wife who goes out of her way to shows interest in the things that I like and I look forward to seeing her again someday when I have graduated and I actually have some free time.

Table of Contents

<u>Chapter</u>	<u>page</u>
1 Introduction	2
1.1 Ubiquitin E3 ligase complexes and the role of Cul3/Rbx1:Keap1 in cancer chemoprevention..	2
1.2 Nrf2 and Chemoprevention.....	8
1.3 Keap1 and Its Domains.....	9
1.4 Keap1 Cysteine Mutants.....	13
1.5 Cul3 and Rbx1	15
1.6 Significance and Impact.....	17
2 Expression, Purification, and In Vitro Ubiquitination Activity of Cul3/Rbx1.....	20
2.1 Introduction	20
2.1.1 Rationale for Co-expression Plasmid and Gene Synthesis	20
2.1.2 <i>In vitro</i> Ubiquitination of Nrf2 Activity Assay for Cul3/Rbx1	21
2.2 Materials and Methods	21
2.2.1 Generation of Expression Construct for Cul3/Rbx1 Co-expression.....	21
2.2.2 Protein Expression and Purification.....	22
2.2.2.1 pETDuet-1-hCul3-Rbx1 Plasmid Expression	22
2.2.2.2 Cul3/Rbx1 Affinity and Size Exclusion Chromatography.....	22
2.2.2.3 Keap1 and Nrf2 Expression and Purification.....	23
2.2.3 <i>In vitro</i> Ubiquitination Assay.....	23
2.3 Results.....	25
2.3.1 Design of Cul3/Rbx1 Co-expression Construct.....	25
2.3.2 Protein Over-expression and Purification	26
2.3.3 <i>In vitro</i> Ubiquitination Assay.....	28
2.3.3.1 Anti-Nrf2 Western Blot at 25 °C	28
2.3.3.2 Anti-Nrf2, -Keap1, and -Cul3 Western Blot at 37 °C.....	29
2.4 Discussion	32
3 Modeling of the Individual Proteins and Their Complex	34
3.1 Introduction	34
3.2 Materials and Methods	35
3.2.1 Cullin3 Homology Model Creation	35
3.2.2 Keap1 Modeling.....	37
3.2.3 Cul3/Rbx1:Keap1 Complex Modeling	38
3.3 Results and Discussion	38
3.3.1 Cullin3 Homology Model	38
4 Structural Characterization of Wild Type Complex.....	47
4.1 Introduction	47
4.1.1 Analytical Ultracentrifugation	48
4.1.2 Small-Angle X-ray Scattering.....	50
4.2 Materials and Methods	52
4.2.1 Protein Crystallization of Cul3/Rbx1.....	52
4.2.2 Analytical Size-Exclusion Chromatography and Binding of Cul3/Rbx1 to Keap1.....	53
4.2.3 Analytical Ultracentrifugation	54
4.2.3.1 Individual Proteins	54
4.2.3.2 Stoichiometry Determination of the Cul3/Rbx1:Keap1 Complex	54
4.2.3.3 Data Analysis	55

Table of Contents (continued)

<u>Chapter</u>	<u>page</u>
4.2.4 Small-Angle X-ray Scattering.....	56
4.2.4.1 Individual Protein Samples	56
4.2.4.2 Complex Protein Samples	57
4.2.4.3 SAXS Data Analysis	58
4.3 Results.....	60
4.3.1 Protein Crystallization of Cul3/Rbx1	60
4.3.2 Size-Exclusion Chromatography	61
4.3.3 Analytical Ultracentrifugation	63
4.3.3.1 Sedimentation Velocity of Individual Proteins	63
4.3.3.2 Sedimentation Velocity of the Cul3/Rbx1:Keap1 Complex	64
4.3.4 Small-Angle X-ray Scattering.....	68
4.3.4.1 SAXS Results for the Individual Cul3/Rbx1 and Keap1 Proteins	68
4.3.4.2 SAXS Results for the Cul3/Rbx1:Keap1 Complex.....	69
4.4 Discussion	72
5 Characterization of Keap1 Mutants and Comparison to Wild Type.....	75
5.1 Introduction	75
5.2 Materials and Methods	76
5.2.1 Expression and Purification of Cul3/Rbx1 and Keap1 Recombinant Proteins.....	76
5.2.2 <i>In vitro</i> Ubiquitination Assay.....	77
5.2.3 Surface Plasmon Resonance	77
5.2.3.1 Cul3/Rbx1 Immobilization to CM5 Chip.....	77
5.2.3.2 Keap1 and Mutant Concentration Series.....	77
5.2.4 Analytical Ultracentrifugation	78
5.2.4.1 Data Collection.....	78
5.2.4.2 Data Analysis	78
5.2.5 Small-Angle X-ray Scattering.....	79
5.2.5.1 Data Collection for Individual Keap1 Mutants	79
5.2.5.2 Data Collection for Cul3/Rbx1:Keap1 Mutant Complexes	80
5.2.5.3 Data Analysis	80
5.2.6 Mass Spectrometry of Isoliquiritigenin-Modified Proteins	81
5.3 Results.....	81
5.3.1 <i>In vitro</i> Ubiquitination Assay of Keap1-WT and Mutants	81
5.3.2 Surface Plasmon Resonance	83
5.3.3 Analytical Ultracentrifugation	84
5.3.4 Small-Angle X-ray Scattering.....	87
5.3.4.1 SAXS Profiles for Keap1 Mutants and the Cul3/Rbx1:Keap1-Mutant Complexes	87
5.3.4.2 Pair-Distribution Function Analysis.....	88
5.3.4.3 Ab initio Simulated Annealing of the Mutant Complexes	90
5.3.5 Mass Spectrometry Analysis of Cul3 and Keap1 Alkylation	91
5.4 Discussion	92
<i>Cited Literature.....</i>	<i>100</i>
<i>Appendix A – Codon-optimized Cul3 and Rbx1 Sequences.....</i>	<i>105</i>
<i>Appendix B - Homology Model - Keap1 Cysteine Residues.....</i>	<i>108</i>
<i>Appendix C – SEC – Proteins of Known Molecular Weight.....</i>	<i>110</i>
<i>Appendix D - AUC - Effect of DMSO on Keap1 Sedimentation Velocity.....</i>	<i>109</i>
<i>Appendix E – AUC – Cul3 and Keap1 vHW, 2DSA, GA, and GA-50 Analysis Reports</i>	<i>110</i>

Table of Contents (continued)

<u>Chapter</u>	<u>page</u>
<i>Appendix F – AUC - Wild type Complex vHW Analysis.....</i>	<i>128</i>
<i>Appendix G - AUC – Wild type and Mutant Keap1 vHW Analysis Reports.....</i>	<i>142</i>
<i>Appendix H - SAXS - Moore’s Auto Correlation of C3/R1:K1 Complex SAXS Results.....</i>	<i>147</i>
<i>Appendix I – SAXS - Batch File Programming Codes</i>	<i>148</i>

List of Tables

<u>Chapter</u>	<u>page</u>
Figure 1. General ubiquitination pathway overview.....	2
Figure 2. Examples of Cullin-based E3 ligase complexes	3
Figure 3. Molecular Mechanism of Electrophilic Induction of the ARE.....	5
Figure 4. Crystal Structure of Cul1/Rbx1	6
Figure 5. Dimeric Model of Cul1/Rbx1:Skp1/Cdc4.....	7
Figure 6. Domain organization diagram for Nrf2	9
Figure 7. Domain organization diagram for Keap1	10
Figure 8. Crystal structures of BTB monomer, dimer, and tetramer	12
Figure 9. Crystal Structures of the Kelch Domain.....	12
Figure 10. Hinge and Latch Model Diagram.....	13
Figure 11. Domain Organization Diagram for Cullin3.....	16
Figure 12. Neddylation-induced conformational change in Cul5.....	17
Figure 13. Cul3 and Rbx1 Gene Placement Diagram for pETDuet-1 Plasmid.....	25
Figure 14. Cul3/Rbx1 Purification Chromatograms and SDS-PAGE Gels.....	27
Figure 15. SDS-PAGE Gel of Cul3/Rbx1 Purification Overview	28
Figure 16. Anti-Nrf2 Western Blot of Nrf2 Ubiquitination Assay.....	29
Figure 17. Anti-Nrf2, -Keap1, and -Cul3 Western Blot of Ubiquitination Assay.....	30
Figure 18. Primary Sequence Alignment of Cul3 and Cul1	36
Figure 19. BTB Oligomer Models	40
Figure 20. BTB and Skp1 Superposition	41
Figure 21. Cul1/Cul3 Crystal Structure/Homology Model Comparison	41
Figure 22. Keap1 Monomer Homology Model	42
Figure 23. Keap1 Dimer Homology Model.....	43
Figure 24. Complex Models	45
Figure 25. Analytical Ultracentrifugation Equipment	55
Figure 26. Beamline Photos from the Advanced Photon Source	59
Figure 27. SAXS Data Analysis Workflow Diagram.....	60
Figure 28. Analytical Size Exclusion Chromatogram.....	62
Figure 29. Complex Stoichiometry Diagram	63
Figure 30. van Holde-Weischet Analysis of Cul3/Rbx1, Keap1, and Their Complex.....	65
Figure 31. Edited Complex Data Scans Used in Molar Ratio vHW Analysis.....	67
Figure 32. Small-Angle X-ray Scattering Profiles for Cul3/Rbx1 and Keap1	68
Figure 33. Comparison of Cul3/Rbx1 SAXS Model and Homology Model	69
Figure 34. Comparison of SAXS Keap1 Model and Homology Model.....	71
Figure 35. Complex SAXS Model and Refined Complex Homology Model.....	71
Figure 36. In vitro Ubiquitination Assay with Keap1 Mutants Comparing Nrf2 Ubiquitination.....	82
Figure 37. In vitro Ubiquitination Assay of Keap1-WT and C151W Comparing Keap1 Ubiquitination.....	82
Figure 38. Sedimentation Velocity Results for Keap1-WT, Keap1-C151W, and Keap1-C151S.....	84
Figure 39. Sedimentation Velocity Results for Wild type and Mutant Complexes.....	85
Figure 40. van Holde-Weischet Distribution Comparison Plot of Wild type and Mutant Complexes.....	87
Figure 41. SAXS Profiles for Mutant Complexes and Mutant Keap1 Proteins	88
Figure 42. SAXS Analysis of Mutant Complexes – Kratky Plot and $p(r)$ Normalization.....	89

Table of Contents (continued)

<u>Chapter</u>	<u>page</u>
<i>Figure 43. Difference Pair-Distribution Function Plots.....</i>	<i>90</i>
<i>Figure 44. Low-Resolution Scattering Densities for Wild type and Mutant Complexes.....</i>	<i>91</i>
<i>Figure 45. Conformational Change Model of Ubiquitination Impairment.....</i>	<i>98</i>
<i>Figure 46. Differential Rate Model Summarizing Cul3/Rbx1:Keap1 Complex Formation and Catalysis.....</i>	<i>99</i>
<i>Figure 47. Homology model - Keap1 Cysteine Residues.....</i>	<i>147</i>
<i>Figure 48. A standard curve derived from the analytical size exclusion data.....</i>	<i>147</i>
<i>Figure 49. The Effect of DMSO on Keap1 Sedimentation Velocity.....</i>	<i>147</i>
<i>Figure 50. Wild type and mutant complex SAXS fitting results using Moore's indirect Fourier transform.....</i>	<i>147</i>

Table of Contents (continued)

<u>Chapter</u>	<u>page</u>
<i>Table I. Components of the in vitro ubiquitination assay.....</i>	<i>24</i>
<i>Table II. Cul3/Rbx1 Purification Yield Results</i>	<i>27</i>
<i>Table III. Summary of Molecular Homology and Structural Models.....</i>	<i>44</i>
<i>Table IV. Protein concentrations used in various crystallography screens.....</i>	<i>52</i>
<i>Table V. Sedimentation Velocity Ultracentrifugation Samples for Stoichiometry Determination.....</i>	<i>55</i>
<i>Table VI. Individual protein samples used in SAXS experiments at Bio-CAT Beamline</i>	<i>57</i>
<i>Table VII. Protein complex samples used in SAXS experiments</i>	<i>58</i>
<i>Table VIII. SEC Results – Comparison of Calculated vs. Estimated MW using K_{av}.....</i>	<i>62</i>
<i>Table IX. Results from the Surface Plasmon Resonance Experiments.....</i>	<i>83</i>
<i>Table X. Detection of cysteine residues modified by isoliquiritigenin in the Cul3/Rbx1:Keap1 or Cul3/Rbx1:Keap1-C151W complexes.....</i>	<i>92</i>

List of Abbreviations

2DSA	Two Dimensional Spectrum Analysis
Amp	Ampicillin
APS	Advanced Photon Source
ARE	Antioxidant Response Element
AUC	Analytical Ultracentrifugation
BACK	BTB and C-terminal Kelch
BESSRC	Basic Energy Sciences Synchrotron Radiation Sciences Center
BTB	Brick-a-brack, Tramtrack, Broad complex
C3	Cullin3
CAPS	N-cyclohexyl-3-aminopropanesulfonic acid
CAT	Collaborative Access Team
CDC4	Cell Division Cycle Protein 4
CPC	Chemopreventive Compound
cryo-EM	cryo-Electron Microscopy
Cul1	Cullin1
Cul2	Cullin2
Cul3	Cullin3
Cul4	Cullin4
Cul5	Cullin5
DDB1	DNA Damage-Binding Protein 1
DLG	Aspartate-leucine-glycine peptide
DNA	Deoxyribonucleic Acid
DTT	Dithiothreitol

List of Abbreviations (continued)

EDTA	Ethylenediaminetetraacetic acid
EMSA	Electrophoretic Mobility Shift Assay
ETGE	Glutamate-threonine-glycine-glutamate
Fbw7	F-box and WD repeat domain-containing 7
GSH	Reduced glutathione
GSSG	Oxidized glutathione
HEPES	4-(2-hydroxyethyl)-1-piperazineethanesulfonic acid
His6	hexahistidine
IAB	N-iodoacetyl-N-biotinylhexylenediamine
ID	Insertion device
IPTG	Isopropyl β -D-1-thiogalactopyranoside
ITC	Isothermal Titration Calorimetry
IVR	Intervening Region or Intervening Variable Region
K	Lysine
K1	Another notation for Keap1
Keap1	Kelch-like ECH-associated protein 1
LB	Lysogeny broth
LDS	Lithium dodecyl sulfate
LRF/ZBTB7	Zinc finger and BTB domain containing protein 7
MW	Molecular weight
Nedd8	Neural Precursor Cell Expressed, Developmentally Down-Regulated 8
Neh2	Nrf2 ECH Homology 2

List of Abbreviations (continued)

Ni ²⁺	Nickel ion
NMR	Nuclear Magnetic Resonance
Nrf2	NF-E2-related Factor 2
NTS	N-terminal Strand
PAGE	Polyacrylamide Gel Electrophoresis
PDB	Protein Data Bank
R1	Another notation for Rbx1
<i>Rbx1</i>	RINGBox 1
redox	reduction-oxidation
RMSD	Root Mean Square Deviation
S	Sedimentation Coefficient
SANS	Small-Angle Neutron Scattering
SAXS	Small-Angle X-ray Scattering
SCF	Skp1-Cul1-Fbox Complex
SDS	Sodium dodecyl sulfate
SEC	Size Exclusion Chromatography
Skp1	S-phase kinase-associated protein 1
<i>sp.</i>	species
SPR	Surface Plasmon Resonance
SV5-V	V protein from Simian Virus 5
tBHQ	tert-butyl hydroxyquinone
TCEP	tris(2-carboxyethyl)phosphine
Tris	<i>tris</i> (hydroxymethyl)aminomethane

List of Abbreviations (continued)

UBCH5	Ubiquitin-conjugating Enzyme H5
UBE1	Ubiquitin-like modifier activating enzyme 1
UPS	Ubiquitin-Proteasome System
V_c	Geometric bead volume
vHW	van Holde-Weischet
V_o	Void volume
V_r	Retention volume
XOR	X-ray Operations Research

Summary

Just as our bodies have an immune response system to combat foreign pathogens and harmful cells from within the body, they also have chemo-response systems to counteract the effects of toxic chemicals from inside and outside the body. Genes for glutathione metabolism and redox homeostasis, along with the antioxidant-related transcription factor, Nrf2, are involved in this dynamic signaling pathway that is regulated by an E3 ubiquitin ligase protein-complex, which ligates ubiquitin to a target protein. The atomic structure and stoichiometry of this important ligase complex is currently unknown. It has been hypothesized that structural changes within the complex are responsible for modulating the levels of Nrf2 in the cell and therefore control the transcriptional activation of the beneficial genes mentioned above. These changes are engendered by toxic substances such as arsenic or by chemopreventive compounds such as sulforaphane from the *Brassica* genus of plants. By studying these compounds and the structural changes within the E3 ligase that they induce, a greater understanding of this system will be achieved and therefore new methods for the prevention of cancer may be uncovered. This dissertation aimed to elucidate the molecular structure and mechanism of the Cul3-based E3 ubiquitin ligase complex and how modification of this complex by electrophiles or mutation brings about a change in Nrf2 ubiquitination.

Because of the difficulty in expressing cullin proteins, a vital component of a group of E3 ligases, specific precautions were taken in the creation of an expression construct for Cul3 to ensure success and a robust yield. Full gene synthesis was chosen over traditional cloning methods as a way to fast track the production of purified protein so that structural studies could begin. The codons of the human *cul3* and *rbx1* genes were optimized for expression in *E. coli*, and the genes were then synthesized and subcloned into a pETDuet-1 expression vector. The two proteins, Rbx1 and Cul3, were co-expressed in the BL21 bacterial expression system with a

Summary (continued)

hexahistidine affinity tag on the N-terminus of Rbx1, and the complex of Cul3/Rbx1 was purified in a two-step chromatography procedure. The expression system results in 15 mg of highly purified Cul3/Rbx1 per liter of bacterial cell culture. To ensure purified Cul3/Rbx1 is active, its ability to ubiquitinate Nrf2 was tested through the creation of an *in vitro* ubiquitination assay that consists of fully reconstituted components of the ubiquitination cascade. The results of the activity assay indicated Nrf2 is ubiquitinated only in the presence of Cul3/Rbx1 and confirmed that the purified Cul3/Rbx1 protein from the co-expression system was ready for structural characterization. In addition, the results showed that the Nrf2 ubiquitination reaction can be performed *in vitro* and easily monitored by anti-Nrf2 western blots.

Since there are very few structural models of the Cul3-based E3 ubiquitin ligase components, one of the aims of this work was to obtain structural information on the Cul3/Rbx1 and Keap1 proteins alone and in complex. The only X-ray structures available are of a single domain of the Keap1 protein, the Kelch domain. Therefore, molecular homology modeling was performed to learn more about the structure of the Cul3/Rbx1 and Keap1 proteins being studied. Keap1 and Cul3 homology models, created using the SWISS-MODEL web server, were structurally aligned to the crystal structure of the Cul1-based complex structure to create the Cul3/Rbx1:Keap1 models, a group of models containing either one or two Cul3/Rbx1 proteins and one or two Keap1 proteins. These models were then used to test hypotheses about the oligomeric nature of this intriguing macromolecular complex of proteins and used to refine experimentally derived models in later experiments.

The stoichiometry of the E3 ligase complex was elucidated through a combination of analytical size exclusion chromatography (SEC), sedimentation velocity analytical ultracentrifugation (AUC), and small-angle X-ray scattering (SAXS) approaches, which also

Summary (continued)

determined the hydrodynamic properties, stoichiometry and solution structures of the individual Cul3/Rbx1 and Keap1 proteins. Cul3 and Rbx1 when co-expressed, fold together into a rod-shaped heterodimer of one Cul3 and one Rbx1. The Keap1 protein was confirmed to be an extended, V-shaped obligate homodimer. The same techniques were also used to discover that the Cul3/Rbx1:Keap1 complex consists of one Cul3/Rbx1 heterodimer bound to one Keap1 homodimer. This appears to be a novel organization for cullin proteins with dimeric substrate adaptors and this organization is hypothesized to be formed and controlled through the accessory N-terminal loop found in the Cul3 homology model.

The solution scattering structures of Cul3/Rbx1, Keap1, and their complex are proposed from the SAXS scattering profiles measured at the APS and analyzed via a collection of data analysis programs. Once the low-resolution structure of the Cul3/Rbx1:Keap1 complex was elucidated, it was compared to complexes containing one of two important functional mutations in the Keap1-BTB domain, C151W and C151S, so that the structural mechanism which modulates Nrf2 ubiquitination through this cysteine can be understood.

A paradox exists in the field regarding Keap1 modification of Cys151. Cul3 and Keap1 have been postulated to dissociate from one another when Keap1 Cys151 is modified by electrophiles. Yet, other studies indicated that modification of Keap1 at position 151 causes a switch in the ubiquitination target from Nrf2 to Keap1. The ubiquitination reaction requires the components of the complex to be bound, properly orienting catalytic residues for chemical linkage, and therefore Keap1 cannot freely dissociate from Cul3 *and* be polyubiquitinated at the same time. Further investigation was needed to understand this paradox.

Previous results from the Mesecar lab show that site-directed mutagenesis of Keap1 at position 151 has an effect on the transcription of ARE-controlled genes depending on which

Summary (continued)

amino acid is incorporated into the protein. Two important mutants C151W and C151S were chosen for study because while the C151W mutant promotes an enhanced stability of Nrf2 and a decrease in the rate of ubiquitination, the C151S mutant promotes a loss of induction by electrophilic compounds. The results with C151S suggest that the mutation abolishes the trigger that these compounds utilize to alter the structure of the complex and thereby shut down the ubiquitination of Nrf2. The Keap1 mutants were tested in the *in vitro* ubiquitination assay to confirm that the mutation caused an effect on the rate of ubiquitination as opposed to some accessory pathway that leads to an alteration in ARE regulation. The *in vitro* assay from purified proteins showed vast differences in the Nrf2 ubiquitination rates when either C151W or C151S was present.

Surface plasmon resonance experiments were performed to measure the strength of the interaction between Cul3/Rbx1 and the three Keap1 samples. When the resulting data were analyzed by two different methods within the Biacore T100 Evaluation software, slightly different K_d values were generated, but the trend in the results was consistent: mutation at position 151 to a tryptophan increases the dissociation constant of the complex relative to wild type. The C151S mutation, on the other hand, was found to have a stronger interaction with Cul3/Rbx1 than wild type, since its K_d values were lower. However, the greater difference in K_d values was found between wild type and C151W.

The results from sedimentation velocity experiments further support the results from the surface plasmon resonance experiments. When Keap1 and its mutants are fully saturated with Cul3, each of the three Cul3/Rbx1-Keap1 samples has a unique molecular population. The stronger-interacting C151S sample has two distinct populations of molecules, the complex and the free Cul3. As the interaction becomes weaker in the wild type sample and even less stable in

Summary (continued)

the C151W sample, the two distinct populations begin to merge due to the interconversion of species being faster than the timescale of the experiment.

Small-angle X-ray scattering experiments were performed on the mutant complexes to determine if the complexes, when formed, have a difference in shape, which could contribute to the variability in catalytic rates observed between the wild type and the mutant Keap1 proteins in the *in vitro* assay. Differences in the complexes are apparent when the SAXS profiles are analyzed by Kratky plot and when pair-distribution functions are created and compared, using the GNOM program. Finally, when the data are analyzed via *ab initio* simulated annealing approaches, and replicate models are averaged, the resulting structural models show structural differences in the Cul3/Rbx1:Keap1 mutant complexes. The mutant complex models show a difference in global conformation between the C151W mutant when compared to Keap1 wild type (Keap1-WT or K1C) and the Keap1-C151S mutant (K1S). Two of the lobular portions of the SAXS-derived density, hypothesized to be the Keap1 Kelch domains, appear at an alternative angle with respect to Cul3 when compared to wild type or C151S. The C151S scattering model shows a very similar shape to wild type but is more defined. It is believed that the increased strength of the interaction is what causes this greater resolution. These results suggest that modification of Keap1 Cys151 to Trp results in a deformation or alteration in the global conformation of the complex formed between Keap1 and Cul3, thereby decreasing the strength of the interaction and hence the angle at which the two proteins come together.

In addition to Keap1 modification by electrophiles, results of mass spectrometry experimentation with the Cys151 dependent ARE-inducer, isoliquiritigenin, show that Cul3 cysteine alkylation is also produced by this electrophilic compound and was observed to have differential patterning when wild type Keap1 or the C151W mutation is present. Cys636 of Cul3

Summary (continued)

is modified by the electrophilic ARE-inducer isoliquiritigenin. This cysteine residue is modified in the presence and absence of Keap1, however it is not modified in the presence of Keap1-C151W. This final result further supports the conformational change model of Keap1 modification. Together with the experiments probing the strength of the interaction between Cul3 and the Keap1 proteins, the results of this dissertation indicate that mutation of Keap1 Cys151 to a tryptophan residue causes a difference in conformation when bound to Cul3, resulting in a 5 to 10-fold increase in the dissociation constant and a decrease in the catalytic rate of Nrf2 ubiquitination, resulting from an reorientation of catalytic residues and protein-binding surfaces.

Chapter 1: Introduction

1 INTRODUCTION

1.1 Ubiquitin E3 ligase complexes and the role of Cul3/Rbx1:Keap1 in cancer chemoprevention

The levels of many cellular proteins are regulated by a complex system of enzymes called the ubiquitin-proteasome system (UPS). The ubiquitination part of this system is composed of an ubiquitin-activating enzyme, E1, an ubiquitin-conjugating enzyme, E2, and an ubiquitin ligase complex, E3 (Figure 1). These enzymes function in a cascade, whereby the E1 is initially adenylated in the C-terminus, leading to the formation of a thioester linkage between E1 and ubiquitin (1). Ubiquitin is then transferred to a cysteine residue on the E2, forming the second thioester bond of the cascade (2). Finally, ubiquitin is transferred to an ϵ -amino group on one or more of the substrate protein's lysine residues via an isopeptide bond (3).

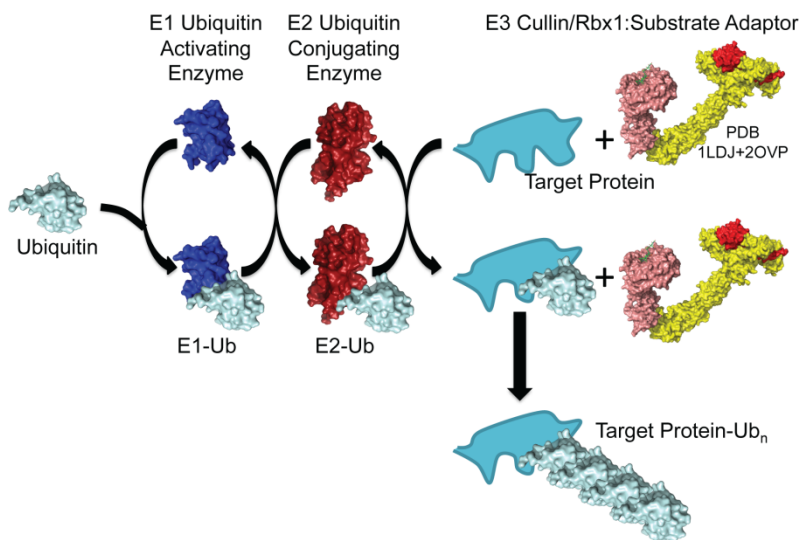


Figure 1. General ubiquitination pathway overview

Ubiquitin (light blue) is activated by E1 (royal blue); it is then conjugated to the E2 (brick red), which binds to the E3 (salmon/yellow/red). This orients the ubiquitin molecule for proper ligation to the target protein (blue). After multiple cycles of this reaction, the target protein has become polyubiquitinated and subsequently degraded by the proteasome.

The E3 ubiquitin ligases are multi-subunit complexes that catalyze the third and final step in the conjugation of ubiquitin to target substrate proteins (3, 4). During the addition of ubiquitin to a target protein, the cullin subunit serves as a scaffold that orients the adaptor-bound target protein for efficient ubiquitin transfer from the ubiquitin-charged E2 (5). Seven different human cullin proteins form a subset of E3 ligases that each has its own unique set of substrate adaptors. This variety of substrate adaptors enables cullins to catalyze the ubiquitination of a wide range of proteins that are involved in numerous cellular processes including cell cycle progression, signal transduction, and transcriptional regulation (Figure 2) (6, 7). Ubiquitination can have various effects on target proteins such as moderating subcellular localization, changing protein stability and protein-protein interactions, or targeting a protein for proteasomal degradation (8).

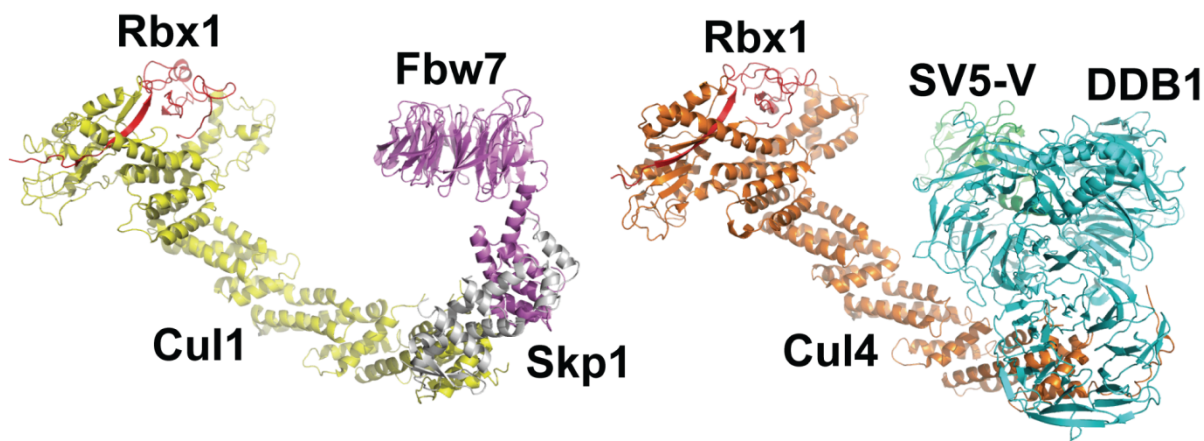


Figure 2. Examples of Cullin-based E3 ligase complexes

Shown are two examples of cullin-based complexes. The SCF complex on the left is composed of Cul1 in yellow, Rbx1 in red (PDB: 1LDJ), Skp1 in gray, and Fbw7 in magenta (PDB: 2OVP). The Cul4/Rbx1:DDB1 complex on the right (here hijacked by the viral SV5-V protein in green) is composed of Cul4 in orange, Rbx1 in red, and DDB1 in teal (PDB: 2HYE).

Cullin3 (Cul3), and one of its substrate adaptors, Kelch-like ECH-associated protein 1 (Keap1), together play an important role in the signaling pathway that regulates the transcription of genes involved in combating oxidative stress and promoting cell survival. The Cullin3-Keap1 mediated signaling pathway controls the cellular levels of the transcription factor nuclear factor (erythroid-derived 2)-like 2 (Nrf2), which is a key protein involved in regulating the expression of numerous cytoprotective genes. Nrf2 is a critical determinant of a cell's ability to survive exposure to oxidative stress, toxic heavy metals, metabolic transformation of xenobiotics, and endogenous oxidized metabolites (9). Under basal conditions, Nrf2 is constitutively expressed but maintained at low levels via ubiquitination by the Cullin3 E3 ligase complex and subsequent degradation by the proteasome (10, 11) (Figure 3 A). Under conditions of oxidative stress or xenobiotic assault, Nrf2 ubiquitination decreases and Nrf2 accumulates in the nucleus (Figure 3 B). Once in the nucleus, Nrf2 forms heterodimeric, transcription factor complexes with small Maf proteins, and these complexes bind to cis-acting DNA promoter sequences called antioxidant response elements (AREs) (12) (Figure 3 C and D). Binding to the ARE initiates transcription of a battery of antioxidant and detoxification genes that protect the cell against damage. Upregulation of these genes is a promising therapeutic strategy for the prevention of numerous diseases including cancer.

The core of the Cullin3 E3 complex is composed of the Cul3 protein bound to the small, 12 kDa protein RINGBox 1 (Rbx1) and the protein Keap1 (4, 6). So far, the X-ray structures of Cul3, Keap1, or the complexes they form remain unsolved. However, the X-ray structure of

Rbx1 has been determined in a complex with the protein Cullin1 (Cul1) (5). The X-ray structure of Cul1-Rbx1 shows an extended rod-shaped protein complex with Rbx1 integrally bound within the C-terminal domain of Cul1 (Figure 4). By analogy, the Cul3-Rbx1 structure is likely to adopt a similar rod-shaped tertiary structure to that of the Cul1-Rbx1 structure since Cul3 shares high sequence homology with Cul1. However, since Cul3 recruits entirely different protein substrates for ubiquitination than Cul1, this is likely where the analogy ends in terms of the formation of higher-order protein complexes. In addition, the stoichiometry of each protein, e.g. Cul3-Rbx1-Keap1-Nrf2, within the functional Cul3-based complex is unknown, yet it is the quaternary structure and the associated conformational changes within the complex that are believed to be an important feature of the ubiquitination mechanism of all cullin-based ligases (13).

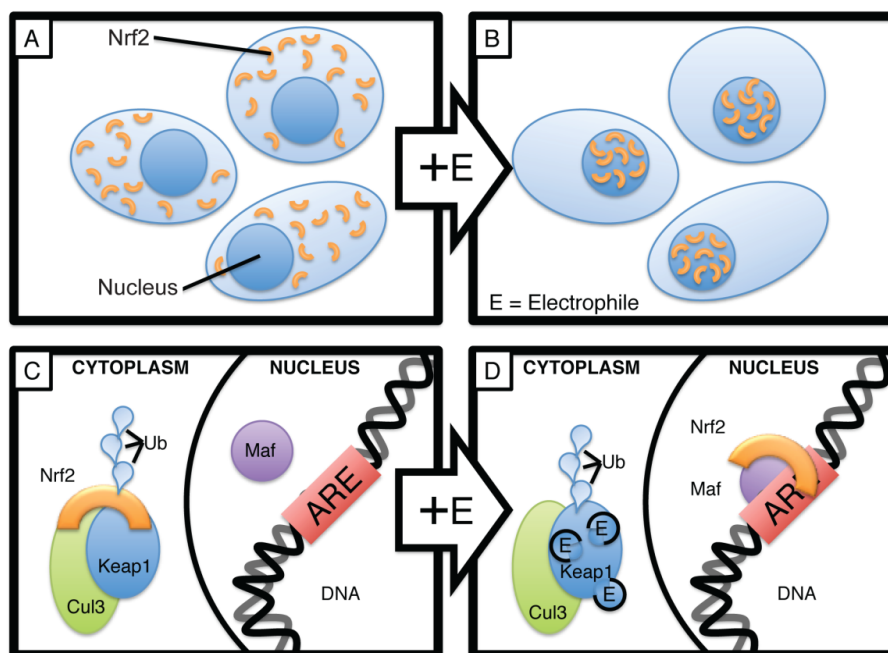


Figure 3. Molecular Mechanism of Electrophilic Induction of the ARE

Under basal conditions, Nrf2 is observed in the cytoplasm (A), where it is sequestered by Cul3-based E3 ligase and polyubiquitinated (C). After the addition of electrophilic inducers, Nrf2 localizes in the nucleus (B), where it complexes with small MAF proteins and binds to the ARE (D).

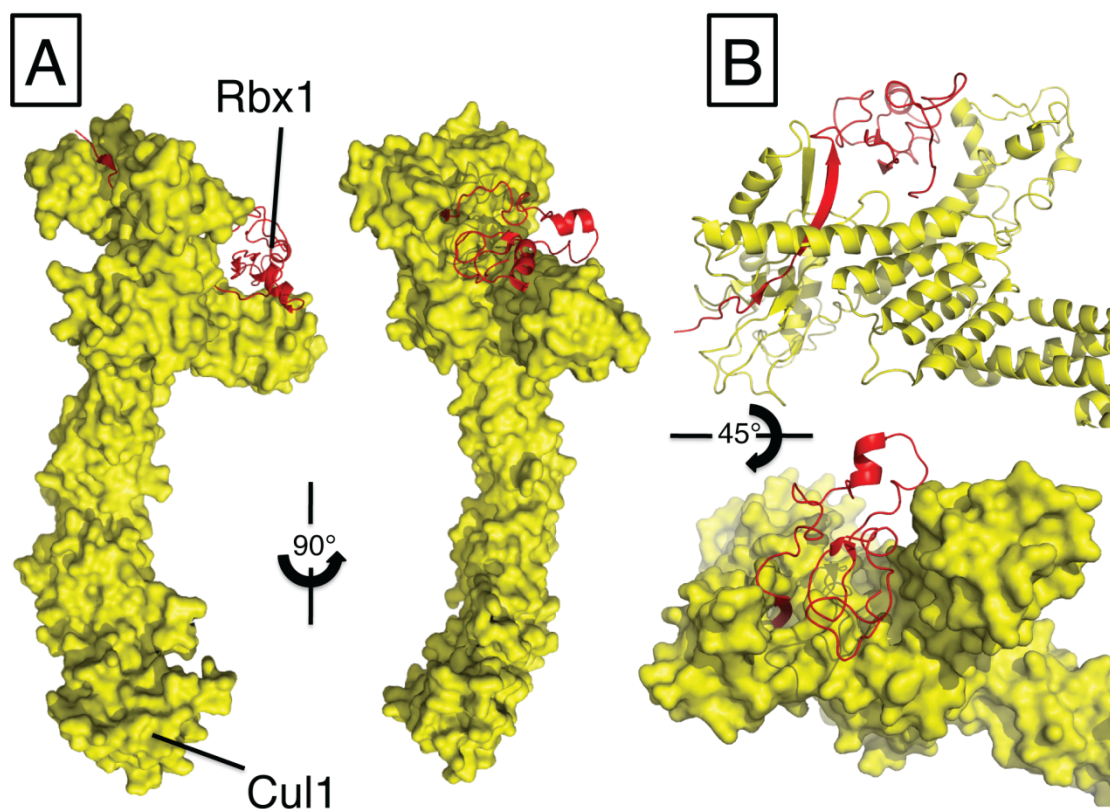


Figure 4. Crystal Structure of Cul1/Rbx1

A. Surface representation of the Cullin1 crystal structure in yellow with Rbx1 in red cartoon. The globular head domain is visible at the top with Rbx1 partially embedded within it. The substrate adaptor-binding N-terminus is seen as the rod-shaped domain extending down. B. Close up view of the Rbx1 molecule sitting within its cleft in Cul1. Rbx1 contributes one beta strand into a Cul1 beta sheet, anchoring it within the cullin.

Cul3/Rbx1:Keap1 is a specific E3 ligase within the cullin RING ligase family (4). It consists of Cullin3 (C3 or Cul3), a scaffolding protein with protein: protein interaction domains on both its N- and C-termini. The C-terminus binds RING Box 1 (Rbx1), which in turn binds to the E2 to allosterically activate it for ubiquitin transfer, to substrate (14, 15). The N-terminus of Cul3 binds to a large family of BTB domain-containing substrate adaptors (16, 17). Therefore, Cul3 functions to indirectly connect Rbx1 and the E2 to the substrate protein via the substrate adaptor protein.

Cullin ligases require substrate adaptors for proper binding and orienting of the protein targeted for ubiquitination. Several substrate adaptors have been shown to form homodimers and this formation of higher-order structure has been implicated as possibly being important in the function of these complexes (13). X-ray crystal structures and molecular homology modeling based on X-ray scattering data for the SCF^{Cdc4} complex from yeast have revealed this higher-order quaternary structure. The functional complex appears to be composed of a dimer of substrate adaptors each bound to one Cul1 scaffold (Figure 5). Further research on this complex shows that dimer disruption compromises the ability of the E3 ligase to initiate ubiquitination and chain elongation. Only after a subsequent phosphorylation step does the substrate have high enough affinity to bind the monomeric complex (18). In addition, the SCFFbx4 complex requires dimerization in order to ubiquitinated its substrate (19). This evidence points towards substrate adaptor dimerization as a potential regulation step in the activity of ubiquitin E3 ligase complexes. Whether dimerization of Cul3 occurs via a similar mechanism is addressed in Chapters 2-5.

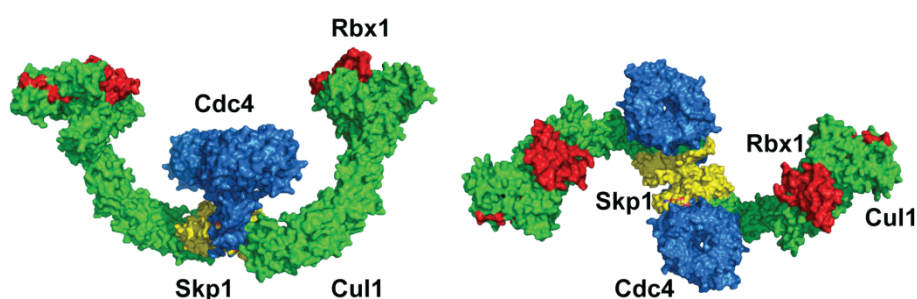


Figure 5. Dimeric Model of Cul1/Rbx1:Skp1/Cdc4

This large macromolecular complex is composed of a dimeric substrate adaptor at its core, flanked by two cullin proteins. Adapted from Tang, et al (13). It is hypothesized that the E3 complex containing the dimeric Keap1 would also have two cullin subunits like this one.

1.2 Nrf2 and Chemoprevention

Cancer chemoprevention uses nontoxic compounds to prevent, slow, or reverse the process of carcinogenesis (20-22). Cells have evolved multi-faceted, highly regulated defense mechanisms to protect against toxic insult from the environment. Nrf2, a major transcription factor, which regulates the expression of numerous cytoprotective genes, serves as one of the critical determining factors of a cell's ability to survive exposure to oxidative stress, toxic heavy metals, metabolic transformation of xenobiotics, and endogenous oxidized metabolites (9). Nrf2 is constitutively expressed and sequestered in the cytoplasm by Keap1 where it is targeted for ubiquitination (23). This process keeps the cellular concentration of Nrf2 low enough to prevent significant nuclear accumulation.

Nuclear accumulation results in the up-regulation of cytoprotective genes under control of the antioxidant response element (ARE), a cis-acting DNA promoter sequence controlling transcription levels of detoxifying or antioxidant genes (12). Several natural products, including sulforaphane from cruciferous vegetables (24), isoliquiritigenin from licorice (25), and curcumin from the turmeric spice (26-28), have been shown to be electrophilic and to cause this nuclear accumulation of Nrf2 as well as a decrease in the progression of carcinogenesis and thus are called cancer chemopreventive compounds or ARE-inducer. By studying how these natural products affect the Cul3/Rbx1:Keap1 complex, greater understanding of their potential use in chemoprevention regimens will be achieved.

The Nrf2 protein is a basic leucine zipper (bZip) transcription factor with a Cap "n" Collar (CNC) structure. It is divided into several domains (**Figure 6**). The Neh2 domain (amino acids 1-97) is the domain that binds to Keap1 (29). It contains two short motifs, ETGE and DLG, which each bind to the kelch domain of Keap1 (discussed in depth in 1.3). Between these two Keap1-binding regions lies a stretch of the Neh2 domain that contains 7 lysines, which are the

final attachment points for ubiquitin in the E1-E3 cascade of reactions. Very little structural data exists for Nrf2, but it is believed to be largely unstructured until bound to small Maf proteins and DNA in the nucleus.



Figure 6. Domain organization diagram for Nrf2

The Neh2 domain contains two Keap1-binding motifs, DLG and ETGE. In between these two sequences within Neh2, lies a region with 7 lysines, which are the targets for ubiquitination by the Cul3/Rbx1:Keap1 sequence.

1.3 Keap1 and Its Domains

The substrate adaptor protein, Keap1, contains several functional domains and 27 cysteines and is therefore thought to act as a redox sensor (Figure 7) (29-33). A subset of these cysteines has been shown to be highly reactive to modification by ARE-inducing compounds. These cysteines are found in each domain of Keap1, however a large percentage of them are found within the intervening region (IVR, also called central linker or BACK domain). So far there have been no structural studies on the IVR domain of Keap1, but the IVR domain has been implicated in playing a role in binding to Cul3 (34). Knowing the locations of the cysteines within this domain may yield a greater understanding of their role in the molecular signaling mechanism brought about by modification with electrophilic ARE-inducers.

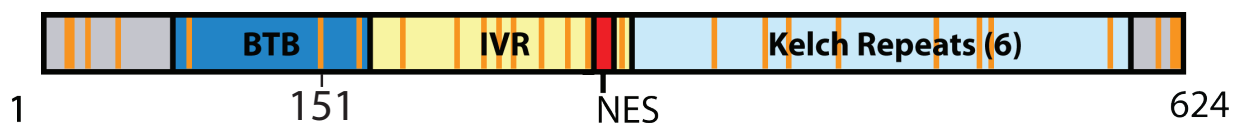


Figure 7. Domain organization diagram for Keap1

The Keap1 protein has 5 domains, the N-terminus, the BTB dimerization domain, the intervening region (IVR), the Kelch repeats domain, and the C-terminus. It contains 27 cysteine residues (orange lines) located throughout the 5 domains as well as a nuclear export sequence (NES).

Keap1 links the substrate, Nrf2, with Cul3 and the rest of the E3 ligase complex and it has been postulated to be a sensor of the redox state within the cell (30, 35). When electrophiles are reacted with Keap1 followed by trypsin digestion and subsequent mass spectrometry analysis, peptide fragments containing several important Keap1 cysteines are found to have covalent adducts with the electrophiles (36). In addition, intra- and intermolecular disulfide bonds are also found when different ratios of oxidized/reduced glutathione (GSH) are reacted with Keap1 (37). Specific Keap1 cysteine residues are readily modified, by these agents and this modification is thought to be an underlying mechanism through which different electrophiles and cancer chemopreventive agents exert their chemical influence on the system. The exact structural roles of these disulfide bonds and covalent adducts in the overall mechanism are poorly understood.

Keap1 consists of N-terminal, BTB, IVR, kelch and C-terminal domains (Figure 7) (38). So far, only the X-ray crystal structure of the kelch domain has been determined (1.85 Å, PDB code: 1U6D and 1.35 Å, PDB code: 1ZGK) and this domain is monomeric (39). The crystal structures of the BTB domains from several other BTB domain-containing proteins have been solved as well, however the oligomeric state of the BTB domain does not appear to be consistent between proteins (Figure 19) (40). The BTB domain of the LRF/ZBTB7 transcription factor

dimerizes (Figure 8 A and B) (PDB code: 2NN2), whereas the BTB domain of Miz-1 forms a tetramer (Figure 8 C) (PDB code: 2Q81) (40, 41). The BTB domain has also been postulated to form even higher-order oligomers, through the formation of a BTB domain fiber (42, 43). Although Keap1 has been shown to dimerize using the BTB domain, the possibility of Keap1 forming higher-order tetramers or oligomers should not be ignored. The BTB domain of Keap1 has also been shown to bind directly to the N-terminal domain Cul3 (34). This interaction with Cul3 may prevent the higher order structuring of the BTB domain.

Keap1 uses its C-terminal kelch domain (6-bladed β -propeller) to bind the N-terminal Neh2 domain of Nrf2 (29). The Neh2 domain contains two motifs, ETGE and DLG, which each bind to the kelch domain in distinct, yet overlapping regions (Figure 9). Differences in the binding affinity of each motif for the kelch domain have been measured by ITC and a “hinge and latch” model has been proposed where each motif binds to one kelch domain from a Keap1 dimer, such that each end of a single Neh2 domain is anchored to a kelch domain from each kelch monomer of the Keap1 dimer (Figure 10) (44-47). It is postulated that this binding mode would allow the proper orientation of the lysine-rich α -helix of Nrf2, which resides between the ETGE and DLG binding sites, to be positioned an optimal distance from the ubiquitin-conjugated E2. Despite extensive study of the Neh2:Keap1-kelch interaction, no structural characterization of the Nrf2:Keap1 complex has been performed.

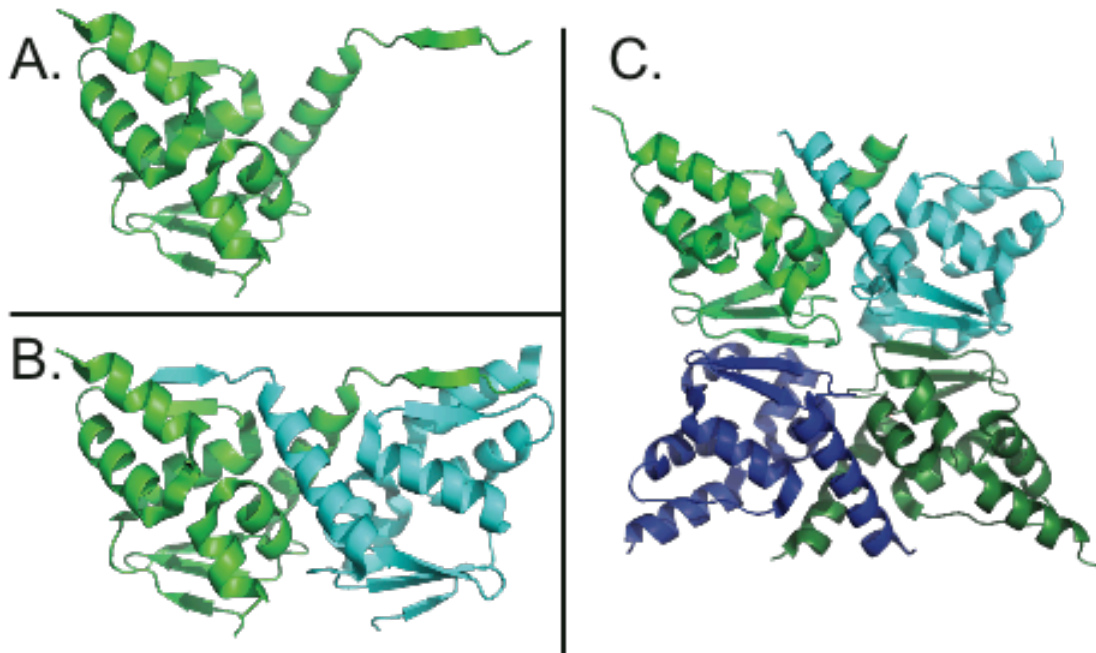


Figure 8. Crystal structures of BTB monomer, dimer, and tetramer

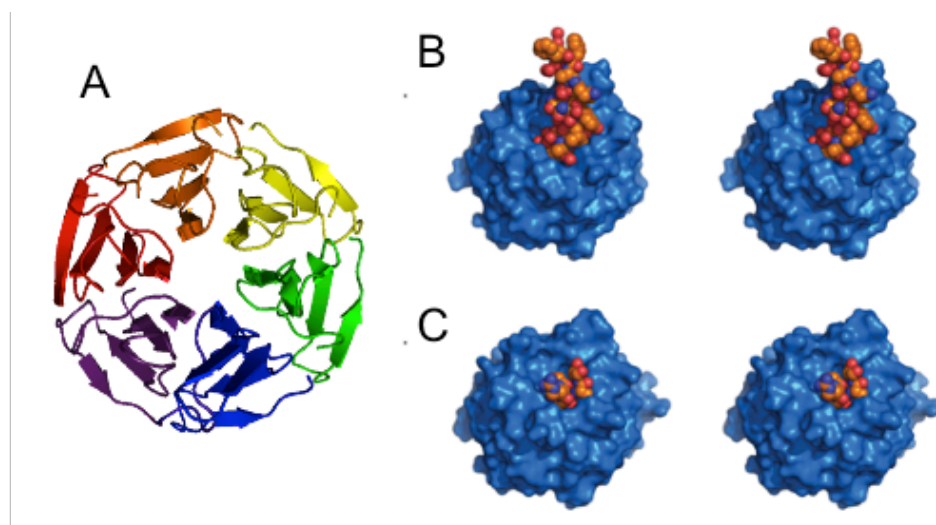


Figure 9. Crystal Structures of the Kelch Domain

A. The crystal structure of the kelch domain of Keap1 (PDB 1ZGK). Each color represents a different kelch repeat forming a blade of the propeller. The kelch domain of Keap1 has been crystallized in the presence of the ETGE (B) and DLG (C) peptides from the Neh2 domain of Nrf2. The crystal structures (2FLU, 2DYH) show that while the peptides both appear to bind the same site, they actually bind to discrete, overlapping sites near the central channel of the kelch domain.

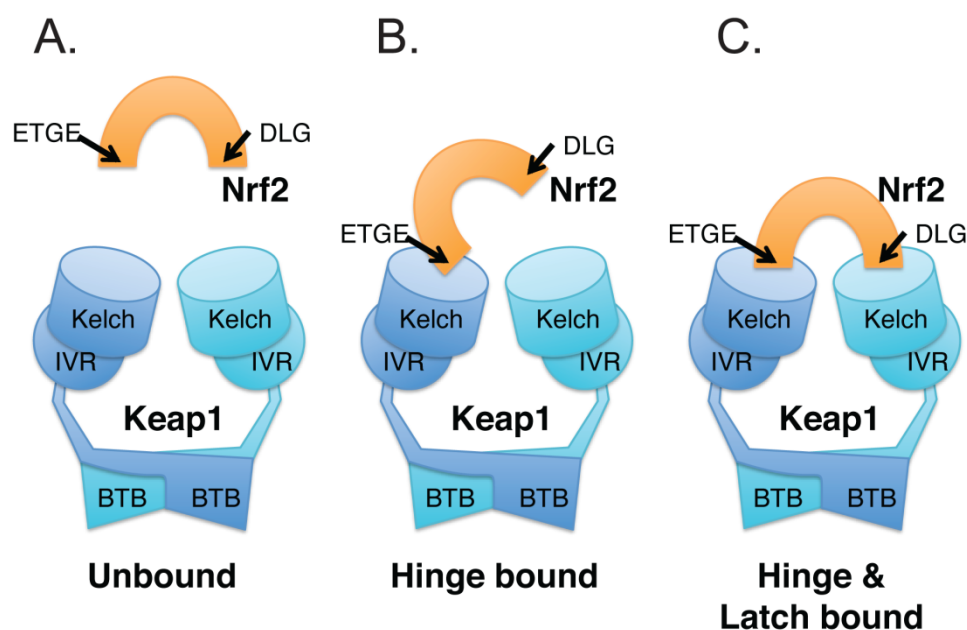


Figure 10. Hinge and Latch Model Diagram

Nrf2 binds to Keap1 in a 1:2 ([Cul3/Rbx1]:[Keap1 monomer]) molar ratio. The two separate proteins (A) come together first when the higher-affinity ETGE motif binds to one of the Keap1 dimer's two kelch domains (B). This allows the lower-affinity DLG motif to bind the other kelch from the dimer (C).

1.4 Keap1 Cysteine Mutants

Keap1 contains 27 cysteines and a number of these cysteines are reactive towards electrophiles (36, 48). In addition, a number of these cysteines are phenotypically different upon mutation, so it is assumed that these cysteines may play an important role in the molecular signaling events controlled by the Keap1-containing E3 complex (49). The significance of these important cysteines is still poorly understood since there is a lack of direct structural characterization of the Keap1 protein.

An important and reactive Keap1 cysteine that may be involved in the signaling mechanism is Cys151. It has been shown by the Mesecar group to be one of the most highly modified cysteine residues in Keap1 (36). The Keap1-C151S mutant has been shown to be unresponsive to modification by electrophiles (49). Zhang et al, have shown that when cells

transfected with the Keap1-C151S mutant are treated with tert-butyl hydroxyquinone (tBHQ), expression of the ARE-driven reporter gene is comparable to untreated cells indicating no increase in gene expression as observed when cells with wild type Keap1 are treated (49). Therefore, it has been proposed that Cys151 is required for “induced escape” (49). Published results from the Mesecar Lab suggest that mutation of Cys151 to a larger, bulkier residues such as phenylalanine, tyrosine, or tryptophan, results in increased expression of ARE-driven genes (50). Activation of the ARE was found to correlate with the partial molar volume of the side chain at position 151 (50). Mutation of Cys151 to tryptophan may mimic a covalent adduct of formed via modification with electrophiles, whereas mutation to serine may cause a loss of the cysteine reactivity without causing any steric interactions that a bulkier tryptophan residue may produce.

A dissociation model for Cul3 and Keap1 has been proposed based on co-immunoprecipitation results of modification of Cys151 by N-iodoacetyl-N-biotinylhexylenediamine (IAB) using purified proteins (51). In the proposed dissociation model, modification of Keap1 Cys151 by IAB results in the dissociation of the Nrf2-Keap1 complex from Cul3; however, publications from other research groups show that modification of Keap1 Cys151 resulting in a switch in the ubiquitination target from Nrf2 to Keap1 (52). These results conflict with one another and further investigation is needed to better understand this dynamic regulatory system.

Two additional cysteines within Keap1 have been implicated to play a role in regulation of the signaling mechanism. Zhang et al, have shown that a Keap1-C288S mutant caused constitutive activation of ARE-driven genes and that the presence of Cys288 is required for Keap1-dependent ubiquitination of Nrf2 (49). Results from Holland et al, show that

intermolecular disulfide bonds were formed between Cys319 on two separate Keap1 molecules in the presence of oxidized glutathione (GSSG) (53). The same experiments showed the formation of an S-glutathionylated Cys434 residue (53). Cys434 is positioned adjacent to the Nrf2 binding pocket in the kelch domain of Keap1. Any alteration of the structure around Cys434 could greatly affect the binding surface for interaction with Nrf2.

By displaying different ubiquitination phenotypes, the above results suggest that these reactive cysteines may play an important role in the overall ubiquitin signaling mechanism. These cysteines may act individually or in concert to disassemble the multiple subunit interactions within the complex. The phenotypic diversity and differences in structural positioning may possibly allow for different mechanisms of ARE-driven gene up-regulation by Nrf2.

By studying mutants of the cysteines mentioned above, particularly Cys151, the structural significance of these cysteines to the ubiquitin signaling mechanism may be better understood. Cys151 has been deemed to be the most important signaling cysteine within the Keap1 molecule, because of its ability to greatly affect ARE-driven gene expression upon mutation to serine or tryptophan. Structure-function studies described in chapter 5, focus on uncovering the role of Cys151 in the mechanism behind this pivotal switch point in the Nrf2 ubiquitin-signaling cascade.

1.5 Cul3 and Rbx1

Cul3 is homologous to the Cullin1 (Cul1) protein found in the Cul1/Rbx1:Skp1 (SCF) ubiquitin ligase complex (6). It contains binding sites for Rbx1 and BTB domain-containing substrate adaptors, including Keap1 (Figure 11). The N-terminal domain that binds these BTB proteins contains three cullin repeat regions, which, based on the structure of Cul1, are

postulated to separate the substrate from the E2 at the proper distance to allow both ubiquitination and chain elongation to occur (5). Cullin proteins have been notoriously difficult to express and purify. Efforts in the past have been to split the gene up into 2 pieces and express the pieces in insect and bacterial cells to be assembled later (54). No efficient bacterial expression systems have been created for these proteins.

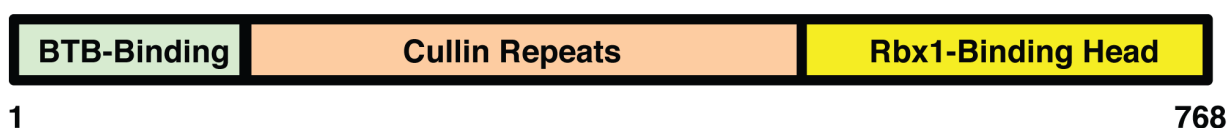


Figure 11. Domain Organization Diagram for Cullin3

The Cul3 protein is divided into three main parts, the globular Rbx1-binding C-terminal domain, the cullin repeats, and the region that binds BTB-containing proteins, found at the N-terminus.

Rbx1 is an evolutionarily conserved protein containing a RING-H2 fingerlike motif, which binds to cullins (14, 15). In the crystal structure of the Cul1/Rbx1 complex (PDB code: 1LDJ), Rbx1 occupies a large cleft on the C-terminal end of Cul1 and inserts its N-terminal β -strand (NTS) into Cul1's head domain, contributing to a β -sheet. In the SCF complex, Rbx1 recruits the E2 to bind to the E3 complex. In addition to Cul1 and Cul3, Rbx1 is involved with forming other E3 complexes with Cul2 and Cul4 (5, 55). While the C-terminal end of each of these cullin complexes binds Rbx1 in the same way, it is the N-terminal region, the substrate adaptor binding domain, which differs from one complex to the next (7).

The Rbx1 molecule is activated once its corresponding cullin is post-translationally modified, by the ubiquitin-like molecule, Nedd8 (56). This modification induces a conformational change in the C-terminal head domain of the cullin molecule that then liberates

the Rbx1 molecule from its cleft (Figure 12) (56). Rbx1 remains tethered to the cullin head by the NTS. It is hypothesized that the increase in conformational freedom of range that modification by Nedd8 induces, contributes to the ability of the complex to polyubiquitinate its substrates (56).

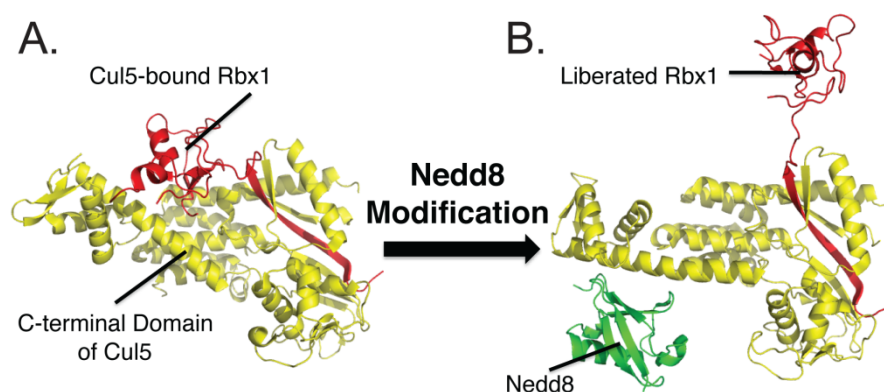


Figure 12. Neddylated-induced conformational change in Cul5

The crystal structures of the head domain of Cul5/Rbx1 can be seen before (A) and after neddylation (B). Covalent modification of Cul5 by Nedd8 causes a conformational change in the head domain, liberating Rbx1 from its cleft. Although still integrally bound through the contribution of a beta strand into a Cul5 beta sheet, Rbx1 now experiences many more degrees of freedom, catalyzing the ubiquitination of its substrate. Adapted from Huang et al. (56).

1.6 Significance and Impact

A major gap exists in our understanding of the structure and signaling of Cul3/Rbx1:Keap1 complex. Since the control of this system using regimented doses of chemopreventive compounds is the goal of the field, structural characterization of the Cul3/Rbx1:Keap1 complex and any structural changes induced by modification would be a major step in the process of understanding how this complex functions and how the regulation of Nrf2 ubiquitination occurs within the cell.

Therefore, the structure of this complex was sought using a combination of high- and low-resolution techniques, such as protein X-ray crystallography, analytical size exclusion chromatography, analytical ultracentrifugation, and small-angle X-ray scattering. After a low-

resolution structural model of the complex was created based on the experimental results, comparison to similar experimental results of complexes formed from Keap1 mutants at position 151, suggests a mechanism by which electrophiles may affect signaling.

CHAPTER 2: EXPRESSION, PURIFICATION, AND IN VITRO UBIQUITINATION ACTIVITY OF
CUL3/RBX1

2 EXPRESSION, PURIFICATION, AND IN VITRO UBIQUITINATION ACTIVITY OF CUL3/RBX1

Portions of the data and text in this chapter have been published in the journal article titled "Development of an efficient E. coli expression and purification system for a catalytically active, human Cullin3-RINGBox1 protein complex and elucidation of its quaternary structure with Keap1." (57)

2.1 Introduction

2.1.1 Rationale for Co-expression Plasmid and Gene Synthesis

In an effort to accelerate the structural and biochemical characterization of Cul3-based ligase complexes, we sought to develop a new, efficient expression and purification system for Cul3-Rbx1 that would enable the production of large quantities of soluble, full-length protein. In general, cullin proteins have been difficult to express in *E. coli* due to solubility issues. In the past, production of cullin proteins has been achieved via expression in insect cells or by a "Split-N-Co-express" approach utilizing *E. coli* as an expression host (58). In the latter method, two separate fragments of Cul1 are expressed and then co-folded to produce a functional version of Cul1 but with a peptide-chain break (58). Since neither method is currently able to easily produce large quantities of full-length Cullin protein, we sought to develop a more efficient expression and purification system that would be applicable to all cullin proteins. We therefore developed an *E. coli* expression and purification system for large-scale production of the full-length Cul3 protein in complex with Rbx1.

Large-scale protein expression and purification procedures were performed to create sufficient quantities of the proteins of interest for the structural characterization studies described in Chapters 4 and 5. A recombinant expression system for *E. coli* was chosen as the optimal system to accomplish this requirement. Expression in *E. coli* allows for optimization and scale-up procedures so that a large amount of highly purified proteins can be obtained. One potential

caveat of this technique however, is that any post-translational modification of the proteins of interest, including neddylation as discussed in Chapter 1, will not be included in the final sample.

2.1.2 *In vitro* Ubiquitination of Nrf2 Activity Assay for Cul3/Rbx1

To ensure the purified Cul3/Rbx1 expressed from the synthetic plasmid was viable and folded correctly, an *in vitro* ubiquitination activity assay was developed based on similar assays developed by Dr. Brenda Schulman (56). This assay combines Nrf2 and Keap1 with the E1, E2, and E3 components and ubiquitin. ATP is consumed in the reaction that leads to the accumulation of Nrf2-ubiquitin conjugates. Analysis of the assay by anti-Nrf2 western blot allows for the observation and comparison of samples in an easy and cost-effective manner.

2.2 Materials and Methods

2.2.1 Generation of Expression Construct for Cul3/Rbx1 Co-expression

Full-length sequences of both proteins (Cul3: NP_003581, Rbx1: NP_055063) were codon-optimized for expression in *E. coli*, synthesized (BioBasic, Inc.), and cloned into a pUC57 vector. Codon-optimized sequences can be found in Appendix A. The two genes were then subcloned into the Novagen pETDuet-1 vector with BamHI and HindIII restriction sites for the Cul3 gene, and NdeI and XhoI restriction sites for Rbx1. The restriction sites within the resulting expression vector, pET-hCul3-Rbx1, position Rbx1 such that it expresses with an N-terminal His6-tag for affinity purification.

2.2.2 Protein Expression and Purification

2.2.2.1 pETDuet-1-hCul3-Rbx1 Plasmid Expression

The expression plasmid pETDuet-1-hCul3-Rbx1 was transformed into *E. coli* BL21 (DE3) cells via electroporation for protein over-expression. Transformed bacteria were plated onto Luria-Bertani (LB)-Amp (100 µg/mL) plates and grown overnight. Single colonies from plates were used to inoculate 10 mL LB-Amp (100 µg/mL) starter cultures that were grown for 8 hours at 37 °C. One milliliter of starter culture was then used to inoculate 1 L of LB-Amp (100 µg/mL) cultures that were grown at 25 °C until the optical density at 600 nm (OD_{600nm}) of the culture reached 0.6. IPTG was then added to a final concentration of 200 µM, and the cells were grown at 18 °C for an additional 8 hours.

2.2.2.2 Cul3/Rbx1 Affinity and Size Exclusion Chromatography

The cells were harvested by centrifugation at 5,000 rpm (4,225 x g) for 15 minutes (Sorvall SLC-4000) and re-suspended to 0.33 g/mL of cell pellet in lysis buffer (50 mM Tris-HCl, pH 8.0, 500 mM NaCl, EDTA-free Protease Inhibitor Cocktail (Roche), 0.2 mg/mL lysozyme, and 0.002 mg/mL DNase I). The cellular suspension was homogenized manually and then lysed by sonication at 65% power for 0.6 seconds every 1.5 seconds for a total of 22.5 minutes. The cell debris was then centrifuged at 18,000 rpm (40,760 x g) for 45 min (Sorvall SA-600). The clarified cell lysate was loaded onto a 5 mL HisTrap affinity column (GE Healthcare), charged with Ni²⁺, and equilibrated with 50 mM Tris-HCl, pH 8.0, 500 mM NaCl, 10 mM imidazole, and 2 mM dithiothreitol (DTT). His6-Rbx1 in complex with Cul3 was eluted by a linear gradient of 0% – 50% imidazole in elution buffer (50 mM Tris-HCl, pH 8.0, 500 mM NaCl, 0.5 M imidazole). The fractions containing both His6-Rbx1 and Cul3, as judged by SDS-PAGE, were pooled and concentrated from 5 mg/mL to 30 mg/mL in a final volume of 5 mL.

The entire 5 mL of protein was then injected onto a HiLoad 26/60 Superdex 200 prep grade size-exclusion column (GE Healthcare). The fractions (5 mL) containing pure His6-Rbx1-Cul3 complex (Cul3/Rbx1 from here on) were pooled, concentrated to 10 mg/mL, and dialyzed into 2L of storage buffer (50 mM Tris-HCl, pH 8.0, 0.25 M NaCl, 20% glycerol) overnight at 4 °C. The following morning the protein was concentrated, to a final concentration of 50-200 μ M (depending on the experiment it was to be used for), using Amicon Ultra (Millipore) concentrator devices with a molecular weight cut-off of 30 kDa. The final protein, in 5-500 μ L aliquots in 1.7 mL Eppendorf tubes, was flash-frozen in ethanol and dry ice for long-term storage at -80 °C.

2.2.2.3 Keap1 and Nrf2 Expression and Purification

The protocols for Keap1 and Nrf2 expression and purification were adapted from our original procedure developed by Dr. Aimee Egger (48). The only change was the removal of the MonoQ Keap1 purification step and the inclusion of the S200 gel filtration step using a buffer containing 50 mM Tris, pH 8.0, 150 mM NaCl, and 2 mM DTT. There were no observable differences in purity or yield between Keap1 samples purified on either the S200 gel filtration column or the MonoQ. This change enabled greater simplicity in the purification steps as both Keap1 and Cul3/Rbx1 could be purified using the same buffers, columns, and equipment.

2.2.3 In vitro Ubiquitination Assay

In order to assess the catalytic activity of Cul3/Rbx1, an *in vitro* ubiquitination assay was developed, based on similar assays developed by Dr. Brenda Schulman (56). Each ubiquitination reaction contained 65 nM human ubiquitin-activating enzyme 1 (UBE1), 5 μ M ubiquitin-conjugating enzyme H5 (UbcH5), 100 nM Cul3/Rbx1, 100 nM human Keap1, 100 nM human

Nrf2, 46 μ M chicken egg white albumin, 75 mM Tris pH 8.0, 15 mM MgCl₂, and 7.5 mM ATP in 5.5 μ L, and was initiated with the addition of 1 μ L of ubiquitin to a final concentration of 169 μ M. The reactions were incubated at room temperature or 37 °C for 5, 10, 20, or 30 minutes and then quenched by the addition of 3.5 μ L of stop buffer (final concentration of 1X NuPAGE LDS sample buffer (Invitrogen), 1X NuPAGE reducing agent, and 3.5 mM EDTA). Reaction products were resolved by 4-12% Bis-Tris PAGE gels and transferred to PVDF membranes. The membranes were blocked with 5% dry milk in TBS-T (50 mM Tris-HCl, 150 mM NaCl, 0.1% Tween 20, pH 8) prior to incubation with rabbit anti-Nrf2 (Santa Cruz). Additional experimentation used goat anti-Keap1 and rabbit anti-Cul3 antibodies using the same procedure as above. Detection of bound antibodies was carried out by enhanced chemiluminescence using bovine anti-rabbit (for Nrf2 or Cul3) or anti-goat (Keap1) antibodies conjugated to horseradish peroxidase (Santa Cruz).

Table I. Components of the *in vitro* ubiquitination assay

Component	Concentration	Order Added to Reaction tube
E1 (UBE1)	65 nM	1
E2 (UbcH5)	5 μ M	1
Cul3/Rbx1	100 nM	1
Nrf2	100 nM	1
Ovalbumin	2 mg/mL	1
Ubiquitin*	169 μ M	3
<i>one of the following:</i>		
Keap1-WT	100 nM	2
Keap1-C151W	100 nM	2
Keap1-C151S	100 nM	2

*reaction initiator, added at time = 0 min

2.3 Results

2.3.1 Design of Cul3/Rbx1 Co-expression Construct

The field of synthetic biology is ushering in a new generation of strategies for the design and synthesis of novel expression systems for proteins that are difficult to produce. Since synthesis of codon-optimized genes and construction of expression vectors is now mainstream and cost-effective, we decided to take advantage of this technology for the difficult-to-produce cullin proteins (59). The full-length, codon-optimized genes for Cul3 and Rbx1 were synthesized by BioBasic, Inc. Both genes were then inserted into the pETDuet-1 system for co-expression in *E. coli* (Figure 13). The Rbx1 protein, but not the Cul3 protein, was designed to have an intact hexahistidine tag for affinity purification. This strategy was more desirable than having both proteins tagged since the purified material would be used for structural characterization and crystallization trials. Highly mobile affinity tags decrease the likelihood of obtaining diffraction quality crystals. In addition, a thrombin cut site was engineered between the His6–affinity tag and Rbx1. This allows the His6 tag to be easily removed for crystallization. A stop codon was added to the Cul3 sequence so that the native S-tag located within the pETDuet-1 vector would not translate with the Cul3 protein.

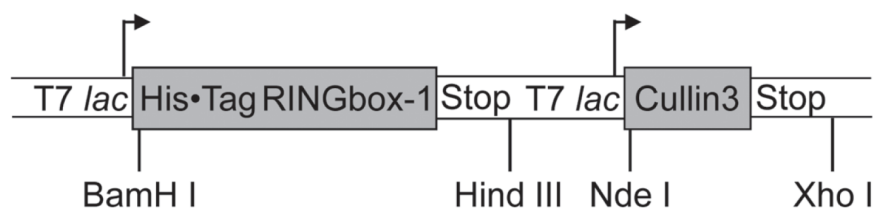


Figure 13. Cul3 and Rbx1 Gene Placement Diagram for pETDuet-1 Plasmid

Cul3 and Rbx1 DNA sequences were cloned into the pETDuet-1 vector using Nde I & Xho I and BamH I & Hind III, respectively. Rbx1 was placed so that an N-terminal His-Tag transcribes along with the gene. The two individual genes are co-expressed and fold together.

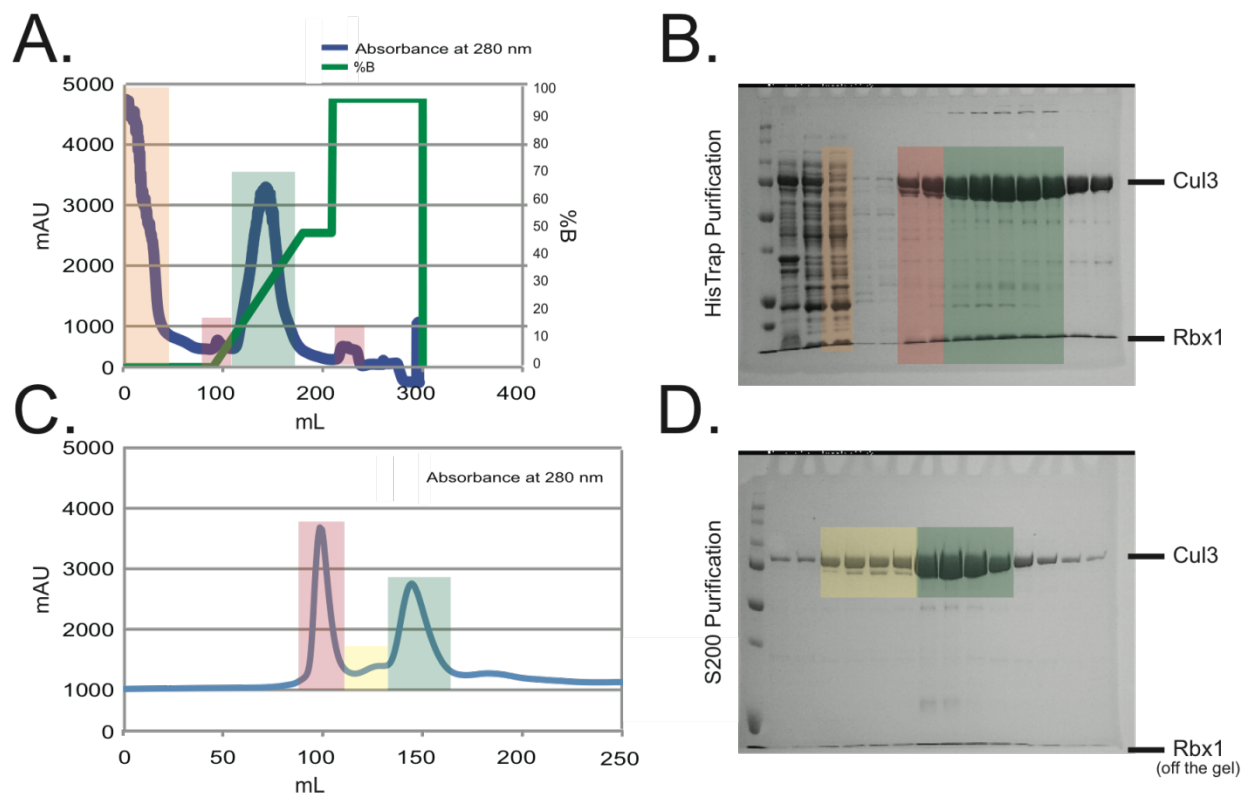
2.3.2 Protein Over-expression and Purification

Expression studies for Cul3/Rbx1 were performed to maximize co-expression and to obtain significant yields of purified protein. These studies consisted of varying incubation temperatures (18°C, 25°C, and 37°C), IPTG concentrations (200 μ M to 1 mM), length of induction time (2, 4, 18 and 24 hours), and the use of different bacterial cell strains including BL21 (DE3) and Rosetta (DE3). The conditions leading to the highest expression were 25°C incubation temperature, 200 μ M IPTG, and 18 hour induction time at 18°C using BL21 (DE3) expression cells.

The optimized expression conditions were adapted for large-scale expression and purification of the Cul3/Rbx1 complex. Cul3/Rbx1 was found to elute from the HisTrap and size-exclusion column as a single species (Figure 16 A and C), indicating that the Cul3 and Rbx1 proteins form a stable complex. The Cul3/Rbx1 complex, visible on a Coomassie-stained SDS-PAGE gel as two bands (88 kDa Cul3 and 12 kDa His6-Rbx1), was highly purified after two chromatographic steps (Figure 17, lane 6). An SDS-PAGE gel of the overall purification procedure and final purified product can be found in Figure 15. The tightly associating Cul3/Rbx1 protein complex was found to be more soluble at high NaCl concentrations; low salt concentrations led to precipitation of the protein. Therefore, the concentration of NaCl was maintained at 250 mM over the course of purification. The final optimized purification strategy yields on average about 15 mg of pure protein per liter of bacterial cell culture.

Table II. Cul3/Rbx1 Purification Yield Results

Sample	Step of Purification	Protein (mg)
1	Wet Cell Paste	38,400
2	Lysate	1417.5
3	Soluble Fraction	964.9
4	Post Histrap ^a	72.9
5	Post S200 ^b	45 ^c

^a Yield: 7.5%^b Yield: 61.7%^c for three liters of cell culture (15 mg/L)**Figure 14. Cul3/Rbx1 Purification Chromatograms and SDS-PAGE Gels**

A. His6-tag affinity purification chromatogram for Cul3/Rbx1 B. SDS-PAGE analysis of HisTrap fractions (orange = loading, red = wash, green = Cul3/Rbx1 peak) C. Size exclusion purification chromatogram for Cul3/Rbx1 D. SDS-PAGE analysis of S200 fractions (red = void, yellow = impurity peak, green = Cul3/Rbx1 peak)

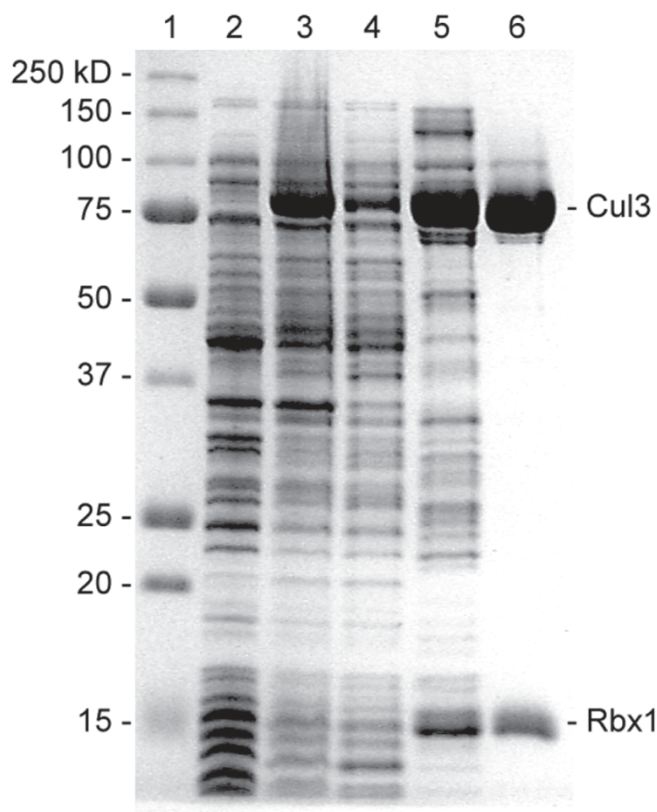


Figure 15. SDS-PAGE Gel of Cul3/Rbx1 Purification Overview

Lane 1 contains a standard protein marker. Lane 2 shows the insoluble protein content from the whole cell lysate. Lane 3 contains soluble proteins. Lane 4 shows the proteins contained in the Histrap flow-through. Lane 5 is the pooled HisTrap elution fractions, which contain Cul3/Rbx1. Lane 6 contains the final purified Cul3/Rbx1 after elution from the S200 SEC column.

2.3.3 *In vitro* Ubiquitination Assay

2.3.3.1 *Anti-Nrf2 Western Blot at 25 °C*

The Cul3/Rbx1 E3 ligase catalyzes Nrf2 ubiquitination in concert with other proteins from the ubiquitin cascade. A discontinuous *in vitro* ubiquitination assay was developed to ensure that co-expressed and purified Cul3/Rbx1 functions to bind and orient the Nrf2-bound substrate adaptor properly for ubiquitin transfer from UbcH5. This is the first reported assay to reconstitute Nrf2 ubiquitination entirely from purified proteins.

The transcription factor Nrf2 was found to be readily ubiquitinated by the recombinant Cul3/Rbx1:Keap1 complex in the presence of the other required ubiquitin-ligase components *in vitro* (Figure 16). The reaction proceeds rapidly and with higher-order Nrf2-ubiquitin conjugates forming and accumulating over time. The Nrf2-ubiquitin conjugates are visible as a short ladder of bands above Nrf2 (Figure 16, Lanes 2 to 4). Each band above Nrf2 represents an additional ubiquitin being added to Nrf2 through the catalytic efforts of the E3-ligase complex. The ladder of Nrf2-ubiquitin intensifies and higher molecular weight forms accumulate, the unmodified Nrf2 band decreases, corresponding to a decrease of free Nrf2 in the reaction.

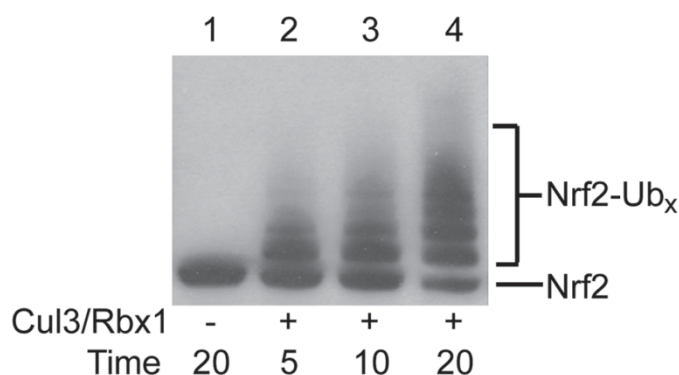


Figure 16. Anti-Nrf2 Western Blot of Nrf2 Ubiquitination Assay

The *in vitro* ubiquitination assay of Nrf2 combines all the components (Table I.) of the reaction cascade. Without the addition of Cul3/Rbx1, Nrf2 remains unmodified (Lane 1). Cul3/Rbx1 catalyzes the ubiquitination of Nrf2 (Lane 2) and the reaction proceeds over time (Lanes 2-4) with the buildup of Nrf2-ubiquitin conjugates.

2.3.3.2 Anti-Nrf2, -Keap1, and -Cul3 Western Blot at 37 °C

When the previous experiment was repeated, except at 37 °C and this time also blotting for Cul3 and Keap1, the results revealed more information about this sophisticated ubiquitination reaction. In the anti-Nrf2 blot of Figure 17, non-ubiquitinated Nrf2 can be observed in Lane 1.

Lane 2 contains Nrf2-Ub_n conjugates that are the results of Keap1-independent ubiquitination. It is not fully understood how this ubiquitination occurs in the absence of Keap1. Comparing lanes 2 and 5 reveals the catalytic power of the addition of Keap1 to the reaction. Nrf2 is conjugated to Nrf2 at a much higher level. Lane 3 contains a similar amount of Nrf2-ubiquitin conjugates when compared to lane 2; however the reaction in the sample in lane 3 was quenched 15 minutes before the sample in lane 2. As the reaction was allowed to proceed even further, Nrf2-Ub_n accumulated more ubiquitins. Their continually expanding MWs caused a streaking on the gel visible in lanes 4 and 5 (Figure 17).

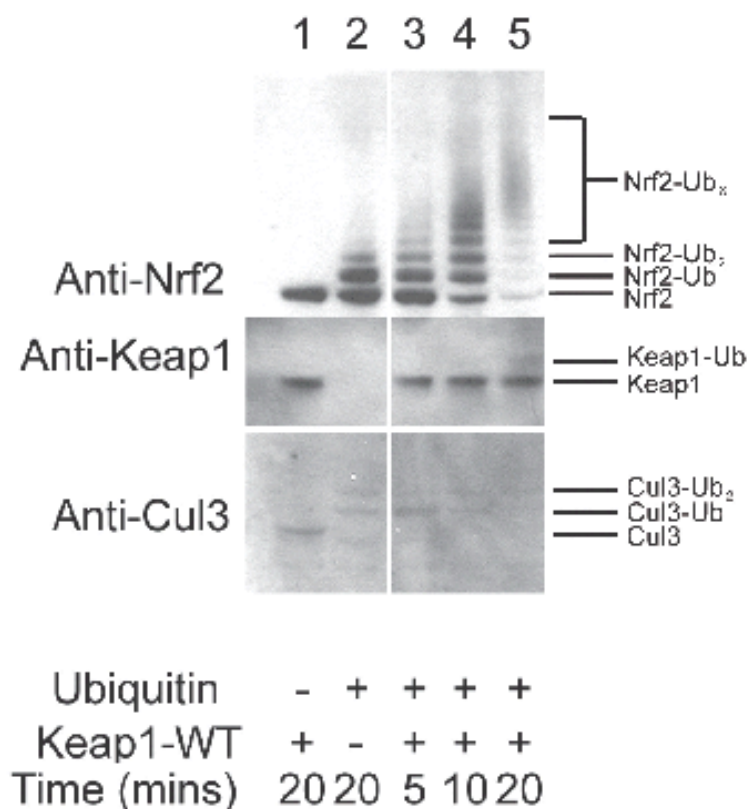


Figure 17. Anti-Nrf2, -Keap1, and -Cul3 Western Blot of Ubiquitination Assay

This is an *in vitro* ubiquitination assay showing the modification of Nrf2, Keap1, and Cul3 over time. The noticeably higher rates of ubiquitination in this blot compared to the previous blot are attributable to the increase in temperature.

The anti-Keap1 blot in Figure 17 reveals an ubiquitination event on Keap1 (lane 5). This modification appears to be very low in concentration and occurs later on in the reaction, as it is not visible at the 5-minute time point. It is not understood whether this ubiquitination of Keap1 is relevant to the reaction mechanism, but it has been postulated that Keap1 undergoes ubiquitination at Lys298 following modification with electrophiles (60).

The anti-Cul3 blot in Figure 17 supports the theory put forth by Huang, et al., that in the absence of Nedd8, cullin proteins undergo ubiquitination to activate their respective Rbx1 molecule (56). In the absence of ubiquitin (lane 1) Cul3 is present as a singular, weak band (the anti-Cul3 antibody is of a much poorer quality than the more robust anti-Nrf2 antibody). Lane 2 shows the presence of two slightly higher MW bands with the absence of the original Cul3 band. These results suggest two ubiquitination events occur on Cul3 within 20 minutes. It is unknown whether these two ubiquitin molecules are present on the same lysine as diubiquitin or on two separate lysines as monoubiquitins. Lanes 3-5 show the formation of the second ubiquitination event over time, but not the first. The first ubiquitination event had already fully occurred by the 5-minute time point. It is believed that since the modification of Cul3 by either Nedd8 or ubiquitin supposedly activates the Rbx1 molecule that is responsible for the ubiquitination of Nrf2, the first Cul3 ubiquitin modification event occurred before the ubiquitination of Nrf2 within the same sample. This theory is based on the conclusions from experiments on Cul5, where Rbx1 in unmodified Cul5 is positioned to ubiquitinate the cullin prior to its release from the cullin cleft (56). It is unknown what effect the second ubiquitin has on the reaction mechanism or rate.

2.4 Discussion

The Cul3/Rbx1 pETDuet-1 co-expression system, resulting in 15 mg per 1 liter of bacterial cell culture, was an easy and cost-effective method of producing full-length, active Cul3/Rbx1 protein. This co-expression system should allow for increased structural and biophysical studies for structure-function analyses of this important and interesting system.

The *in vitro* ubiquitination assay is a powerful tool in the investigation of the Nrf2-ubiquitin signaling system. The anti-Nrf2 western blots show that Nrf2 is readily modified by ubiquitin after the addition of Cul3/Rbx1 and that modification is greatly enhanced in the presence of Keap1. How Nrf2 is ubiquitinated by Cul3/Rbx1, in the absence of Keap1, is not well understood. Nrf2 is not thought to bind to Cul3 or Rbx1. Whether any interaction between them exists is addressed in the surface Plasmon resonance section of Chapter 5.

The *in vitro* assay can also be used to study the effects on Cul3 and Keap1, using their respective antibodies. Cul3 undergoes modification as observed by the higher-MW band directly above whether the Cul3 band migrates. It is hypothesized that this modification of Cul3 is the same as the ubiquitination Rbx1-activation event described by Huang for Cul5 (56). Keap1 appears to be ubiquitinated after 20 minutes, but to a much less degree than Nrf2 or Cul3. Keap1 has been shown to be ubiquitinated at Lys298, but it is unknown whether the ubiquitination of Keap1 observed in the assay occurs at that position.

There are 7 lysine residues on Nrf2 that are potential sites for ubiquitination. They all appear to be the targets of polyubiquitination (59, 61). Now that it is known that Keap1 and Cul3 are also modified in the reaction that catalyzes the ubiquitination of their substrate, Nrf2, more information is needed to determine if these events play a role in the signaling mechanism through this important, cancer-related system.

CHAPTER 3: MODELING OF THE INDIVIDUAL PROTEINS AND THEIR COMPLEX

3 MODELING OF THE INDIVIDUAL PROTEINS AND THEIR COMPLEX

3.1 Introduction

Molecular modeling, based on homologous sequences and structures, was performed to better understand the structure and interactions of Cul3/Rbx1 and Keap1. This technique creates a three-dimensional structure of the protein of interest using a high-quality template structure that shares some sequence similarities. The most critical step in the creation of a homology model is choosing a suitable template structure. This is accomplished using the program BLAST, which searches the database for proteins that share identical or homologous stretches of amino acids (62). Then, the modeling program SWISS-MODEL can be used to create a modeled structure of the proteins of interest based on the sequence alignment of the target and template sequences and the PDB file of the template's X-ray crystal structure (62-65). The resulting output is a PDB file of the three-dimensional modeled protein. This file can be further refined using energy minimization and can be visualized or manipulated in PyMOL (66). Structural alignment, a technique that globally aligns backbone residues, can be used within PyMOL to further manipulate proteins or domains relative to one another spatially. A large amount of information can be learned from these types of models. However, it must be understood that the model quality is highly dependent on the suitability of the template chosen, including % homology, % identity, resolution, and functional similarity.

The reason for creating these models was to guide experimentation and analysis of structural studies. For example, model parameters such as size and shape were used to define ranges for variables in the analysis of small-angle X-ray scattering data. The Keap1 homology model of the BTB domain was used by a collaborator to guide site-directed mutational studies, by allowing the visualization of residues spatially surrounding important cysteines as potential targets for mutagenesis. Homology models are routinely compared to SAXS-derived ab initio

simulated annealing structures (67). The results of scattering and ultracentrifugation experiments were then used to further refine the models.

3.2 Materials and Methods

3.2.1 Cullin3 Homology Model Creation

The human Cul3 amino acid sequence was retrieved from PUBMED (NP_003581). A BLAST search was performed on the Cul3 sequence that compared it to all known protein sequences in PUBMED and the most homologous protein, Cullin1, was chosen for modeling with SWISS-MODEL. The Cullin1 X-ray crystal structure (PDB: 1LDJ) was used as a template for Cullin3. A sequence alignment, produced using ClustalW in Biology Workbench, revealed the two proteins were 52% homologous and 30% identical (Figure 18). A three-dimensional homology model of Cul3 was produced using SWISS-MODEL workspace web server and visualized using PyMOL. Structurally aligning the Cul3 homology model with the crystal structure of Cul1 and Rbx1 from PDB 1LDJ, then deleting just the atoms pertaining to Cul1, reveals the Cul3/Rbx1 homology model with Rbx1 positioned within the C-terminal domain just as it was in the Cul1 structure (used in Figure 24 B, C, D).

```

Cul1 MSSTRSQNP HGLKQIGLDQIWDDL RAGIQQVYTRQSMASRYMELYTHVYNYCTS VHQSN
Cul3 -MSNLSKGTGSRKDTKMRIRAFPMTMDEKIVNSIWDLLKN-----AIQEIQ
cons m-S--S-----K--l-----l-----V-t---m-K-rymelythvynyct-v---n

QARGAGVPPSSKSKKGQTPGGAQFVGLLEYKRLKEFLKNYLTNLLKDGED-LMDESVLKIFY
RKNNSGLSFEELYRNAYTMVLKHKGEKLYTGLREVVTHELINKVREDVLSLNNNFLTQL
-----Gv-----k-----G--LY--LkE-l---L-N-lkd---n-m---L---

TQQWEDYRFSSKVLNGICAYLNRHWVRRECDEGRKGIYEIYSLALVTWRDCLFRP--LNK
NQAWNDHQ TAMVMIRDILMYMDRVYVQ-----QNNVENVYNLGLIIFRDQVVRYGCI RD
-Q-W-D-----vl--I--Yl-R-wV-recdeg---i--iY-LaLv-WRD-l-R-gcl--

QVTNAVLKLIKERNGETINTRLISGVVQSYVELGLNEDDAFAKGPPTLTVIKESFESQFL
HLRQTLTLDMIARERKGEVVD RGAIRNACQMLMILGLEGR-----SVYEEDFEAPFL
-v-n-vL-lI-kER-GE-i----I---Q--v-LGL---dafakgptltVI-E-FE--FL

ADTERFYTRESTEFLQQNPVTEYMKKAEARLLEEQRVQVYLHESTQDELARKCEQVLI E
EMSAEFFQMESQKFLAENSASVYIKKVEARINEEIERVMHCLDKSTEEP IVKVVERELIS
--t--Fy--ES--FL--N--t-YmKK-EARl-EE--RV---L--ST-d-l-r--E--LI-

KHLEIFHTEFQN---LLDADKNEDLGRMYNLVSRIQDGLGELKLLLETHIHNQGLAAIE
KHKMTIVEMENSGLVHMLKNGKTEDLGC MYKLF SRVPNGLKTMCECMSSYLREQ GKALVS
KHl-----q-glvhlL---K-EDLG-MY-L-SRI--GL--l---l-t-i--QG-A-i-

KCGEAA LNDPKMYVQTVLDVHKKYNALVMSAFNNDAGFVAALDKACGRFINNNAVTKMAQ
EEGEG--KNPVDYIQGLLDLKS RFRDRFLLESFNNDRLFQKTIAGDFEYFLN-----
--GEaal--P--YvQ-vLDv--ky---vm--FNND--F---l-----FiNnnavtkmaq

SSSKSPEL LARYCDSLKKSSKNPEEALEDTLNQVMVVF KYIEDKDVFKQFYAKMLAKR
LNSRSPEYLSLFI DDKLLKKGVKGLTEQEVETILDKAMVLF RFMQEKDVFERIYKQHLARR
--SkSPE-L--y-D--LKK--K---E-EI E--L---MVvFkyi-dKDVf-kfY---LakR

LVHQNSASDDAEAS MISKLLKQACGF EYTSKLRMFQDIGVSKDLNEQFKKHLTNS--EPL
LLTNKSVSDDSEKNMISKLLKTECGCQFTSKLEGMFRDMSISNTTMDEF RQHLQATGVSLG
Lv-q-S-SDD-E--MISKLL--CG--yTSKL--MF-Di-vS-----e-Fk-HL--sgv---

DLDFS IQVLSSGSWPFQQS-CTFALPSELERSYQRF TAFYASRHSGRKLTWLYQLS----
GVDLTVRVLTTGYWPTQSA TPKCNI PPAPRHA FEIFRRFYLAKHSGRQLTLQHMG SADL
-lD-si-VLssG-WP-Q--t-----lP-----y--F--FY--rHSGR-LT-----l-sadl

-----KGELVTNCFKNRYTLQASTFQMAILLQYNTEDAYTVQQLTDS
NATFYGPVKKEDGSEVGVGGAQVTGSNTRKHILOVSTFQMTILMLFNNREK YTFEEIQQE
natfygvpkkedgsevgv-G--VT-----r--LQ-STFQM-ILl-yN--d-YT-----l----

TQIKMDI LAQVLQI LLKSK-LLVLEDENANVDEVELKPD TLIKLYLGYKNKKLRVNINVP
TDIPERELVRALQSLACGKPTQRVLTKEPKSKEIENGHIFTVNDQFTSKLHRVKIQTVA A
T-I----L---LQ-L---Kp---l-----EvE-----i-----K--kIrvn----

MKTEQKQEQETHKNIEEDRKL LIQAAIVRIMKMRKV LKHQQLLGEVLTQLSSRFKPRVP
KQGESDPERKETRQKVDDDRKHEIEAAIVRIMKSRKKMQHNVLVAEVTQQLKARFLPSPV
---E---E---T---ieeDRK--I-AAIVRIMK-RK-l-Hq-LlgEV--QL--RF-P---

VIKKCIDILIEKEYLERVDGEKDTYSYLA
VIKKRIEGLIEREYLARTPEDRKVITYVA
VIKK-Id-LIEKEYL-R---ek--YsYlA

```

Figure 18. Sequence Alignment of Cul3 and Cul1

A sequence alignment of Cul3 and Cul1 as a template is shown here. The program ClustalW was used on SDSC Biology Workbench for the alignment. The alignment tool, BOXSHADE, was used to highlight identical residues (green), similar residues (blue), and extra loops not found in the other polypeptide (yellow).

3.2.2 Keap1 Modeling

In contrast to Cul3, Keap1 was modeled via single domain segments, because of the multiple domains of Keap1 and the fact that no close homolog has had its structure resolved. The kelch domain of Keap1 has been crystallized and the structure determined to high-resolution; therefore the PDB structure of the Kelch domain was used in modeling the overall structures. As for Keap1's other important domains, IVR and BTB, the NMR structure of the homologous protein Kelch-and-BTB-containing Protein 4 (PDB: 2EQX) (68) was used to model the IVR domain. The BTB domain from the LRF/ZBTB7 transcriptional regulator shares 30% sequence identity with Keap1-BTB and was therefore chosen as the template sequence (40). An alignment of the two sequences was performed and a model was produced using the crystal structure of the BTB domain from the LRF/ZBTB7 (PDB code: 2NN2) (40). Once each domain had been modeled individually, the Cullin1-related substrate adaptor complex, Cdc4-Skp1, was used as a structural alignment template (PDB: 1NEX), to create a complete structural model of Keap1 (Figure 22) (69). The individual domains were aligned in PyMol, which attempts to minimize the RMSD between sequence-aligned residues. This model of Keap1 was monomeric however; Keap1 is dimeric based on previously published size exclusion results (30) and results from Chapters 4 and 5 as well as newly published cryo-EM results (70). The crystal structure of dimerized human LRF/ZBTB7 protein was used to create a dimeric Keap1 model by creating two duplicate copies of the Keap1 model and structurally aligning them with each LRF/ZBTB7 monomer.

After the publication of the Keap1 cryo-EM structure, our homology model of Keap1 was further refined through comparison. The two structures are very similar with one noted exception. In our original model, the long axis of the Keap1 BTB domain was oriented perpendicular to an imaginary line drawn from one kelch domain to the other. In the cryo-EM

cross-sectional images of Keap1, the long axis of the BTB domain is clearly observed to be parallel to this line.

3.2.3 Cul3/Rbx1:Keap1 Complex Modeling

Once homology models of the individual proteins were completed, a model of their macromolecular complex was created by structurally aligning Cul3 and Keap1 to Cul1 and Skp1 within the Cul1-Skp1 complex crystal structure (PDB: 1LDJ) (5). The resulting structural model of Cul3/Rbx1:Keap1 was used to guide structural characterization experiments and for comparisons to experimental models produced in Chapters 4 and 5.

3.3 Results and Discussion

3.3.1 Cullin3 Homology Model

A list of all models created and templates used can be found in Table III, page 44. When Cul3 was superimposed over the Cul1 crystal structure, the resulting RMSD was 0.7 Å across 4,034 backbone atoms. Visualization of the Cul3 model in PyMOL revealed a structure sharing many similarities to Cul1's structure, with minor exceptions (Figure 21).

Two distinct loop regions (residues 41-66 and 555-575), not present in the Cul1 structure, are found at each end of the Cul3 homology model. The model also reveals the diametric nature of the cullin molecule, with the globular, Rbx1-binding "head" region on one end and the rod-like Keap1-binding "tail" region on the other end.

Several families of proteins contain BTB and BTB-like domains. They form dimer, tetramers, and higher-order oligomers, such as the BTB fiber and models were created to represent these different oligomeric states (Figure 19). Keap1-BTB and Skp1 contain similar folds, and a superimposition of the two structures aligned 5 of the 6 α -helices, and all three β -

strands of Keap1-BTB, with the corresponding α -helices and β -strands of the BTB-fold within Skp1 (Figure 20). The RMSD of the superposition was 6.874 Å across 296 backbone atoms. The overlay of major helices and low RMSD indicate that if Keap1's BTB domain is used to bind Cul3 in the same way Skp1 binds to Cul1, then the Keap1 BTB domain likely occupies a similar binding site on Cul3.

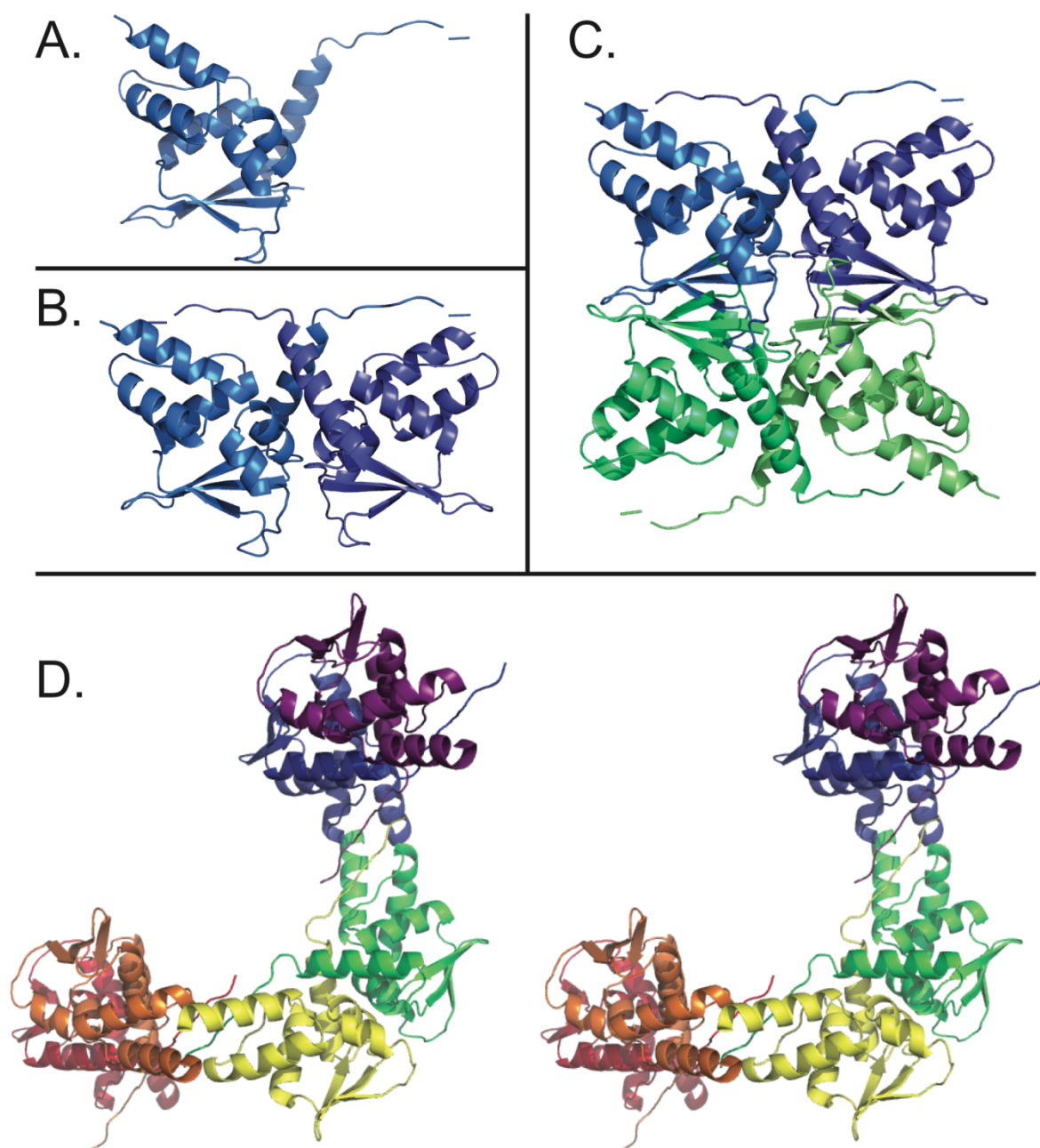


Figure 19. BTB Oligomer Models

The domain from Keap1 was modeled from a number of these examples to create the Keap1-BTB monomer (A), dimer (B), tetramer (C), and a stereo view of the Keap1-BTB fiber model.

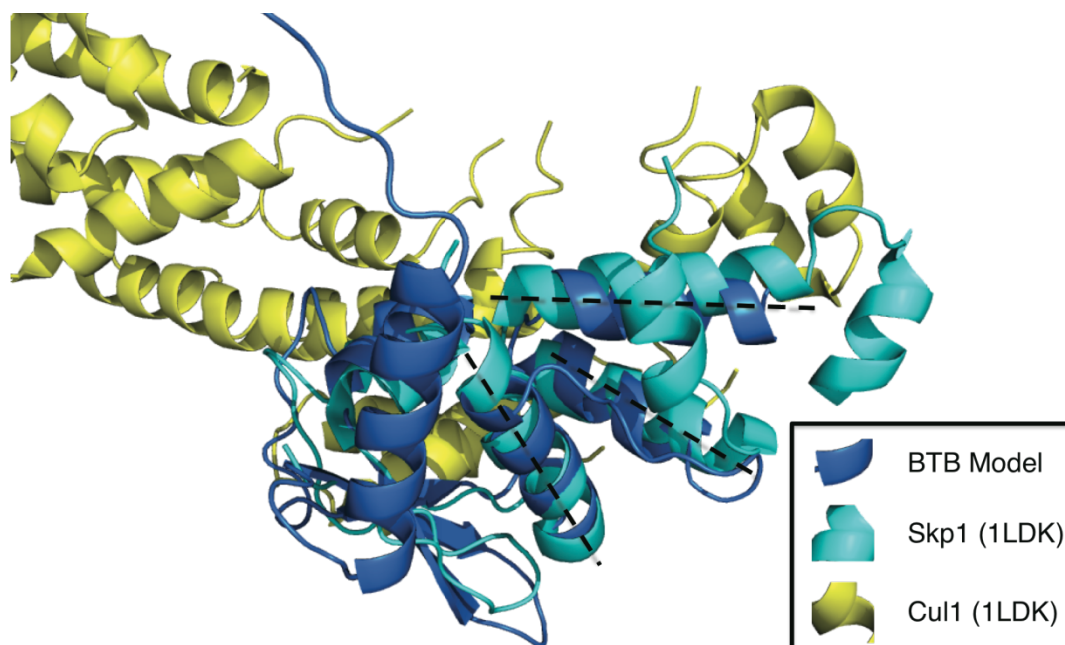


Figure 20. BTB and Skp1 Superposition

The BTB homology model was superimposed on the Skp1 protein from the SCF complex (RMSD = 6.874 for 439 Atoms). Three main helices overlay and are indicated by the dashed lines. Two additional overlaying helices can be observed to the left of the main helices.

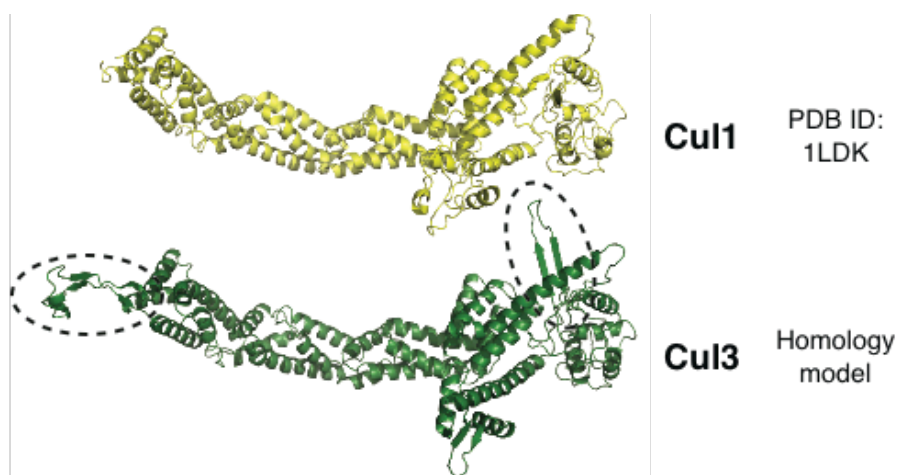


Figure 21. Cul1/Cul3 Crystal Structure/Homology Model Comparison

The crystal structure of Cul1 can be seen in yellow. The homology model of Cul3, which was produced by SWISS-MODEL, is green. Two additional loops are present within the Cul3 model. One of the loops, located near the postulated Keap1-binding region, may play a role in the unique stoichiometry of this complex.

The monomeric Keap1 model (Figure 22) shows the Kelch domain near one end and the BTB domain at the other, with the IVR domain in between them. Many of Keap1's cysteine residues are found decorating the surface in this model, with several of them being found on surfaces that have been hypothesized as binding to either Cul3 or Nrf2 (See Appendix B). The dimeric model of Keap1 displays P2 symmetry around the BTB dimer (Figure 23). The BTB dimer is composed of two small, globular BTB domains, each contributing a beta-strand to the other counterpart. The overall model has a V-shaped appearance with the Kelch domains oriented in the same direction, most likely for binding of the substrate, Nrf2.

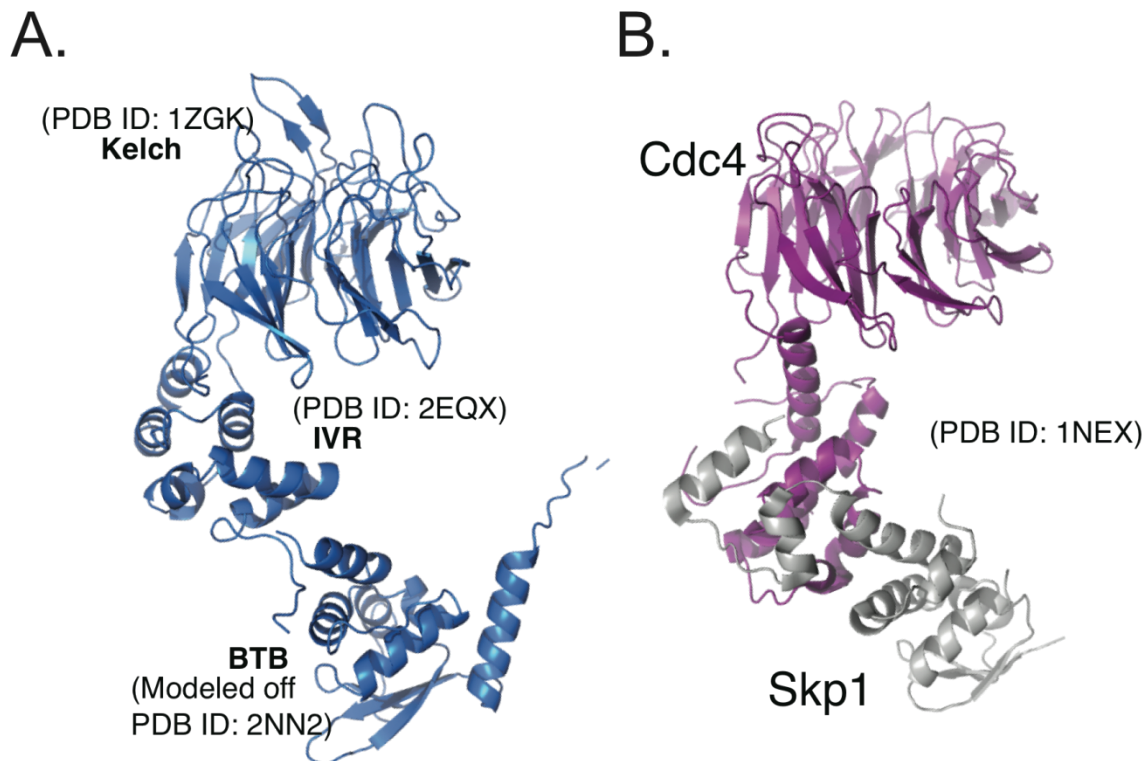


Figure 22. Keap1 Monomer Homology Model

The Keap1 monomer homology model (A) is composed of three pieces: BTB domain, IVR, and Kelch domain. The pieces were structurally aligned in space using the bimolecular complex of Skp1 and Cdc4 (B) as a three-dimensional template.

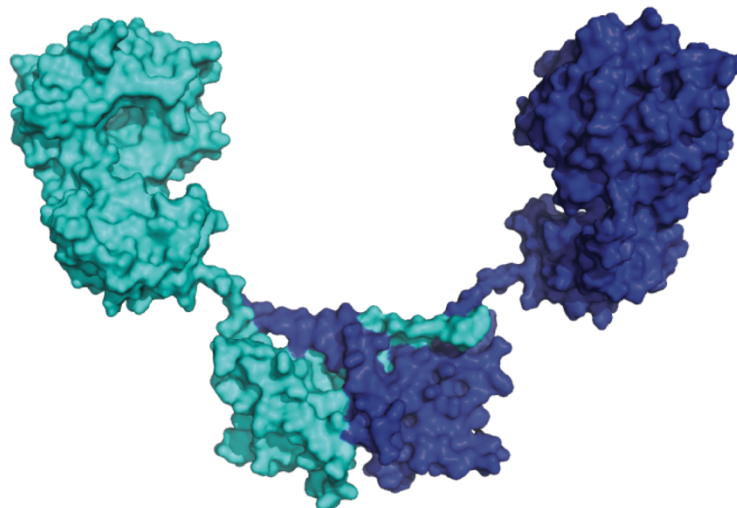


Figure 23. Keap1 Dimer Homology Model

The Keap1 monomer homology model was used to create the dimeric model shown here. Two copies of the monomer model were structurally aligned to the LRF/ZBTB7 dimer. The model was then further refined with proper BTB alignment upon publication of the Keap1 cryo-EM structure by Yamamoto (70).

The complex model has a unique shape (Figure 24 C, page 45). It is reminiscent of a scorpion with Keap1's kelch domains forming the scorpion's claws and the long, curved Cul3 molecule forming the scorpion's tail. It is believed that the complex has this unique structure so that the E2-charged tail of the scorpion can be in close proximity to the substrate-bound claws of the scorpion so that proper transfer of the ubiquitin molecule from the E2 to the Nrf2 lysines can take place. The complex model has a maximal linear dimension of 225 angstroms and a proposed molecular weight of 240 kilo-Daltons, with Cul3 contributing 88 kDa, Rbx1, 12 kDa, and the Keap1 dimer, 140 kDa. This model resembles other cullin-based E3 ligase structures generated for Cull1 complexes, which are shown in 1.1, in terms of the orientation of substrate adaptor relative to the cullin protein, however, the stoichiometry is different. Dimeric substrate adaptors bind two cullin proteins and monomeric substrate adaptors bind one (13, 19). As mentioned

previously, this modeling may have many inherent flaws and should not be used as a substitute for X-ray crystal structures. The modeling does however give us molecular details, such as size and shape of predicted complex, which can be used to guide further experiments.

Table III. Summary of Molecular Homology and Structural Models

Homology Model	Figure	PDB Template(s) Used
Cul3/Rbx1	22	1LDJ
Keap1 substructures		
BTB Domain	21, 23	2NN2
IVR Domain	23	2EQX
Kelch Domain	23	1ZGK
Keap1 Monomer	23	2OVP, 1NEX
Keap1 Dimer	24	2OVP, 2NN2
Cul3/Rbx1:Keap1 Complex	25	1LDK, 2OVP, 2NN2

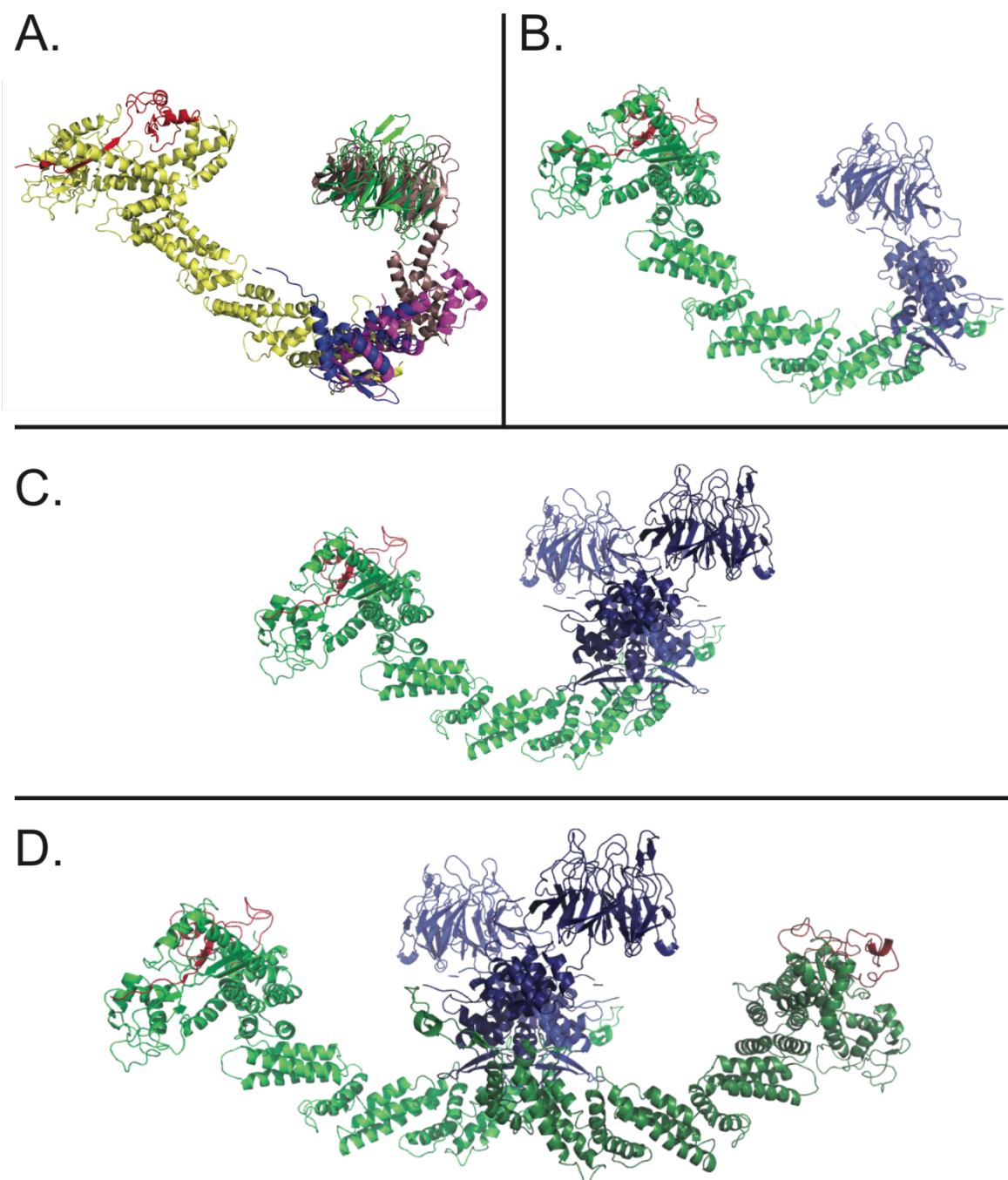


Figure 24. Complex Models

The BTB and Kelch domains from the Keap1 model were structurally aligned with INEX (A). Keap1 monomer model was used to create the monomer-monomer model (B). Keap1 dimer model was used to create the monomer-dimer model (C) and an additional CuI3 was added on to create the dimer-dimer model (D). These models' attributes were used in the other techniques to guide experimentation and analysis.

CHAPTER 4: STRUCTURAL CHARACTERIZATION OF THE WILD TYPE COMPLEX

4 STRUCTURAL CHARACTERIZATION OF WILD TYPE COMPLEX

Portions of the data and text in this chapter have been published in the journal article titled "Development of an efficient E. coli expression and purification system for a catalytically active, human Cullin3-RINGBox1 protein complex and elucidation of its quaternary structure with Keap1." (57)

4.1 Introduction

Structural characterization of Cul3/Rbx1 and Keap1 is required for a better understanding of the function and regulation of the ubiquitin E3 ligase complex that they form. Currently, even the most fundamental structural properties are unknown, including the stoichiometry of the components within the complex. Cullin complexes have been found to contain either one or two cullin proteins depending on the oligomeric nature of the substrate adaptor. The Cul1-containing ligase complex that is responsible for the ubiquitination of Cdc4 contains a dimerized substrate adaptor bound to two Cul1 molecules (13). This dimeric complex containing Cul1 and Cdc4 is partially regulated through a change in oligomerization, as the substrate is unable to bind to a Cul1-substrate adaptor monomer complex. The substrate readily binds to the dimeric complex and is ubiquitinated (13). When the substrate adaptor dimerization in the D domain of Cdc4 is disrupted, the substrate can only bind to the substrate adaptor with the subsequent concerted effort of a phosphorylation event on the substrate. Only upon phosphorylation can the substrate bind and be ubiquitinated by the monomeric complex (13).

Other cullin-containing complexes are not regulated through oligomerization and have only monomeric substrate adaptors and hence only one cullin per complex (55). It is not fully understood what effect more than one cullin has on an E3 ligase complex, but we hypothesize that an additional cullin protein in the complex potentially doubles the catalytic power of the complex, as each cullin binds ubiquitin-charged E2 molecules through its C-terminally bound Rbx1 subunit. One of the main goals of this project was to determine how many Cul3 molecules

are found within the complex containing dimeric Keap1. Therefore, structural characterization techniques, such as analytical size exclusion chromatography (SEC) and sedimentation velocity ultracentrifugation (AUC), were performed on recombinant Cul3/Rbx1 and Keap1 to elucidate the Cul3/Rbx1:Keap1 molar ratio within the complex as well as the size of the complex in kilodaltons. More refined structural information on the complex was sought through studies focusing on protein X-ray crystallography and small-angle X-ray scattering (SAXS).

4.1.1 Analytical Ultracentrifugation

Analytical ultracentrifugation (AUC) is a powerful tool in the solution phase characterization of proteins and protein complexes (71). Invented over 75 years ago, the use of this type of instrumentation experienced a lengthy hiatus during which AUC was rarely performed, until a modern version of the analytical ultracentrifuge became available to research communities in the later part of the 20th century (71). This technique is capable of measuring the dynamics of protein complex assembly by exposing samples to a large centrifugal force field and observing the macromolecular sedimentation and diffusion over time (72). AUC can provide details about dynamic interactions, solution conformation, oligomerization properties, and binding stoichiometry and can be used to study mixtures of molecules covering a wide range of molecular weight ($10^2 - 10^8$ Da) (72).

The sedimentation can be measured with absorbance, interference, fluorescence, and multi-wavelength detectors. Absorbance detectors, the most widely used optical system, measure the intensity of the transmitted light at 280 nm (73). This type of optical system allows for the detection of DNA and protein samples at dilute concentrations, where their sedimentation is unaffected by concentration-dependent nonideality effects (72). Interference optical systems measure the difference in refractive index between a sample and a reference cell. The pattern of

shifted fringes generated by the refractive index differences are converted by a fast Fourier transform into concentration profile, which can then be evaluated by standard methods (72). The interference optical system can be used when the absorption of buffer components masks the sample, resulting in absorbance optical data misrepresenting the actual sedimentation of the sample (73).

Fluorescence optics have a high degree of sensitivity and selectivity and can be used to measure picomolar concentrations of proteins (74). All molecules must be labeled with fluorescent probes whose wavelength coincides with the excitation laser's wavelength (488 nm). Proteins expressed with intrinsically located fluorescent protein tags, at either end of their amino acid sequences, can be used to study complex assembly dynamics or the hydrodynamic properties of proteins without purification in whole cell extract suspensions or in blood serum (75, 76). Multi-wavelength detectors, just now becoming available, allow for additional detection using wavelengths other than 280 nm. Multiple wavelengths can be simultaneously detected, which reduces the number of experimental runs when measuring several different areas of the UV/vis spectrum (77).

Data are collected in sequential time scans and analyzed by observing the change in concentration over time as a function of the radial position. The program Ultrascan is used in the analysis of AUC data and is an integrated editing and analysis environment. Several analysis programs are utilized within Ultrascan, such as van Holde-Weischet (vHW) data analysis or 2-dimensional spectrum analysis (2DSA). Van Holde-Weischet data analysis is a model independent method of analyzing sedimentation velocity experimental data. This type of analysis provides S-value distributions that are corrected for diffusion effects. 2DSA is a composition

analysis used in sedimentation velocity studies. It generates sedimentation coefficient, diffusion coefficient, frictional coefficient, and molecular weight distributions.

In the AUC experiments performed as part of this dissertation, intensity data were collected using absorbance optics at 280 nm. Buffer components with minimal absorbance at 280 nm were chosen for experimentation, and collected data results were analyzed using the Ultrascan program (72).

4.1.2 Small-Angle X-ray Scattering

Small-angle X-ray scattering (SAXS) has recently become a fundamental tool in studies of the solution structure of biological macromolecules and can be applied to a broad range of conditions and particle sizes, which can range from a few kDa to several MDa (78). SAXS samples do not require special preparation (78). In a SAXS experiment, a solution of proteins or DNA is exposed to X-rays and the scattered intensity $I(s)$ is recorded as a function of the momentum transfer s ($s = 4\pi\sin\theta/\lambda$, where 2θ is the angle between the incident and scattered radiation), and the solvent scattering is subtracted (78). The resulting SAXS profile contains information about the gross structural features – shape and quaternary and tertiary structure. The one-dimensional SAXS profile is not suitable for the analysis of atomic structure, however, because although SAXS profiles are unique at low scattering angles (2-3 nm resolution) for different proteins, the differences are much less pronounced at higher scattering angles (smaller than 2 nm resolution) (78).

The GNOM program is an indirect transform program for SAXS data processing and analysis. One-dimensional SAXS profiles are used to evaluate a distance or pair distribution function ($p(r)$ or PDF). The idea of the indirect transform method was first proposed by Glatter (79) and also implemented in other packages (80, 81). The algorithms used in GNOM (82-85)

are based on Tikhonov's regularization technique (86). The resulting output data generated by GNOM have characteristic shapes when viewed as a plot of the distribution of interatomic distances contained within the experimental sample's measured scattering particle. A perfectly spherical particle would be observed through GNOM analysis as a Gaussian distribution, where the function approaches the x-axis at two locations, $x = 0$ and $x = D_{\max}$, where x is in angstroms and D_{\max} is the maximal linear dimension within the particle. The distribution pattern for a rod-shaped particle would have a skew to the left, with a greater number of lower angstrom distances (representing the width of the rod) and a lesser number of medium and higher angstrom distances (representing the length of rod). The $p(r)$ curve output file obtained from the GNOM program, along with the SAXS scattering profile, can be used in further analytical steps to create structural models.

Ab initio simulated annealing structure prediction aims to create three-dimensional structural models from one-dimensional SAXS profile patterns. The DAMMIN program uses a genetic algorithm and the previously described GNOM output file to produce models described by densely packed beads (87). This program creates low-resolution structural models of chaotically oriented particles (e.g., biological macromolecules) from isotropic scattering profiles. Multiple *ab initio* runs are often performed and analyzed to reveal the most persistent features of the model using the DAMAVER program suite (88, 89). This SAXS data analysis procedure has been performed and validated using proteins with known X-ray crystal structures (87).

If good quality homology models of SAXS samples exist, they can be used to refine the SAXS models *a priori*. Occasionally, *ab initio* simulated annealing creates a model that fits the experimental data but does not represent the actual structure of the complex. This is because the DAMMIN program begins at a random configuration and uses a simulated annealing algorithm

to explore the landscape of acceptable low-resolution structures. It is possible for the algorithm to get stuck in local minima within this landscape, resulting in a less accurate depiction of the complex. By comparing these DAMMIN models to the homology model, aberrant DAMMIN replicates, which may potentially inaccurately depict the complex, may be discontinued from the analysis, resulting in a more refined model of the data. Conversely, SAXS-derived *ab initio* models can be used to refine homology models, because of the shape and structure information they contain.

4.2 Materials and Methods

4.2.1 Protein Crystallization of Cul3/Rbx1

Crystallization trials consisted of large-scale, coarse screening using the sitting-drop method by a Tecan liquid handling robot. The sitting-drop method of crystallization was used for the robot screens with 1 μ L of protein mixed with 1 μ L of well solution. Crystallization screening trays were stored at 25 °C. Finer hand screening using the hanging-drop method was performed to recreate published crystallization conditions for Cullin1 (5). This included using 2 μ L protein drops mixed with 2 μ L of well solution and storing crystal trays at 4 °C. A list of crystal screens used and protein concentrations tested can be found in Table IV.

Table IV. Protein concentrations used in various crystallography screens

Screen Name	Cul3/Rbx1 (mg/mL)	Keap1 (mg/mL)	Cul3/Rbx1:Keap1 (mg/mL)
Classics I *	5, 12.5, 22	15	11.3
Classics II*	5, 12.5, 22	15	11.3
PEG I*	5, 12.5, 22		
PEG II*	12.5		
JCSG+*		15	11.3
EG*	22, 44		
Published [†]	5, 15, 30		

*Produced by Qiagen

[†]100 mM Tris HCl, 0.2-0.5 M NaCl, 12-18% EtOH, 5 mM DTT, pH 8.0

4.2.2 Analytical Size-Exclusion Chromatography and Binding of Cul3/Rbx1 to Keap1

Purified Cul3-Rbx1 was subjected to analytical size-exclusion chromatography (SEC) in the absence and presence of Keap1 to assess its ability to form a stable complex and to determine the stoichiometry of the components of the Cul3/Rbx1:Keap1 complex. The experiment was performed at 4°C, using a 300 x 7.8 mm Bio-Silect® SEC 250-5 column (Bio-Rad), equilibrated with 50 mM Tris, pH 8.0, 250 mM NaCl, and 2 mM DTT. Several molecular weight standards were used for calibration, including ovalbumin, conalbumin, aldolase, catalase, ferritin, thyroglobulin, and blue dextran (GE Healthcare). Cul3/Rbx1 and Keap1 were first run individually (50 µL of 8 µM Cul3/Rbx1 and 50 µL of 16 µM Keap1). The proteins were then mixed and incubated on ice for 30 minutes prior to injecting 50 µL of 8 µM complex (consisting of 8 µM Cul3/Rbx1 and 16 µM Keap1) on the column. The resulting fractions (500 µL volumes) were visualized by SDS-PAGE. The retention volumes for each of the standards and samples were measured and used to calculate the partition coefficients, K_{av} :

$$K_{av} = (V_r - V_o) / (V_c - V_o) \quad (\text{Equation 1})$$

where V_r is the retention volume, V_o is the void volume (calculated based on the retention time of the blue dextran standard), and V_c is the geometric bead volume for the column. The K_{av} for each standard was plotted against the log of the molecular weight in order to generate a standard curve, which was then used to calculate the approximate molecular weight for each experimental sample.

4.2.3 Analytical Ultracentrifugation

4.2.3.1 Individual Proteins

Purified Cul3/Rbx1 and Keap1 were assessed by analytical ultracentrifugation. The samples were then subjected to sedimentation velocity experiments performed at a temperature of 25 °C and a rotor speed of 60,000 rpm using a Beckman Optima XL-I analytical ultracentrifuge equipped with 1.2 cm boundary-forming epon centerpieces in an An60TI rotor (Figure 25). After temperature and pressure reached the set points, loaded samples were allowed to reach thermal equilibrium before data collection began. Measurements of the intensity of transmitted light were collected at 280 nm as a function of radial position. Each centrifuge cell was scanned sequentially with 3-minute delay between scans until no further sedimentation was observed. An additional experiment assessing the effect of DMSO on Keap1 used three samples of Keap1 with 0, 7.5, and 15% (v/v) DMSO. The same collection method as above was used for the DMSO samples.

4.2.3.2 Stoichiometry Determination of the Cul3/Rbx1:Keap1 Complex

The stoichiometry of binding of Cul3/Rbx1 to Keap1 was assessed by analytical ultracentrifugation. Purified Cul3/Rbx1 and Keap1 were first incubated on ice at three different molar ratios (2:1, 1:1, and 1:2) ([Cul3/Rbx1]:[Keap1 monomer]) for 30 minutes. The samples (Table V) were then subjected to sedimentation velocity experiments performed at a temperature of 25 °C and a rotor speed of 60,000 rpm using a Beckman Optima XL-I analytical ultracentrifuge equipped with 1.2 cm boundary-forming epon centerpieces in an An60TI rotor (Beckman). After temperature and pressure reached the set points, loaded samples were allowed to reach thermal equilibrium before data collection began. Intensity data were collected at 280

nm as a function of radial position. Each centrifuge cell was scanned sequentially with 3-minute delay between scans until no further sedimentation was observed.

Table V. Sedimentation Velocity Ultracentrifugation Samples for Stoichiometry Determination

AUC Sample	Cul3 (μM)	Keap1 (μM)	Cul3/Rbx1:Keap1 Molar Ratio
1	0.25	2	1 to 8
2	0.5	2	1 to 4
3	1	2	1 to 2
4	2	4	1 to 2
5	4	4	1 to 1
6	8	4	2 to 1

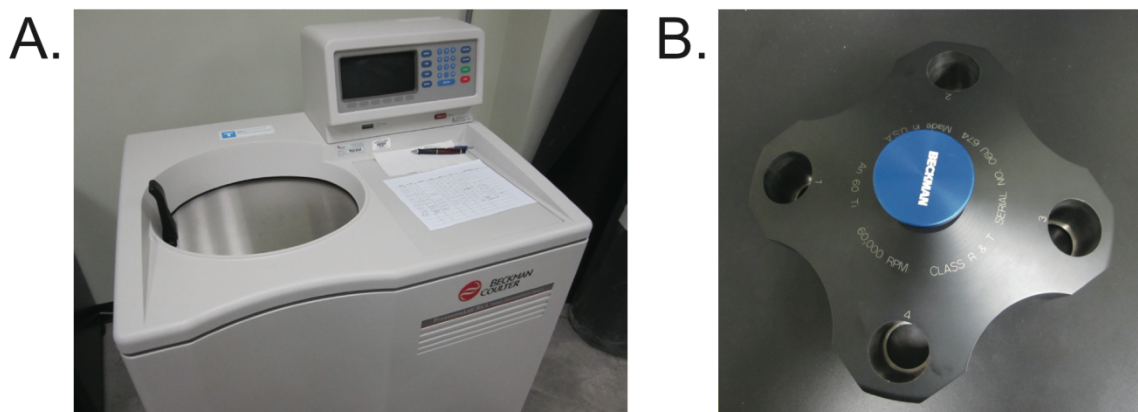


Figure 25. Analytical Ultracentrifugation Equipment

The Beckman Coulter XL-I Analytical Ultracentrifuge (A) is a modified preparatory centrifuge with the optics equipment retrofitted within the vacuum chamber. The An60i rotor is equipped with 3 rotor cells and a counterbalance (B).

4.2.3.3 Data Analysis

The program Ultrascan 2.0 used for analysis of the primary data as described by Demeler (72). Solution density and viscosity were calculated from buffer composition as 1.00994 g/mL

and 1.0363 cP. A value of 0.732442 mL/g was assumed for the partial specific volume. Intensity data were converted to pseudo-absorbance, which was used in a two-dimensional spectrum analysis (2DSA). The 2DSA was performed with S-value limits of 1 and 15 (resolution: 10), f/f_0 limits of 1 and 4 (resolution: 10), 6 uniform grid repetitions, and no Monte Carlo iterations at that time. Time invariant noise and meniscus (range: 0.03 cm) was also fit using the iterative ($n=3$) method. Radially invariant noise was fit in the subsequent 2DSA, as it should not be done at the same time as time invariant noise fitting (72, 90). The model with the lowest RMSD for each cell was chosen, and its corresponding noise file was used for subtraction. For complex (interacting) samples with more than one protein, further 2DSA analysis with 50 Monte Carlo iterations was performed until no additional decrease in RMSD was noted.

For those samples containing only one individual protein, a different approach was taken and additional fitting was performed using parsimonious regularization by genetic algorithm with 50 Monte Carlo iterations until no further decrease in RMSD was observed. Enhanced van Holde-Weischet analysis was also performed on noise-subtracted data to determine sedimentation coefficients and distribution within each sample. Sedimentation coefficients plotted against the relative frequency distributions were exported to Excel (Microsoft) for graphing.

4.2.4 Small-Angle X-ray Scattering

4.2.4.1 Individual Protein Samples

Individual protein samples for SAXS (Table VI) were prepared in a buffer containing 50 mM HEPES, pH = 8.0, 150 mM NaCl, 3% glycerol, and 2 mM Tris(2-carboxyethyl)phospine (TCEP) and 10 mM DTT. Immediately prior to injection into the flow cell, 1 mL samples were centrifuged at 15,000 rpm for 10 min and the top 200 μ L were carefully removed so as not to

collect any higher order aggregates found near the middle or bottom of the tube. SAXS data were collected at beamline 18-ID-D at the Advanced Photon Source on July 15, 2010. The instrument was configured with a sample-detector distance of 2.430 m with a range of 0.006-0.37 \AA^{-1} at an X-ray wavelength of 1.03 \AA . The flow cell was pre-equilibrated at 37 $^{\circ}\text{C}$. The small sample volume, the copper enclosure surrounding the sample area, and the length of tubing between the sample vial and the 1-mm ID quartz capillary ensured that the sample had reached experimental temperature by the time it was exposed to X-rays. Raw data collected from the MAR-CCD detector were reduced to I versus Q using the Bio-CAT Igor Pro macros.

Table VI. Individual protein samples used in SAXS experiments at Bio-CAT Beamline

SAXS Sample	Cul3 (μM)	Keap1 (μM)
1	2	-
2	4	-
3	6	-
4	-	4
5	-	8
6	-	12

4.2.4.2 *Complex Protein Samples*

Complex samples for SAXS (Table VII) were prepared in a buffer containing 50 mM Tris, pH = 8.0, 250 mM NaCl, and 2 mM Tris(2-carboxyethyl)phospine (TCEP). Immediately prior to injection into the flow cell, samples were filtered using 0.65 micron Ultrafree-MC spin filters (Millipore) and centrifuged at 15,000 rpm for 10 min. SAXS data were collected at beamline 12-ID-C at the Advanced Photon Source on March 10, 2009 (Figure 26). The instrument was configured with a sample-detector distance of 2.3 m with a range of 0.006-0.37

\AA^{-1} at an X-ray wavelength of 1.03 \AA . The sample flowed through a 1-mm ID quartz capillary maintained at 25 °C such that the protein was exposed to X-rays for less than 100 ms. Collected raw data were reduced to I versus Q using the BESSRC-Cat Igor Pro macros. Moore's autocorrelation analysis was performed using the low-Q portion range of the data where $R_g Q < 1$ and data were visualized by Kratky plot.

Table VII. Protein complex sample used in SAXS experiments

SAXS Sample	Sector and Beamline at APS	Cul3 (μM)	Keap1 (μM)
1	BESSRC-CAT Sector 12-ID-C	15	30

4.2.4.3 SAXS Data Analysis

The statistical plotting program, Igor Pro, and sector-specific Igor Macros (small programs written by beamline scientists) were used to reduce the raw SAXS data and subtract the background scattering from the sample data. The program GNOM was used to calculate the $p(r)$ pair-distance distribution function for both groups of reduced data by an indirect Fourier transform of the scattering data over the range 0.008-0.37 \AA^{-1} . The value of $p(r)$ was constrained to be 0 at $r=0$ but was unconstrained at the maximum distance (D_{max}). The shapes of the $p(r)$ curves were essentially independent of the value of D_{max} (350 \AA) used in the transformation in the range between 150 and 500 angstroms.

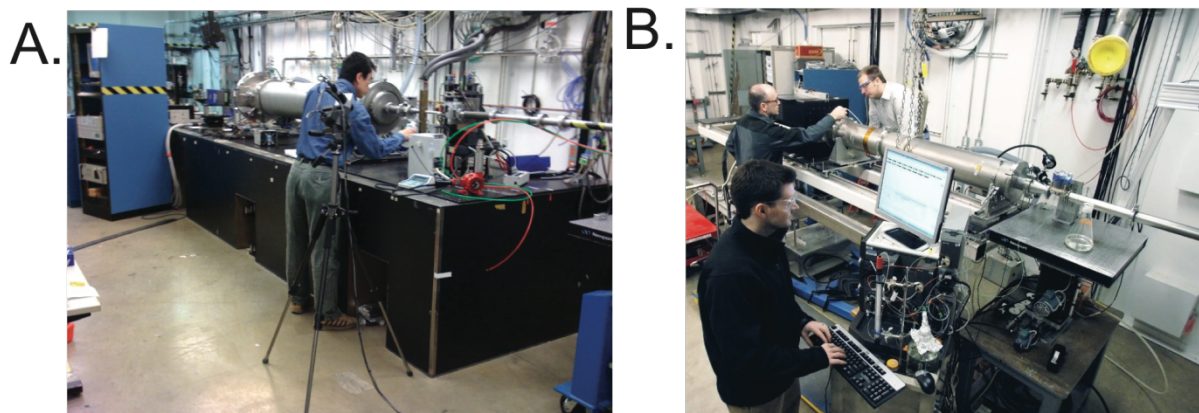


Figure 26. Beamline Photos from the Advanced Photon Source

A. Pictured here is the hutch of Bio-CAT's beamline 18-ID-D. It is very long to accommodate a variety of experimental conditions. Here, Liang Guo, PhD, a beamline scientist can be seen readying the instrumentation for beam transmission. The smaller and simpler hutch at BESSRC-CAT's 12-ID-C beamline is just large enough to fit all the necessary equipment and personnel. Beamline scientist Sönke Seifert, PhD is pictured discussing the detector with Andrew Mesecar, PhD in the background, while the author is pictured in the foreground.

The resulting output files from GNOM were loaded into the *ab initio* simulated annealing structure determination program DAMMIF (91). By default, p1 symmetry was used in all models, except in the case of Keap1, where additional models with p2 symmetry were also created. Using a set of personally created batch files (see Appendix I), twenty rounds of annealing were performed in series for each sample and then automatically averaged using the DAMAVER program suite, which superpositions the annealed structures and averages them. The resulting .pdb file of the averaged scattering envelope was visualized in PyMOL. A flowchart for the general analysis scheme is found in Figure 27.

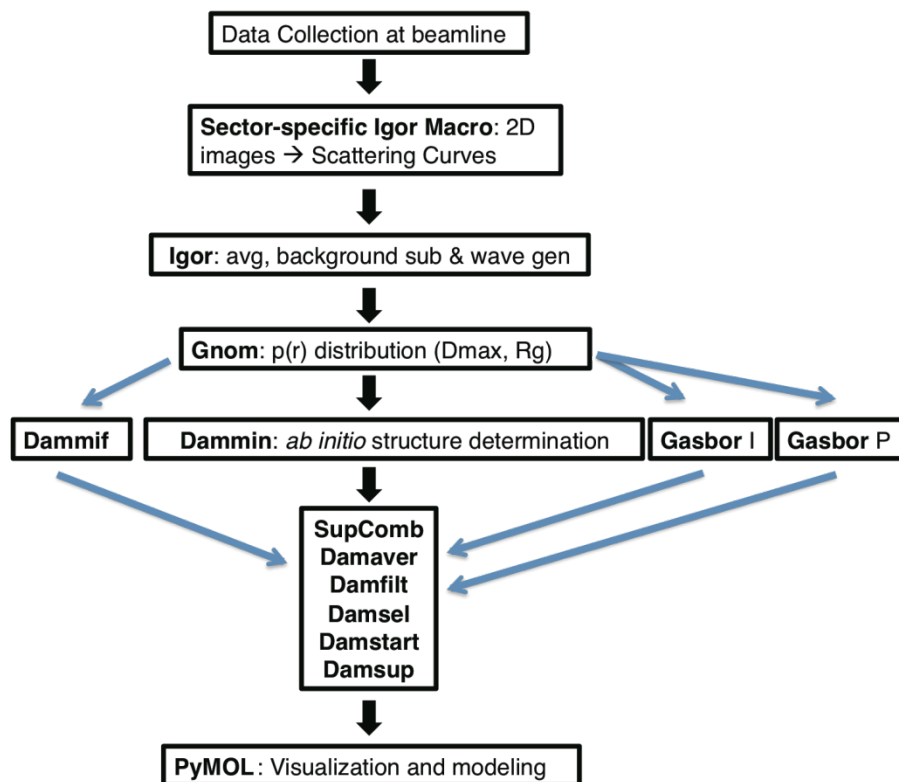


Figure 27. SAXS Data Analysis Workflow Diagram

Many different computer programs are used in the analysis of SAXS data. The overall process takes a 2D image of the scattering and turns it into a 1D scattering profile. $P(r)$ curves are generated from the 1D profiles and are used to create 3D *ab initio* simulated annealing density envelopes. The alternative routes are colored blue. Dammin, Dammif, Gasbor I, and Gasbor P are all simulated annealing programs.

4.3 Results

4.3.1 Protein Crystallization of Cul3/Rbx1

None of the crystallization conditions screened produced diffraction-quality crystals. The most promising condition, 100 mM Tris pH=8.0, 15 % ethanol, 500 mM NaCl, produced microcrystals that could not be reproduced. A list of all the crystal screens used in the trials can be found in Table IV. Crystallization trials were eventually abandoned in favor of SAXS experiments to help elucidate the shape of Cul3/Rbx1.

4.3.2 Size-Exclusion Chromatography

The quaternary structure of the Cul3/Rbx1 complex was determined via analytical size-exclusion chromatography. Based on the retention times of the Cul3/Rbx1 protein when compared to the protein standards, the experimentally derived molecular weight for Cul3/Rbx1 is approximately 111 kDa, which corresponds to a heterodimeric complex of the proteins at a 1:1 ratio (Figure 28). The molecular weight is slightly greater than the calculated molecular weight of 100 kDa, most likely due to the predicted rod-like shape of Cul3/Rbx1 as observed in the Cul-Rbx1 crystal structure (5). This experiment also shows the relatively tight interaction of Cul3 and Rbx1, as no free Cul3 or Rbx1 was detected.

The molecular weight of Keap1, which has recently been shown to be a homodimer via cryoelectron microscopy (92), was determined to be 198 kDa by analytical SEC (Figure 28). As observed for the Cul3/Rbx1 complex, the molecular weight of Keap1 is somewhat greater than the calculated molecular weight of 140 kDa. The cryo-EM structure of Keap1 indicates that Keap1 has an extended dimeric structure suggesting that the larger molecular weight derived from SEC is likely the result of a larger hydrodynamic radius and stokes radii due to non-spherical, molecular geometry (70).

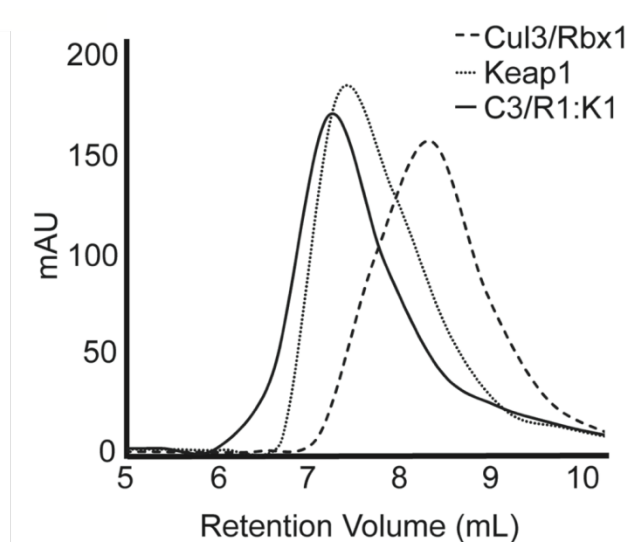


Figure 28. Analytical Size Exclusion Chromatogram

Cul3/Rbx1 and Keap1 were subjected to analytical size exclusion chromatography. The proteins were analyzed individually and in complex with one another. The resulting retention volumes, molecular weights, and K_{av} values are listed in Table VIII. A plot of the proteins of known molecular weight and the resulting standard curve can be found in Appendix C.

Table VIII. SEC Results – Comparison of Calculated vs. Estimated MW using K_{av}

Sample	Calculated MW (kDa)*	Estimated MW (kDa)**	K_{av}
Cul3/Rbx1	100	111	0.25
Keap1 (dimer)	140	198	0.18
Cul3/Rbx1:Keap1	240	280	0.13

*calculated from amino acid sequence

**estimated from SEC experiment using K_{av} and solving for MW in equation 1

Since the quaternary structure of the Cul3/Rbx1:Keap1 complex is also unknown, we determined the approximate molecular size of this complex by analytical SEC. When the Cul3/Rbx1:Keap1 complex was formed at 1:2 ratios ([Cul3/Rbx1]:[Keap1 monomer]), the complex eluted from the SEC column as a single species with no other peak observed in the chromatogram (Figure 28). Analysis of the retention time of this peak with protein standards

indicates the Cul3/Rbx1:Keap1 complex has an estimated molecular weight of 280 kDa, which corresponds to a calculated molecular weight of 240 kDa. These results suggest that Cul3/Rbx1:Keap1 is a heterotetrameric complex consisting of one molecule each of Cul3 and Rbx1 and two molecules, i.e. two monomers or one dimer, of Keap1 (Figure 29). From here on, this complex will be denoted as Cul3/Rbx1:Keap1.

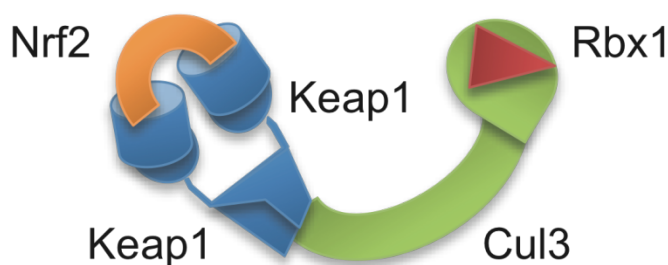


Figure 29. Complex Stoichiometry Diagram

A model cartoon representation of the stoichiometry of the Cul3/Rbx1:Keap1:Nrf2 complex. Two Keap1 proteins forming a dimer are bound to one Cullin3 molecule and one Nrf2 molecule, and Rbx1 is integrally located within the head of Cul3.

4.3.3 Analytical Ultracentrifugation

4.3.3.1 Sedimentation Velocity of Individual Proteins

Cul3/Rbx1 was subjected to a sedimentation velocity experiment to determine its stoichiometry. van Holde-Weischet analysis reveals the Cul3/Rbx1 sample to be a monodisperse population of sedimenting particles with a sedimentation coefficient of 4.9 S, which corresponds to a heterodimeric complex between Cul3 and Rbx1 with one molecule of each per particle. Because of the tight nature of the Cul3 and Rbx1 interaction and the very uniform sedimentation profile, Cul3/Rbx1, when denoted as such, will be referred to as a monomer despite actually being a heterodimer (Figure 30 A). This distinction was made to eliminate confusion when

discussing the Keap1 dimer. Keap1 was also sedimented during the same experiment and was also found to be a monodisperse population, although the sedimentation coefficient was found to be higher at 6.1 S (Figure 30 A)

The effect of DMSO on Keap1 was assessed by AUC. The rationale for this experiment is the frequent use of DMSO as a vehicle for dissolving chemopreventive compounds. In previous experiments as seen in Figure 49, found in Appendix D, the Keap1 peak on the AUC plot shifts in the presence of increasing concentrations of DMSO. The shape of the curve begins to narrow and the main peak shifts to the left on the x-axis resulting in a lower apparent S-value. DMSO does not appear to have any effect on Keap1 dimerization, suggesting the homodimer interaction is strong. If dimerization was affected by DMSO there would likely be the progressive formation of an additional peak at a lower S-value, instead of a single peak with a progressively shifting S-value.

4.3.3.2 Sedimentation Velocity of the Cul3/Rbx1:Keap1 Complex

Sedimentation velocity experiments were performed to confirm the binding stoichiometry observed in the analytical size exclusion experiments. This technique was chosen over the simpler electrophoretic mobility shift assay (EMSA), because the complex does not readily enter a native gel during electrophoresis. As shown from the data in Figure 30, a single peak of Cul3/Rbx1:Keap1 was observed at 8.74 S when Cul3/Rbx1 and Keap1 were mixed in a 1:2 ([Cul3]:[Keap1 monomer]) molar ratio. When additional equivalents of Cul3/Rbx1 are added in a 1:1 or a 2:1 ratio with Keap1, another peak at 4.98 S, representing excess, i.e. free, Cul3/Rbx1, is present. When excess Cul3/Rbx1 is present in the 1:1 and 2:1 ratio samples, the complex peak shifts to 9.28 S and 9.76 S, respectively.

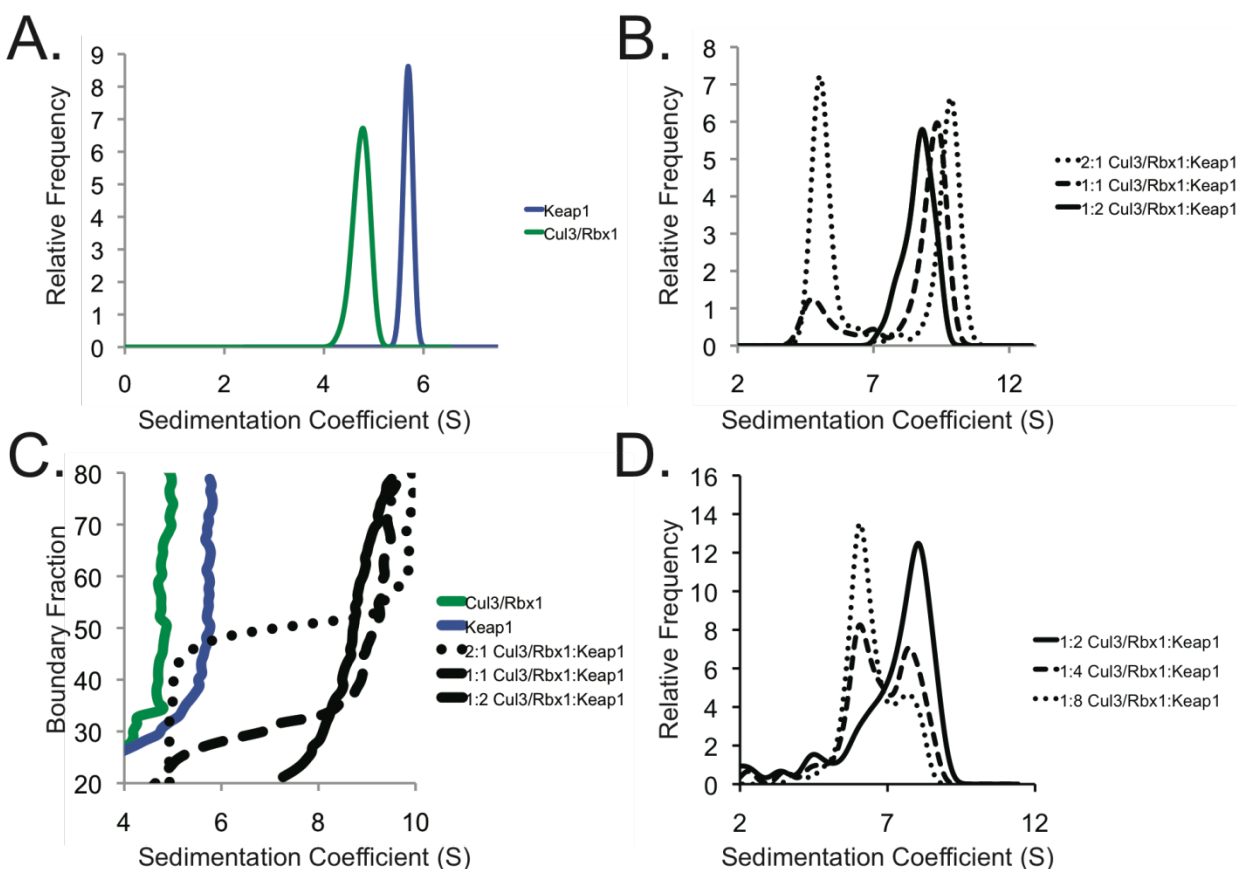


Figure 30. van Holde-Weischet Analysis of Cul3/Rbx1, Keap1, and Their Complex

A. van Holde-Weischet (vHW) envelopes of Cul3/Rbx1 and Keap1 individually. B. vHW envelopes of samples containing different molar ratios of the two individual proteins from panel A. In this experiment, Cul3/Rbx1 is found in excess. C. vHW distribution plot of the same data sets from panel A and B. D. Three additional molar ratios of Cul3/Rbx1 and Keap1 where Cul3/Rbx1 is limiting and Keap1 is in excess instead.

When the above sedimentation results are combined in a van Holde-Weischet distribution plot, the peak shifting-effect discussed earlier can be observed (Figure 30 C). In this type of plot, vertical line segments represent homogenous populations of particles. The Cul3/Rbx1 sample (green) is slightly to the left of the dotted black line of the 2:1 sample in the Cul3/Rbx1 region, representing a lower sedimentation coefficient. The Cul3/Rbx1 only sample is not experiencing the presence of Keap1 that the 2:1 sample is, where the equilibrium with Keap1-bound

Cul3/Rbx1 is causing a shift in the sedimentation coefficient to the right. The phenomenon can also be observed in the ratio samples (solid, dashed, and dotted lines, Figure 30 C), because as more Cul3 is present, it will be less likely Keap1 will be found unbound, resulting in a higher sedimenting species.

The edited ultracentrifugation data for the envelope plot in Figure 30 B can be seen in Figure 31. Time- and radius-invariant noise has been subtracted and the meniscus positions were found by 2DSA analysis (see Appendix E for result files).

An additional AUC stoichiometry experiment was performed, but unlike the previous experiment which looked at molar ratios greater than 1:2 ($[\text{Cul3/Rbx1}]:[\text{Keap1 monomer}]$), this experiment tested 1:2, 1:4, and 1:8 ratios. The results in Figure 30 D show a singular peak for the 1:2 sample as before, and the 1:4 and 1:8 samples show increasing amount of unbound, excess Keap1. Together with the size exclusion experiments, these results conclusively show a binding stoichiometry of one heterodimer of Cul3/Rbx1 bound to one dimer of Keap1. Sedimentation equilibrium experiments were also performed, but because Keap1 is not stable at room temperature over long periods of time, significant precipitation occurred during the run, and the results were inconclusive.

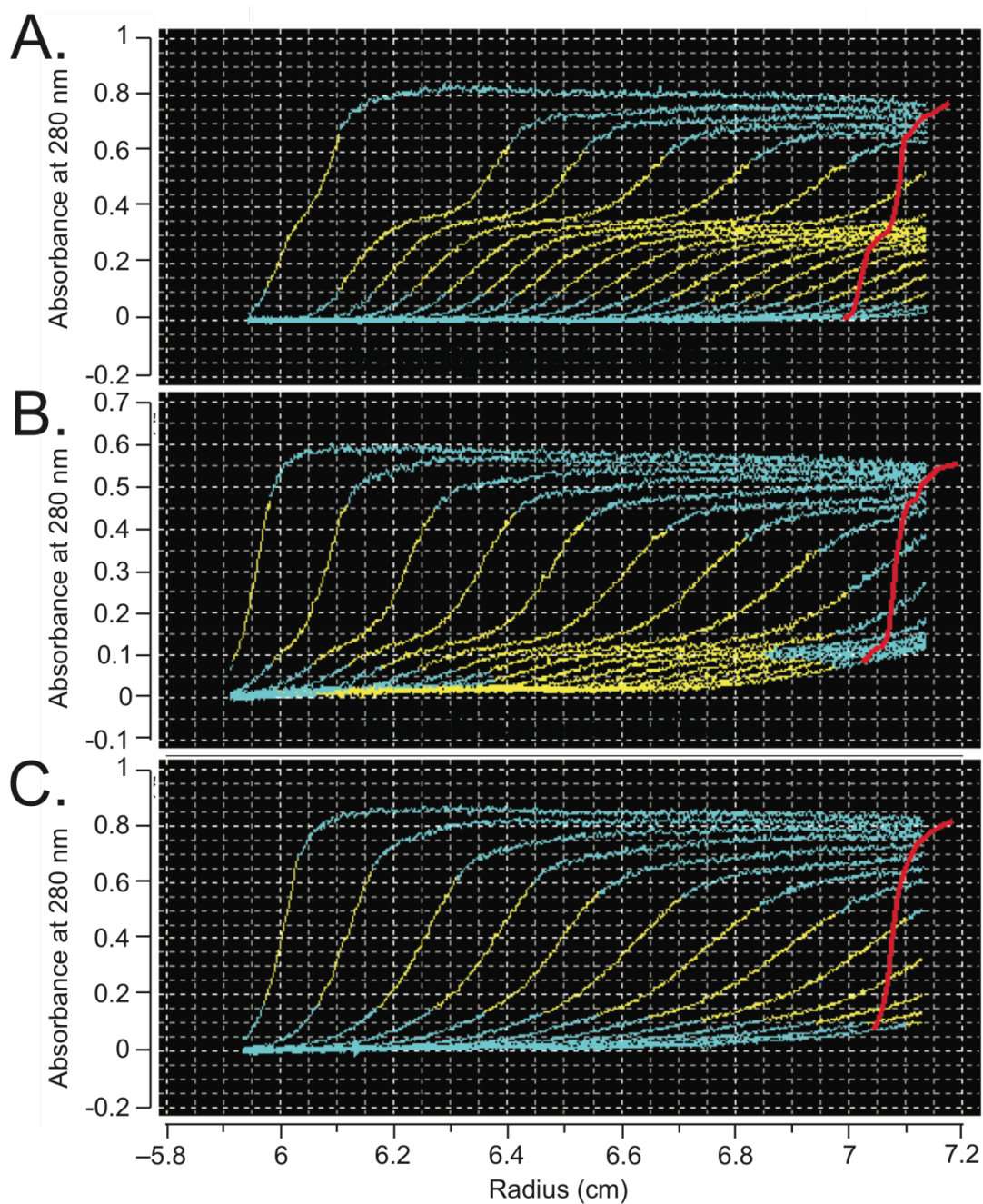


Figure 31. Edited Complex Data Scans Used in Molar Ratio vHW Analysis

A. Edited complex data scans for the 2:1 [Cul3/Rbx1]:[Keap1 monomer] sample. B. 1:1 sample data. C. 1:2 sample data. The area of the boundary used in the analysis is shown in yellow. The unused portion of the data is in cyan. The red line denotes the back diffusion tolerance.

4.3.4 Small-Angle X-ray Scattering

4.3.4.1 SAXS Results for the Individual Cul3/Rbx1 and Keap1 Proteins

The initial results of the SAXS experiments for the individual proteins, in a buffer containing 2 mM TCEP, showed a large amount of aggregation and the absence of a monodisperse system, with the exception of the Cul3 sample. The addition of 10 mM DTT and 3% glycerol (suggested by Dr. Guo) significantly reduced this phenomenon. Background-subtracted scattering profiles of Cul3/Rbx1 and Keap1 are shown in Figure 32 A and B. SAXS analysis of Cul3/Rbx1 reveals its tertiary structure (Figure 33) to be very similar to the predicted structure using homology modeling (3.2.1).

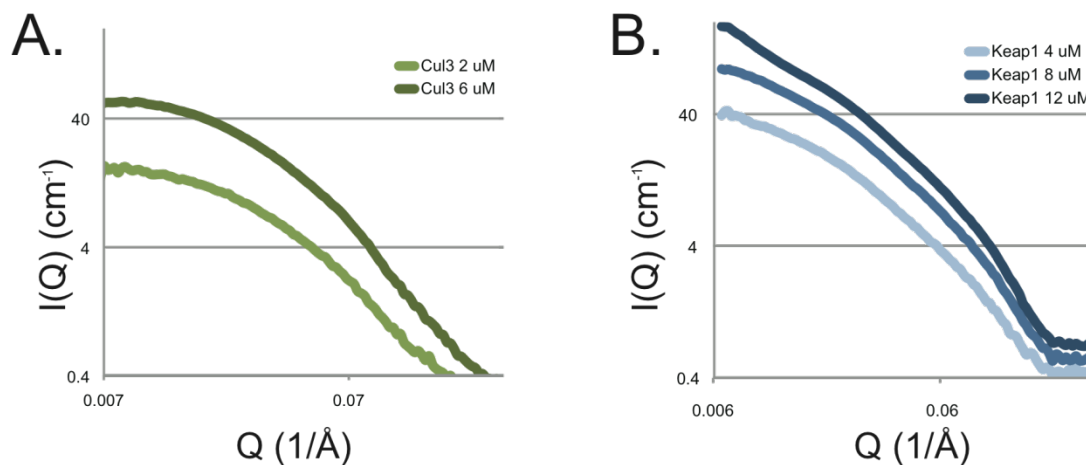


Figure 32. Small-Angle X-ray Scattering Profiles for Cul3/Rbx1 and Keap1

A. Cul3/Rbx1 scattering profiles at two different concentrations. B. Keap1 scattering profiles at three different concentrations. The appearance of aggregation is observed in the 12 μM Keap1 sample as the slope of the curve near the y-intercept is less horizontal than the rest.

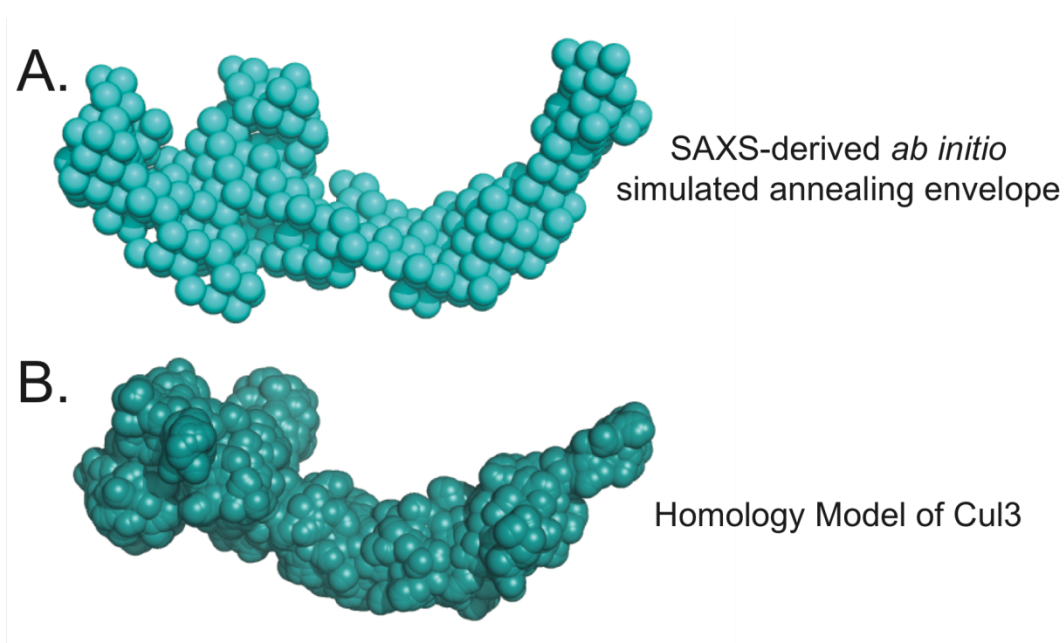


Figure 33. Comparison of Cul3/Rbx1 SAXS Model and Homology Model

A. Cul3/Rbx1 envelope result file as viewed in PyMOL shown in sphere mode. B. The homology model of Cul3/Rbx1, produced as described in Chapter 3, visualized by PyMOL in space-filling mode.

SAXS analysis of Keap1 produced an *ab initio* simulated annealing structure that is also very similar to the homology model and cryo-EM envelope of Keap1 (Figure 34). The V-shaped structure appears slightly larger than the homology model of the Keap1 dimer. This is likely due to the diverse set of conformations Keap1 assumes in solution, as evidenced by the cryo-EM results from Ogura *et al* (70).

4.3.4.2 SAXS Results for the Cul3/Rbx1:Keap1 Complex

When Cul3/Rbx1 and Keap1 are mixed in a 1:2 molar ratio ([Cul3/Rbx1]:[Keap1 monomer]) and subjected to SAXS, the complex has a different scattering profile than the two individual proteins. When the SAXS profile is input into the GNOM program, the shape of the

$p(r)$ curve generated for the Cul3/Rbx1:Keap1 complex was essentially independent of the value of D_{\max} used in the transformation, between 150-500 angstroms. Using a D_{\max} value below that range would cause the $p(r)$ curves to sharply cross the x-axis, a sign of an inappropriately small D_{\max} (93). D_{\max} values above that range caused the $p(r)$ curves to oscillate above and below the x-axis at higher D_{\max} values, indicating the chosen D_{\max} value is too large. When D_{\max} values were chosen from within that range, the $p(r)$ curves gradually approach the x-axis between the 250-300 angstroms range, indicating that the true D_{\max} value lies somewhere in that range. A final $p(r)$ curve was generated using a D_{\max} value of 350 angstroms for use in *ab initio* simulated annealing structure determination programs.

Analysis by the *ab initio* program DAMMIN, shows its quaternary structure to resemble a similar curved-Y or scorpion shape compared to the homology model. In the SAXS complex structure, what is believed to be the Keap1 dimer is visible at one end of the structure, with the C-terminal end of Cul3 visible at the other end. The exact orientation of the Cul3 and Keap1 proteins within the complex is unknown without some additional experimentation with phase-contrast samples, such as in small-angle neutron scattering (SANS). However, the stoichiometry of the complex is in agreement with these results, as the structure does appear to contain one Cul3/Rbx1 protein and one Keap1 dimer.

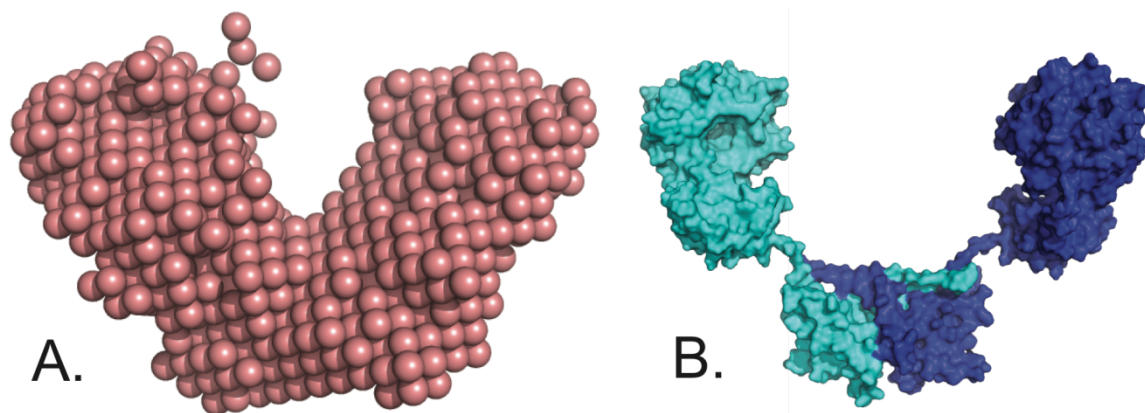


Figure 34. Comparison of SAXS Keap1 Model and Homology Model

A. Keap1 envelope result file as viewed in PyMOL shown in sphere mode. B. The homology model of the Keap1 dimer, produced as described in Chapter 3, visualized by PyMOL in surface mode.

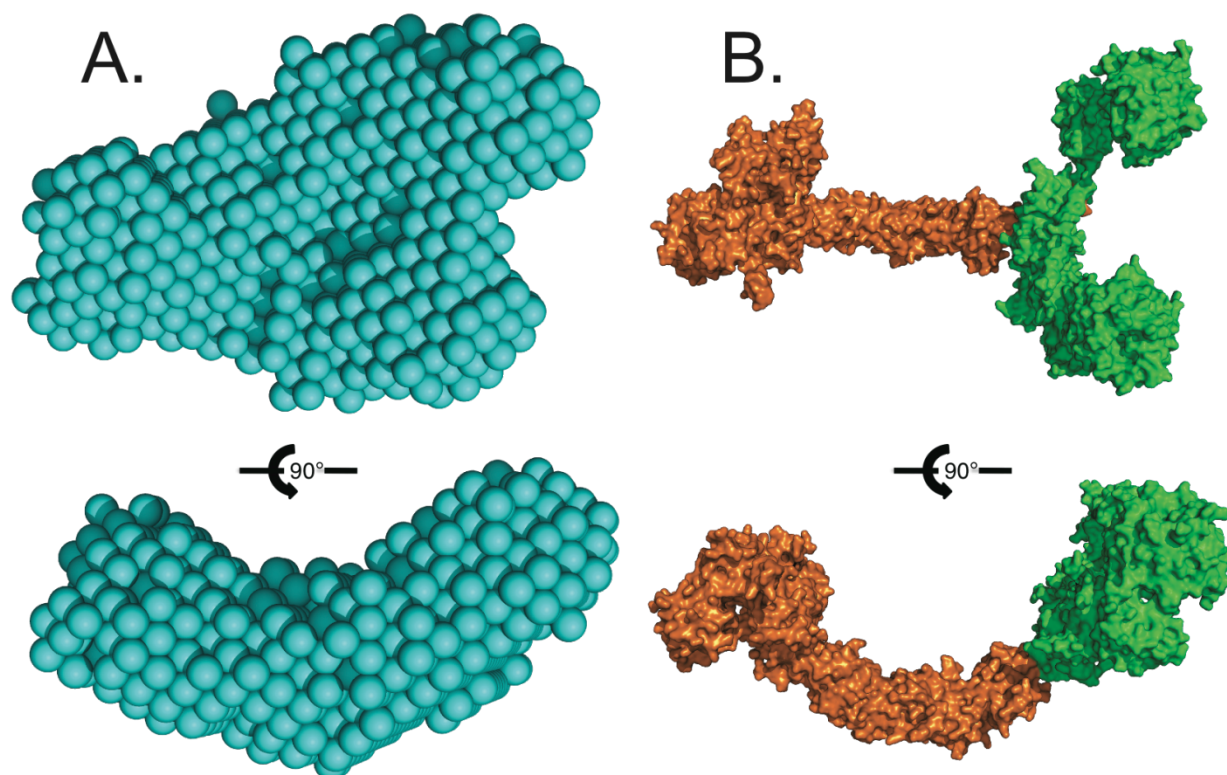


Figure 35. Complex SAXS Model and Refined Complex Homology Model

SAXS analysis on wild type complex data reveals a trilobular structure (A). The density was used to refine the original homology model described in Chapter 3. B. The refined complex homology model.

4.4 Discussion

Cul3's experimental hydrodynamic and structure properties confirm that its structure is very similar to predicted homology models and in comparison to other cullins. Cul3 and Rbx1 have not been observed as individual species in any of the experiments performed, indicating that the Cul3/Rbx1 heterodimer is a very stable protein complex. Once the addition of NaCl to a concentration of 150 mM or higher was implemented to increase Cul3/Rbx1 solubility in solution, this purified complex remained stable at 4 °C for a week before any noticeable precipitation took place.

Keap1 on the other hand, is a more difficult protein to work with because of its poor solubility in water. Keap1 contains a high density of cysteine residues that oxidize easily, leading to aggregation and precipitation from solution. The use of reducing agents such as TCEP or DTT and degassing buffer solutions helped to lower oxidization levels of Keap1 cysteines. In addition, pressurized nitrogen gas was used to rid the empty space within storage containers of oxygen, further increasing the half-life of the purified Keap1. This facilitated the solubility of Keap1 enough to allow for experimentation at room temperature for several hours, making sedimentation velocity ultracentrifugation possible. Keap1 was confirmed to be a homodimeric protein that is capable of binding to Cul3 and Nrf2. In addition, Keap1's solution structure closely resembles the published cryo-EM results (70).

Cul3 binds to Keap1 in a 1:2 molar ratio ([Cul3/Rbx1]:[Keap1 monomer]). This quaternary structure represents a novel organization for cullin ligases since they usually form complexes having one cullin and a monomeric substrate adaptor or an overall dimeric structure with two cullin protomers present and a dimeric substrate adaptor (13, 18, 94).

AUC experiments, using different ratios of Cul3/Rbx1 and Keap1, confirmed the stoichiometric organization of the complex. A molar ratio of 1:2 ([Cul3/Rbx1]:[Keap1

monomer]) sample produced singular peaks in two separate experiments, representing a homogenous population sample of the complex. The presence of accessory peaks, observed in all ratios other than 1:2, is indicative of a heterogeneous population of the complex and a free component (free Cul3/Rbx1, Figure 30 B, or free Keap1, Figure 30 D) The peak-shifting effect observed in the AUC experiments is most likely due to a rapid interconversion of the species during the time-course of sedimentation (95). When more Cul3 is available, such as in the 1:1 and 2:1 samples, the equilibrium between free and bound Keap1 is shifted and Keap1 spends a greater percentage of time in solution bound to Cul3 in a complex. Therefore, those samples each have slightly different S-values from each other and the 1:2 complex.

Despite not having the high-resolution atomic structure like X-ray crystallography, the low-resolution SAXS structure provides a wealth of information about a protein's size and shape. SAXS experimentation and analysis revealed the solution scattering for Cul3/Rbx1, Keap1, and the complex they form. Both of the resulting structural models for Cul3/Rbx1 and Keap1 closely resemble their homology models produced using SWISS-Model. The main difference between the initial complex homology model (section 3.2.3) and the SAXS-derived *ab initio* structure is that the SAXS structure is slightly flatter and less curved than the model. This may be due to the fact that SAXS results are an average of all the complex's conformations in solution, whereas the homology model is built from crystal structures where each protein is locked into a particular conformation because of the molecular contacts within the protein crystal.

Chapter 5: Characterization of Keap1 Mutants and Comparison to Wild Type

5 CHARACTERIZATION OF KEAP1 MUTANTS AND COMPARISON TO WILD TYPE

5.1 Introduction

Keap1 has been identified as an oxidative stress sensor protein because it contains a high number of cysteine residues through the protein (29). The vast majority of ARE inducers are capable of reacting with cysteine residues, and Keap1 contains 27 cysteines, 25 of which are highly conserved. Thus far, C151 is the only cysteine known to be required for stabilization and activation of Nrf2 in response to the ARE inducers sulforaphane and tBHQ (96). In addition, NEPP11, an endogenous neurite outgrowth-promoting prostaglandin (97) and ebselen, a seleno-organic drug (98), are both highly dependent on Keap1 C151 for their upregulation of the ARE response in cells. Importantly, our group has found C151 to be one of the most reactive cysteines in the human Keap1 protein in vitro (48, 99), and the only cysteine consistently and highly modified in vitro by the natural product ARE inducers xanthohumol, isoliquiritigenin and 10-shogaol (36).

Based on the important role that Cys151 appears to play in the regulation of Nrf2 ubiquitination, our group investigated the effect of mutations at position 151 in Keap1. The C151W mutant repressed Nrf2 much less than wild type, causing the ARE activation to increase significantly compared to wild type Keap1 (50). This ARE activation is dependent on the partial molar volume of the residue at amino acid position 151. It has been hypothesized that these observed changes are due to a dissociation of Cul3 and Keap1. Modification of C151 by electrophiles has been shown by Keap1-Cul3 co-immunoprecipitation to disrupt the interaction between Cul3 and Keap1, based on experiments conducted both in cell lysates (61) and with purified proteins (51) in which wild type Keap1 and the Keap1 C151S are compared. Our group also observed a disruption of the Keap1-Cul3 interaction by co-immunoprecipitation by introduction of tryptophan at position 151 (50). Evidence for this

dissociation has not been sought through more direct methods that measure the strength of interaction, however, and little else is known about how Cys151 modification affects the structure of this complex.

In an effort to understand the molecular signaling events that lead to the modulation of Nrf2 ubiquitination, in vitro structural and biochemical studies have been performed in an effort to detect and elucidate any structural and functional changes to the Cul3/Rbx1:Keap1 complex engendered by Keap1 cysteine modification. We have taken advantage of the Keap1 C151W protein as a functional model for Keap1 protein modified at position 151. This strategy provides the benefit of having a homogenous population of modified protein, which is impossible to achieve if modifying wild type Keap1 with electrophiles due to varying numbers of modifications per protein molecule (99). In addition, this mutant protein has been shown to be properly folded and functional in that it binds to Nrf2 in cells as well as wild type Keap1 (50).

Our results indicate that modification of Keap1 C151 leads to a decrease in Nrf2 ubiquitination both by an alteration in the dissociation constant for the Cul3:Keap1 interaction of approximately 5-fold and a conformational change within the complex. A conformational change of the Keap1-Cul3 complex, rather than solely a disruption of the complex, is supported by mass spectrometry analysis of Cul3 cysteine modification in the presence of either wild type Keap1 or Keap1 C151W.

5.2 Materials and Methods

5.2.1 Expression and Purification of Cul3/Rbx1 and Keap1 Recombinant Proteins

Wild type human Cul3/Rbx1 and Keap1 were prepared as previously described in Chapter 2 (57). Keap1-C151W and -C151S mutations were produced using primers and site-

directed mutagenesis. DNA sequencing was used to confirm the mutations. The only difference in expression of the proteins from that for wild type Keap1 is that for Keap1-C151S, 200 μM ZnCl_2 was added to the growth media as no protein expression is obtained without it (48).

5.2.2 In vitro Ubiquitination Assay

The *in vitro* ubiquitination assay was performed as previously described in Chapter 2 (57). The only exceptions were the addition of samples containing Keap1-C151W and Keap1-C151S mutants instead of Keap1-WT. Samples were allowed to equilibrate at 37 °C before the addition of ubiquitin to start the reaction.

5.2.3 Surface Plasmon Resonance

5.2.3.1 Cul3/Rbx1 Immobilization to CM5 Chip

Surface plasmon resonance experiments were performed using a Biacore T100 at 20°C. A list of samples tested by SPR can be found in Table IX. Cul3/Rbx1 was diluted to 1 μM in immobilization buffer (10 mM sodium acetate, pH = 5.0) and was then immobilized onto the CM5 sensor chip (Biacore) using amine coupling with 1-Ethyl-3-[3-dimethylaminopropyl]carbodiimide hydrochloride (EDC) and N-hydroxysuccinimide (NHS). Immobilization proceeded for 30 seconds at a flow rate of 10 $\mu\text{L}/\text{min}$.

5.2.3.2 Keap1 and Mutant Concentration Series

A concentration series for Keap1-WT, Keap1-C151W, and Keap1-C151S of {30, 61, 123, 247, 494, 988, 1976, 3952} nM was used to determine binding affinity for the interaction with Cul3/Rbx1. The flow rate was set at 20 $\mu\text{L}/\text{min}$ for a contact time of 420 seconds

followed by 600 seconds of dissociation time. A regeneration scouting procedure identified a solution of 50% ethylene glycol 100 mM CAPS pH 10.0 as optimal for regeneration of the Cul3/Rbx1 immobilized chip. The results were analyzed by the Biacore Evaluation Software Kinetics and Affinity Wizard. This all-inclusive analysis program subtracts the reference channel measurements from the sample data. On and off rates of binding are fitted in the Kinetics wizard, while the amount of bound analyte at each concentration is used to create binding isotherms in the Affinity wizard. Multiple data sets were analyzed and standard deviations were calculated for Affinity data and reported in Table IX. Data sets with the most accurate fitting, as determined by the lowest χ^2 value, were chosen for the Kinetics data.

5.2.4 Analytical Ultracentrifugation

5.2.4.1 Data Collection

Cul3/Rbx1, Keap1-WT, Keap1-C151W, and Keap1-C151S proteins were subjected to sedimentation velocity experiments individually as well as in complex. These experiments were performed at a temperature of 20 °C and a rotor speed of 60,000 rpm using a Beckman Optima XL-A analytical ultracentrifuge equipped with absorbance and interference optics and an An60TI rotor. After temperature and pressure reached the set points, loaded samples were allowed to reach thermal equilibrium before data collection began. Intensity data were collected at 280 nm as a function of radial position. Each centrifuge cell was scanned sequentially with zero time delay between scans until no further sedimentation was observed.

5.2.4.2 Data Analysis

The program Ultrascan 2.0 used for analysis of the primary data as described by Demeler (100). Solution density and viscosity were calculated from buffer composition as

1.00994 g/mL and 1.0363 cP. A value of 0.732442 mL/g was assumed for the partial specific volume. Intensity data was converted to pseudo-absorbance, which was used in a two-dimensional spectrum analysis (2DSA). The 2DSA was performed with S-value limits of 1 and 15 (resolution: 10), f/f_0 limits of 1 and 4 (resolution: 10), 6 uniform grid repetitions, and no Monte Carlo iterations at that time. Time invariant noise and meniscus (range: 0.03 cm) were also fit using the iterative (n=3) method. Radially invariant noise was fit in the subsequent 2DSA as recommended (90). The model with the lowest RMSD for each cell was chosen, and its corresponding noise file was used for subtraction.

For complex (interacting) samples with more than one protein, further 2DSA analysis with 50 Monte Carlo iterations was performed until no additional decrease in RMSD was noted. For those samples containing only one individual protein, a different approach was taken and additional fitting was performed using parsimonious regularization by genetic algorithm with 50 Monte Carlo iterations until no further decrease in RMSD was observed. Enhanced van Holde-Weischet analysis was also performed on noise-subtracted data to determine sedimentation coefficients and distribution within each sample. Sedimentation coefficients plotted against the relative frequency distributions were exported to Excel (Microsoft) for graphing.

5.2.5 Small-Angle X-ray Scattering

5.2.5.1 Data Collection for Individual Keap1 Mutants

Keap1-WT, C151W, and C151S samples for SAXS were prepared at 4, 6, and 8 μ M in a buffer containing 50 mM Tris, pH = 8.0, 250 mM NaCl, and 2 mM Tris(2-carboxyethyl)phosphine (TCEP), 10 mM DTT, and 3% glycerol. Immediately prior to injection into the flow cell, samples were filtered using 0.65 micron Ultrafree-MC spin filters

(Millipore) and centrifuged at 15,000 rpm for 10 min. SAXS data were collected at beamline 18-ID-D at the Advanced Photon Source on July 15, 2010. The instrument was configured with a sample-detector distance of 2.3 m with a range of $Q=0.006-0.37 \text{ \AA}^{-1}$ at an X-ray wavelength of 1.03 \AA . The sample flowed through a 1-mm ID quartz capillary maintained at 25°C such that the protein was exposed to X-rays for less than 100 ms.

5.2.5.2 Data Collection for Cul3/Rbx1:Keap1 Mutant Complexes

Wild type and mutant complex samples for SAXS were prepared, at $15 \text{ }\mu\text{M}$ for Cul3 and $30 \text{ }\mu\text{M}$ for Keap1-WT, C151W, and C151S, in a buffer containing 50 mM Tris, pH = 8.0, 250 mM NaCl, and 2 mM Tris(2-carboxyethyl)phospine (TCEP). Immediately prior to injection into the flow cell, samples were filtered using 0.65 micron Ultrafree-MC spin filters (Millipore) and centrifuged at 15,000 rpm for 10 min. Complex SAXS data were collected at beamline 12-ID-C at the Advanced Photon Source on March 10, 2009. The instrument was configured with a sample-detector distance of 2.3 m with a range of $Q=0.006-0.37 \text{ \AA}^{-1}$ at an X-ray wavelength of 1.03 \AA . The sample flowed through a 1-mm ID quartz capillary maintained at 25°C such that the protein was exposed to X-rays for less than 100 ms.

5.2.5.3 Data Analysis

Data were reduced to I versus Q using the BESSRC-Cat Igor Pro macros. Moore's autocorrelation analysis was performed using the low-Q portion range of the data where $R_gQ < 1$ as well as visualization by Kratky plot. The program GNOM was used to calculate the $p(r)$ pair-distance distribution function by an indirect Fourier transform of the scattering data over the range $0.008-0.3 \text{ \AA}^{-1}$. The value of $p(r)$ was constrained to be 0 at $r=0$ but was unconstrained at the maximum distance (D_{max}). The shapes of the $p(r)$ curves were essentially

independent of the value of D_{\max} (350 Å) used in the transformation in the range between 150 and 500 angstroms.

As described in Chapter 4, the resulting $p(r)$ output files from GNOM were used in the DAMMIN or DAMMIF program to build three-dimensional scattering densities for each sample. These scattering densities were visualized in PyMol and used to further refine molecular models of the complexes.

5.2.6 Mass Spectrometry of Isoliquiritigenin-Modified Proteins

Nano LC-MS/MS mass spectrometry experimentation and analysis procedures, were conducted by our collaborator from the Van Breeman group, Chenqi Hu. The experimental procedures have been described elsewhere (101). Briefly, sample preparation involved the preincubation of Keap1-WT and C151W with Cul3 for 30 minutes, prior to reaction with varying concentrations of isoliquiritigenin for 2 hours. Following these reactions, nano LC-MS/MS mass spectrometry analysis was performed on tryptic digestion products in order to determine the sites of alkylation.

5.3 Results

5.3.1 *In vitro* Ubiquitination Assay of Keap1-WT and Mutants

Keap1-WT, Keap1-C151W, and Keap1-C151S were compared in the *in vitro* ubiquitination assay. Although each reaction produced ubiquitinated Nrf2, they resulted in varying levels of Nrf2-ubiquitin conjugates (Figure 36). Keap1-C151S samples have the greatest amount of ubiquitinated Nrf2 at the tested timepoints indicated by the absence of unmodified Nrf2 and the presence of a higher MW smear on the gel at the 15 and 20 minute time points, whereas Keap1-C151W samples appear to have the least, with the greatest

amount of unmodified Nrf2. Keap1-WT results indicate the rate of the reaction is intermediary to the two functional mutants. The effect of modification on Keap1 ubiquitination was also assessed by anti-Keap1 western blot. No differences in the ubiquitination patterns of Keap1, were observed for Keap1-C151W when compared to wild type.

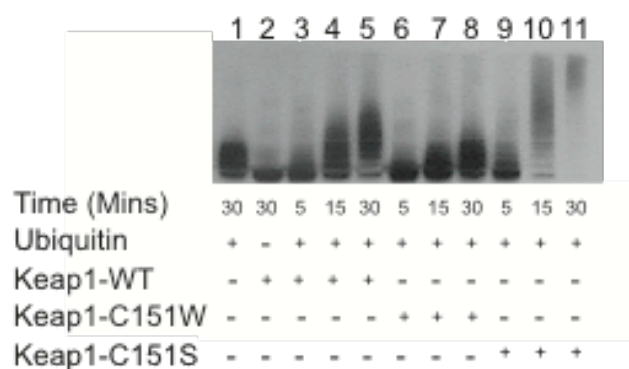


Figure 36. *In vitro* Ubiquitination Assay with Keap1 Mutants Comparing Nrf2 Ubiquitination

An anti-Nrf2 western blot showing the difference in ubiquitination rates for Nrf2 when different Keap1 mutants are used. Keap1-independent ubiquitination of Nrf2 is observed in lane 1.

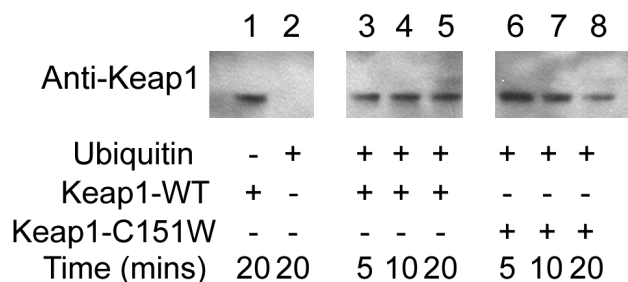


Figure 37. *In vitro* Ubiquitination Assay of Keap1-WT and C151W Comparing Keap1 Ubiquitination

An anti-Keap1 western blot comparing the ubiquitination of Keap1-WT and C151W. A small amount of ubiquitination is observed in the 20 minute timepoint as a faint band above the much darker unmodified-Keap1 band.

5.3.2 Surface Plasmon Resonance

The results of the SPR experiments are summarized in Table IX. Each data set was analyzed by two separate evaluation wizards within the Biacore T100 Evaluation software. The Kinetics wizard uses models to fit the data to determine the on and off rates of association, which are divided by one another to find the K_d . The Affinity wizard uses the response units to create binding isotherms, which are used to calculate the K_d . While the exact K_d value, for wild type and mutant complexes vary somewhat between the two analysis methods, the overall trend of the results is the same: modification of Cys151 to tryptophan decreases the strength of the interaction by 5- to 10-fold, while modification to serine slightly increases the strength of the interaction Table IX.

Table IX. Results from the Surface Plasmon Resonance Experiments

Sample	Analyte	Ligand	Dissociation Constant, K_d (nM)	Analysis Wizard
1	Keap1-WT	Cul3/Rbx1	801 ± 489	Affinity
			306 ($\chi^2=30.5$)	Kinetics
2	Keap-C151W	Cul3/Rbx1	4240 ± 1140	Affinity
			1960 ($\chi^2=9.77$)	Kinetics
3	Keap1- C151S	Cul3/Rbx1	513 ± 277	Affinity
			221 ($\chi^2=397$)	Kinetics
4	Nrf2	Cul3/Rbx1	No measurable binding observed	Affinity
			No measurable binding observed	Kinetics

5.3.3 Analytical Ultracentrifugation

The sedimentation profiles for Keap1-C151W (5.9 S) and Keap1-C151S (5.9 S) overlay with the Keap1-WT sample from Chapter 4 (Figure 38). This result suggests that the overall shape and size of the Keap1 protein are not affected by the site-directed mutation at position 151.

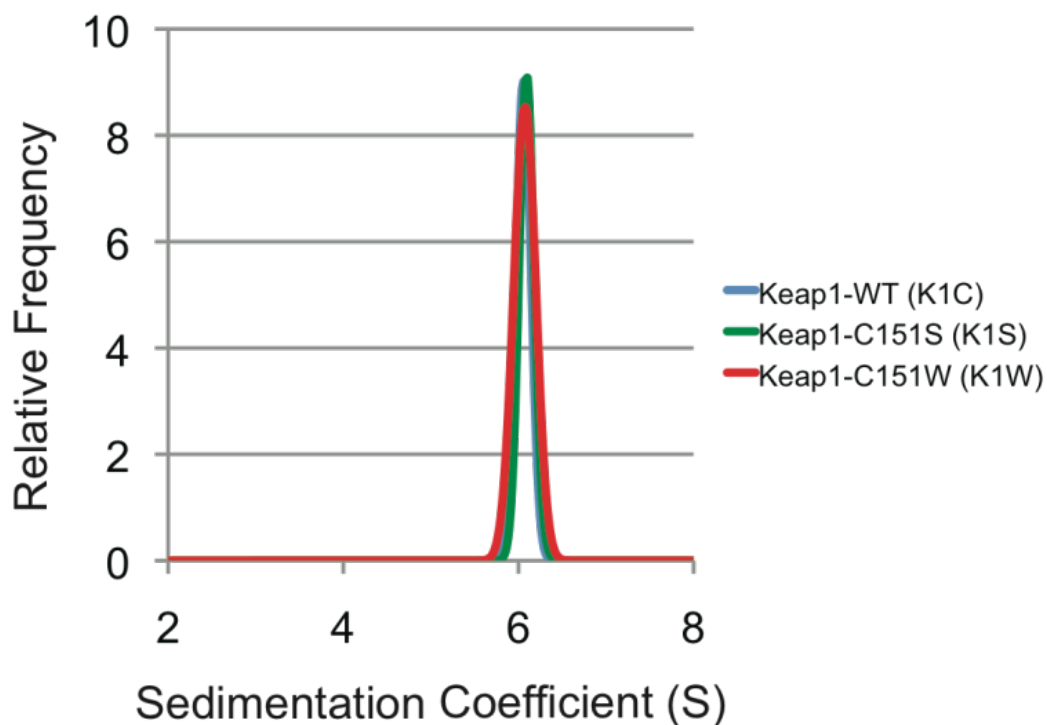


Figure 38. Sedimentation Velocity Results for Keap1-WT, Keap1-C151W, and Keap1-C151S
van Holde-Weischet envelope analysis of individual Keap1-WT and the two functional mutants, Keap1-C151W and Keap1-C151S.

When Cul3/Rbx1 is incubated with each of the Keap1 proteins in a one to one molar ratio, larger complex peaks are observed, but contrary to the individual Keap1 peaks, these complex peaks do not overlay (Figure 39). Each of the complex peaks (8.5 S for Cul3/Rbx1:Keap1-WT, 7.2 S for Cul3/Rbx1:Keap1-C151W, and 9.3 S for Cul3/Rbx1:Keap1-C151S) are larger than the two individual species peaks, indicating that the proteins do form complexes. The shapes of the peaks differ, with Cul3/Rbx1:Keap1-C151S being the sharpest, Cul3/Rbx1:Keap1-C151W being the broadest, and the complex containing Keap1-WT falling in between. In addition to the complex peaks, there are additional peaks, which overlay with the Cul3/Rbx1 only samples, confirming the presence of excess Cul3/Rbx1 in the samples.

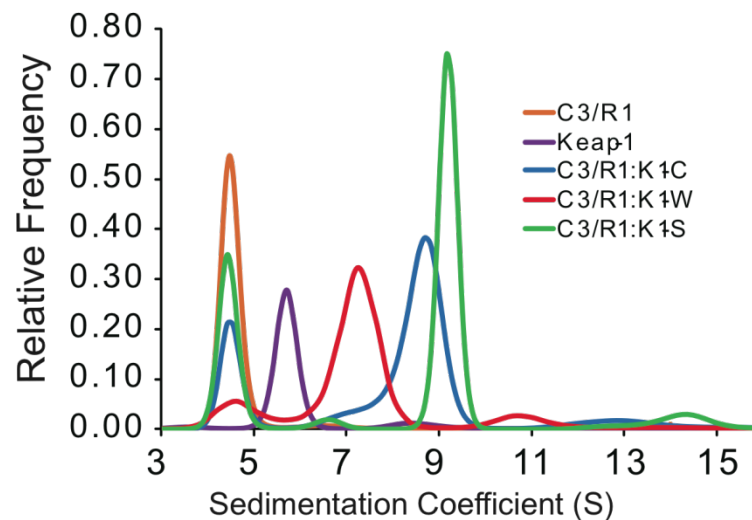


Figure 39. Sedimentation Velocity Results for Wild type and Mutant Complexes

Taking a different look at the same data using an enhanced van Holde-Weischet distribution plot sheds additional light on these results. As shown in Figure 39, this plot of the three complexes at the same 1:1 ratios as above shows how sedimentation differences

between the three complexes can be attributed to the differences in their dissociation constants. The stronger Cul3/Rbx1:Keap1-C151S interaction results in two segregated populations of the formed complex (higher S species) and excess free cullins (lower S species). As the interaction strength decreases, the two populations become less and less segregated as the equilibrium is shifted. With a somewhat greater population of free Keap1, the Keap1 C151W-Cul3 complex's overall sedimentation is retarded and it is observed as a smaller sedimenting species. Conversely, as the amount of Cul3 bound to Keap1 varies, Cul3's apparent sedimentation increases for Keap1-C151W compared to Keap1-C151S. This effect causes the Cul3 boundary and the complex boundary to merge in the C151W-containing sample, as the two are no longer distinct species with complexes forming and coming apart at a timescale must shorter than the experimental setup. These studies highlight a difference in the strength of binding at the interface of the two proteins when Cys151 is modified to different amino acids. It is possible that a conformational change within mutant complexes could be contributing to the differences seen in this plot; however, they may be masked by the contributions of the differences in dissociation constant. The results for experiments probing the existence of the possible conformational change within the complex are shown in the next few sections.

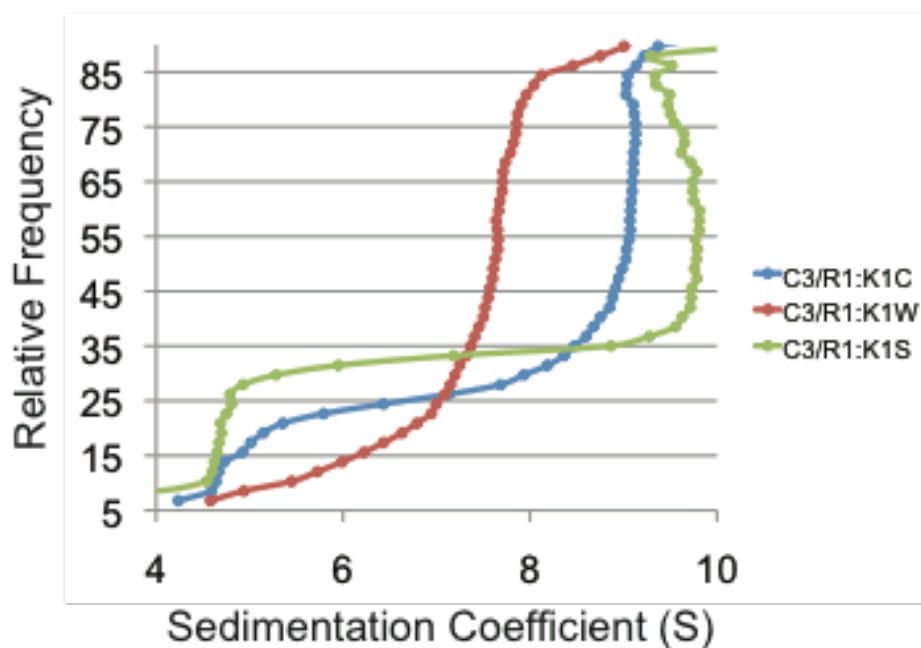


Figure 40. van Holde-Weischet Distribution Comparison Plot of Wild type and Mutant Complexes

5.3.4 Small-Angle X-ray Scattering

5.3.4.1 SAXS Profiles for Keap1 Mutants and the Cul3/Rbx1:Keap1-Mutant Complexes

Figure 41 shows the reduced, background-subtracted scattering curves for the wild type and mutant Cul3/Rbx1:Keap1 complexes as well as wild type Keap1, -C151W, and -C151S only. While the complex samples do appear to be very similar overall, with two humps around the middle of the plot, there are unique differences in the complex which become highlighted in a Kratky plot (Figure 42). This plot is used to examine protein folding and exaggerates the differences between scattering profiles. The bimodal shape of the plot and the decreasing slope of the right-hand portion of the plot suggest that the complexes are between globular and extended, but not unfolded. The differences between the results support the hypothesis that these complexes are structurally distinct.

The Keap1-only scattering profiles are also very similar but look distinctly different from the complex scattering results. These samples appear to only have one smooth broad hump, unlike the two from the protein-complex data.

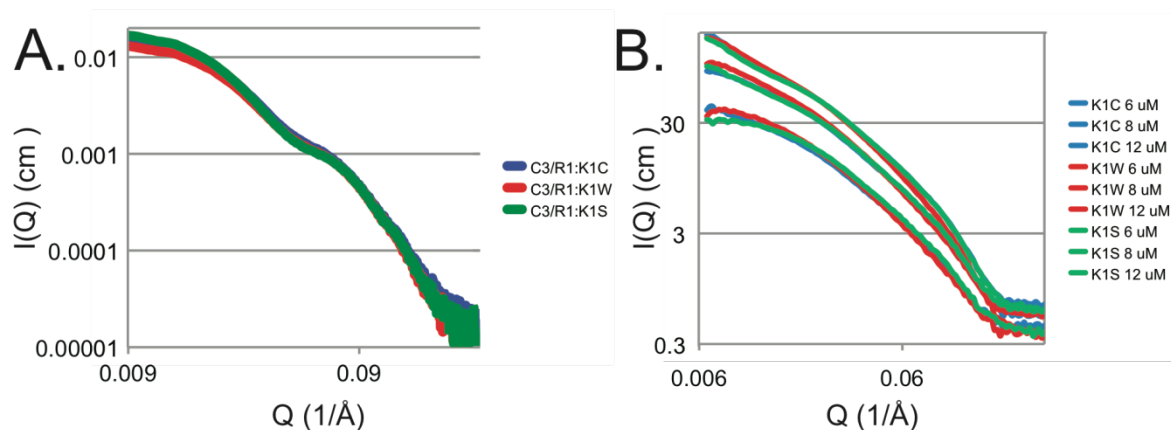


Figure 41. SAXS Profiles for Mutant Complexes and Mutant Keap1 Proteins

Scattering profiles for wild type and mutant complexes are shown here. B. Scattering profiles for different concentrations of the wild type and mutant Keap1 proteins.

5.3.4.2 Pair-Distribution Function Analysis

The exported scattering waves from above were input into GNOM and the $p(r)$ curves generated show differences between the three complexes as well. The complex curves are all skewed to the left, indicating that they are somewhere between rod-shaped and spherical (102, 103). Subtracting the $p(r)$ curves from one another allows for the generation of $p(r)$ difference plots, $\Delta P(r)$. Figure 43 shows that while there are differences in the individual Keap1 proteins, they are much less than the differences between the Cul3-containing complexes.

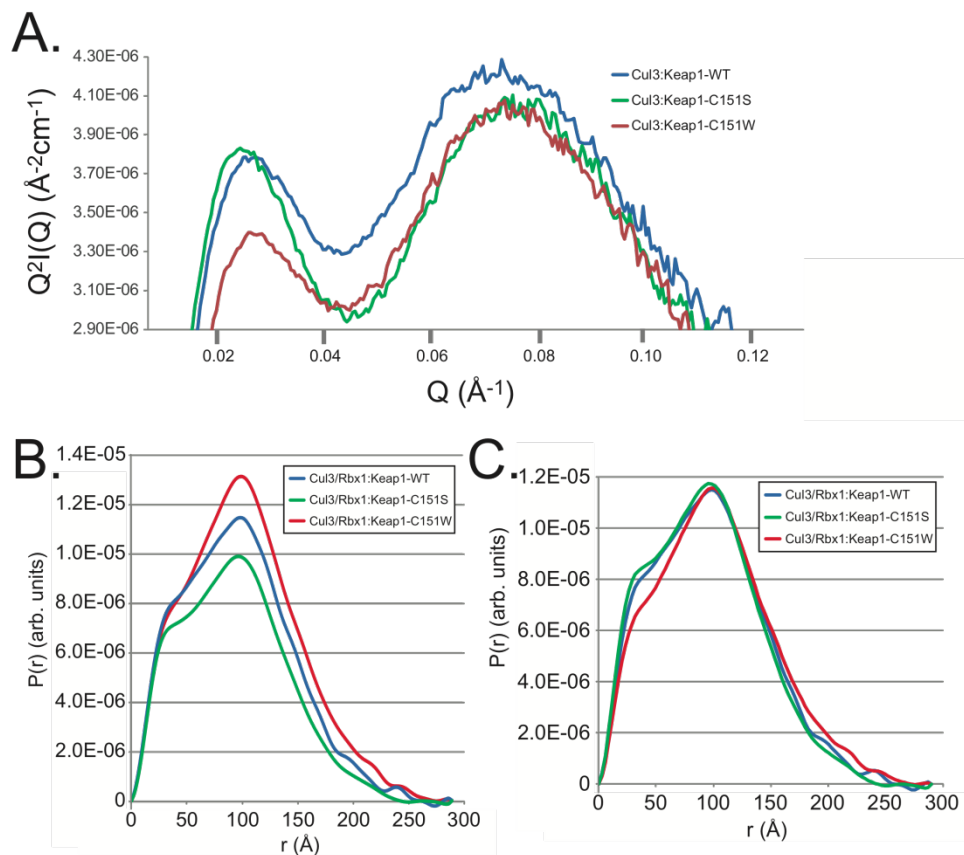


Figure 42. SAXS Analysis of Mutant Complexes – Kratky Plot and $p(r)$ Normalization

A. Kratky plot of the wild type and mutant complex samples, highlighting the structural differences between the three mutants when in complex with Cul3. B. $P(r)$ curves as generated by GNOM. C. The same $p(r)$ curves, normalized to area.

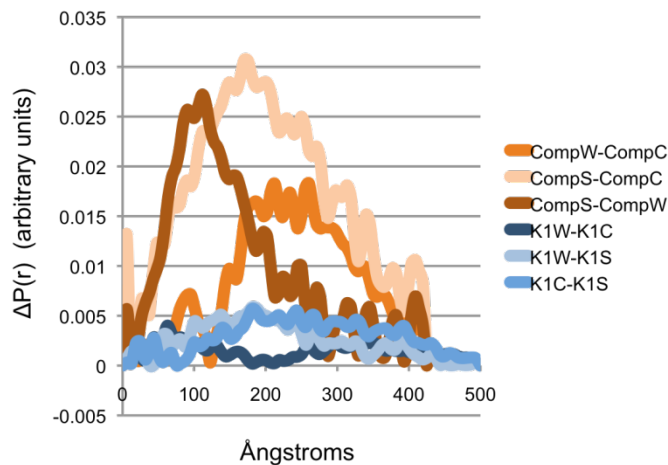


Figure 43. Difference Pair-Distribution Function Plots

Each data set from within its series was subtracted from the other two and the absolute values of the differences are plotted here.

5.3.4.3 *Ab initio Simulated Annealing of the Mutant Complexes*

How these differences in the $p(r)$ curves relate to structural differences becomes more clear when they are input into the *ab initio* simulated annealing program, DAMMIN. Averaged DAMMIN scattering densities appear to show an angular difference of the Keap1-C151W-Cul3/Rbx1 complex when compared with the two other complexes containing Cul3/Rbx1 and either Keap1-WT or Keap1-C151S (Figure 44). SAXS density appears to be similar between Keap1-WT and C151S, except that the wild type density appears more diffuse. The Keap1-C151W density appears marked different from the other two.

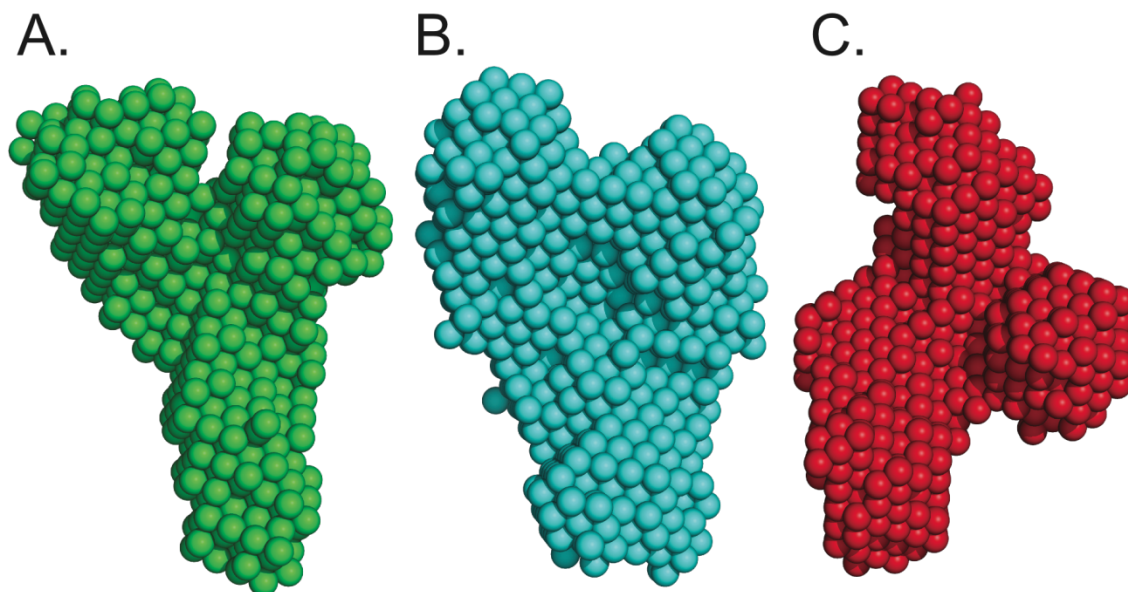


Figure 44. Low-Resolution Scattering Densities for Wild type and Mutant Complexes

A. Solution structure model of Cul3/Rbx1:Keap1-C151S created through the *ab initio* simulated annealing program, DAMMIF. B. The Cul3/Rbx1:Keap1-WT model. C. The Cul3/Rbx1:Keap1-C151W model illustrating what is hypothesized to be a conformational change at the interface Keap1 shares with Cul3.

5.3.5 Mass Spectrometry Analysis of Cul3 and Keap1 Alkylation

To gain further insight of how the modification at Keap1 Cys151 induces a conformational change within the Cul3/Rbx1:Keap1 complex, isoliquiritigenin was used as a chemical probe to look for conformational differences between the wild type and Keap1-C151W complexes. A change in Cul3 alkylation patterns would indicate a conformational change of the complex. As shown in Table X, the cysteine at position 636 on Cul3 was alkylated only when Cul3 was bound to wild type Keap1 and not to the Keap1-C151W mutant.

Table X. Detection of cysteine residues modified by isoliquiritigenin in the Cul3/Rbx1:Keap1 or Cul3/Rbx1:Keap1-C151W complexes

Conditions		Modified cysteines with [ISO]/[Keap1]=2		Modified cysteines with [ISO]/[Keap1]=5	
Preincubation	Addition	Keap1	Cul3	Keap1	Cul3
Keap1-WT+ Cul3 ^b	ISO	C23 ² , C38 ³ , C151 ^{1,2,3} , C196 ^{1,2} , C319 ^{1,2,3} , C613 ¹	C636 ^{1,2,3}	C23 ^{1,2,3} , C38 ^{2,3} , C151 ^{1,2,3} , C196 ^{1,2,3} , C226 ^{1,2,3} , C319 ^{1,2,3} , C368 ³ , C613 ^{2,3}	C636 ^{1,2,3}
Keap1-C151W + Cul3	ISO	C23 ^{1,3} , C38 ^{2,3} , C226 ^{1,3} , C319 ^{1,2,3}	—	C23 ^{1,2,3} , C38 ^{1,3} , C196 ² , C226 ^{1,2,3} , C319 ^{1,2,3} , C434 ³ , C613 ^{1,2,3}	—

^a Isoliquiritigenin is abbreviated as “ISO”.

^b Keap1-WT or C151W mutant was incubated with Cul3 at a molar ratio of 2:1 ([Keap1]/[Cul3]).

^c Triplicate experiments were performed. The numbers indicate the experiments in which isoliquiritigenin-modified peptides were detected using LC-MS/MS.

5.4 Discussion

The resulting van Holde-Weischet AUC curves for wild type Keap1, C151W, and C151S overlay very closely with one another, suggesting that they all behave the same under the experimental sedimentation velocity conditions. These results indicate that modification of Keap1 does not alter the hydrodynamic properties of the protein. They also show that there is no disruption in the homodimerization of Keap1 upon modification at position 151. This conclusion suggests that regulation of the Cul3/Rbx1:Keap1 complex occurs by other means, different from that of the SCF^{Cdc4} complex.

Every other experiment performed on Keap1-WT and its functional mutants, Keap1-C151W and -C151S, points to structural and catalytic differences, not in the individual proteins, but in the complexes they form with Cul3/Rbx1. AUC and SPR studies show that increasing the partial molar volume of the 151 side chain, through site-directed mutagenesis to a tryptophan, decreases Keap1's affinity for Cul3 by approximately 5-fold. In addition, in the model generated by SAXS analysis, Keap1's substrate binding domains appear repositioned due to the altered interaction. The *in vitro* ubiquitination assay experiments with

Keap1 C151W show for the first time that modification of Cys151 alone is sufficient to effect a change in ubiquitin signaling through this complex. Ubiquitination of Nrf2 can still take place when Cys151 is mutated to a tryptophan, albeit in a reduced capacity. These results show that modification does not induce a complete dissociation, as has been suggested by others, because C151W is still able to catalyze the Nrf2 ubiquitination reaction although, not at the same rate as Keap1-WT or C151S. We propose that both the decrease in affinity of Keap1 for Cul3 and the alteration in the complex structure result in a decreased catalytic rate of ubiquitination, as seen in the *in vitro* ubiquitination assay.

No difference in Keap1 ubiquitination was observed for the C151W mutant when compared to wild type in the *in vitro* ubiquitination assay. Keap1-ubiquitin conjugates were only slightly visible as a very faint band above the unmodified-Keap1 band at the 20 minute timepoint for both Keap1-WT and C151W, suggesting that the Keap1 ubiquitination reaction is a rare event in the *in vitro* assay and not influenced by Cys151 alone. Previous described experiments by the Hannink lab showed an increase in Keap1 ubiquitination after modification by an electrophilic ARE-inducer that has also been shown to modify Cys151. Together with our results, it is believed that the modification of Cys151 alone is insufficient to cause an increase in the ubiquitination of Keap1. Because ARE-inducers modify more than one cysteine, additional cysteine besides Cys151 must play an additional, required role in the switch of ubiquitination from Nrf2 to Keap1. These results support the model that initial assault to the complex by oxidation affects Nrf2 ubiquitination first through the most reactive cysteine, 151. Then, as oxidation builds, resulting in modification of other Keap1 cysteines, further structural changes take place exposing Keap1 lysines for ubiquitination.

Mutation of position 151 to a serine affects the complex in a much different way. In the *in vitro* ubiquitination assay, when Keap1-C151S is used, Nrf2 ubiquitination occurs at a much more rapid rate when compared to wild type Keap1 (Figure 36). The inability of a serine at position 151 to undergo cysteine oxidation or form disulfide bonds may be the reason for this increased activity compared to wild type. Disulfide bond formation leading to oligomerization can result in inactive protein, lowering the effective concentration of E3 ligase complex in solution. Cys151 may be oxidized despite the presence of the reducing agent DTT or TCEP. The interaction of Cys151 and the reducing agents themselves may also play a role. Experimental results for the wild type complex tend to lie between the two functional mutants. Therefore Keap1-C151S likely represents a population of Keap1 completely free of any modification at position 151, and Keap1-C151W represents a population of Keap1 entirely modified at position 151.

AUC analysis shows differences in the wild type and mutant complexes. This difference is most likely due to the differences in affinity of Cul3/Rbx1 for each of the Keap1 proteins. The apparent sedimentation observed in AUC velocity experiments for rapidly interconverting species represents an average of the particles in solution. This may be why the Cul3/Rbx1:Keap1-C151W complex sedimentation coefficient is much different than the wild type or the C151S-containing complex, which have been shown to have stronger interactions. The stronger interaction results in less interconversion of species and less averaging of the sample components into a singular species. In addition, no amount of free Keap1-C151W was observed in the experiment, indicating that although modification decreases the interaction with Cul3, it is still strong enough to form a complex at the concentrations tested.

The SAXS data yielded information about the relative positioning of domains within each of the wild type and mutant complexes. It is believed that the observed differences are due to structural changes in the way these proteins combine together and not due to the dissociative effect of modification. Through analysis of the conformational differences between the wild type and mutant complexes, a rudimentary model of Cys151-dependent modification-induced signaling by this complex has been created (Figure 45). This model describes how increased molecular mass, positioned on the side chain of residue 151 within the BTB domain of Keap1, causes a pivoting of the Keap1 axis with respect to Cul3 and Rbx1. The pivoting movement is hypothesized to bring Keap1's substrate binding domains out of proper orientation and alignment with Rbx1's E2-recruitment site, thereby preventing the proper ubiquitination of the target substrate, Nrf2.

The regeneration scouting trial results from the surface plasmon resonance experiments are consistent with interacting surfaces composed of mostly hydrophobic residues, which have a slightly greater tendency to form non-specific interactions when compared to highly ionic interacting surfaces. Hydrophobic interactions are driven by the increase in entropy for the solvation by water molecules and are not direct interactions, like ionic bonds. This leads to a greater freedom in the orientation of binding. A shifting of the interface by only a few angstroms, such as from the addition of a bulky side chain, can result in large changes in position in other parts of the molecule, similar to the action seen by a lever and an off-set fulcrum, where a small displacement on one side of the lever translates into a larger displacement on the other side. These results support the hypothesis that the tryptophan mutation's added bulk, compared to wild type, at position 151 alters the effective binding surface for Cul3, resulting in a less stable complex that falls apart into its components more

readily and when formed, has a slightly altered structure that is in a less favorable orientation for the ubiquitination reaction to occur on target Nrf2 lysines.

As mentioned in the discussion of Chapter 4, Keap1 rapidly experiences oxidation and subsequent precipitation from solution under conditions of increased temperature or oxygen tension. Despite taking precautions against this, Keap1's solubility issues greatly complicated the surface plasmon resonance experiments. Desorb and sanitization protocols, normally performed after numerous experiments, had to be performed after every experiment, otherwise the next set of experimental results was nonsensical, due to clogged tubes and inappropriate injection concentrations as a result of this precipitation. This effect seemed to be the greatest in the C151W mutant, which hampered our ability to achieve many data sets. A great deal of time and reagents were spent trying to acquire useable data sets for analysis of that mutant.

Mass spectrometry has shown us that Cul3 Cys636 is modified by isoliquiritigenin. This is also observed when bound to Keap1-WT, yet not observed as modified when bound to Keap1-C151W. This differential modification of Cul3 Cys636 implies that the binding of C151W to Cul3 results in a different conformation than the binding of wild type Keap1 to Cul3 and that this difference may be propagated through the Cul3 protein where it has an effect on the reactivity or accessibility of the cysteine at position 636 (104). In the LC-MS/MS investigation, Cul3 Cys636 is identified for the first time as a reactive cysteine and it is possibly another promising sensor for ARE activation. Further detailed investigation is needed to determine the role of Cul3 C636 in ARE activation.

All of the information gained from the experiments performed as part of this dissertation point to differences in the structure and catalysis of the E3 ubiquitin ligase

complex that Cul3/Rbx1 forms with Keap1 or its functional mutants. In addition to the conformational change model illustrated above, a differential rate equation model was developed to explain the observed differences in ubiquitination rates between samples containing Keap1-WT, C151W, or C151S proteins (Figure 46). This model highlights how mutation of Keap1 at position 151 affects the formation and activity rate of the Cul3/Rbx1:Keap1 complex.

As with any other enzymatic reaction, the rate of the reaction is dependent on the concentration of the enzyme, in this case, the rate of ubiquitination is dependent on the concentration of the Cul3/Rbx1:Keap1 complex. As seen in other systems, any factors affecting the formation of the complex and the conformational orientation of catalytic residues will also affect the catalytic rate of the reaction (105). In the system studied here, the formation of the complex is affected by Keap1 Cys151 mutation. In addition, it appears that the orientation of important catalytic residues or binding surfaces may also be affected. The combination of these effects is now believed to culminate in the observed differences of Nrf2 ubiquitination seen in the *in vitro* assay with Keap1 function mutants.

In conclusion, we theorize that modification of Keap1 to a tryptophan at position 151 lowers the rate of Nrf2 ubiquitination by compromising both the stability and the orientation of catalytic residues. This dramatic effect on the function of the protein-complex is believed to be due a conformational change that results in an altered interaction with Cul3. The altered interaction has a higher dissociation constant, as observed by SPR and AUC, and results in a different overall shape, suggested by SAXS data analysis. Nrf2 ubiquitination is significantly affected by these changes. Further modification by electrophiles, resulting in multiple Keap1

cysteine adducts, is believed to result in an even greater conformational change that exposes Keap1 lysine residues for ubiquitination.

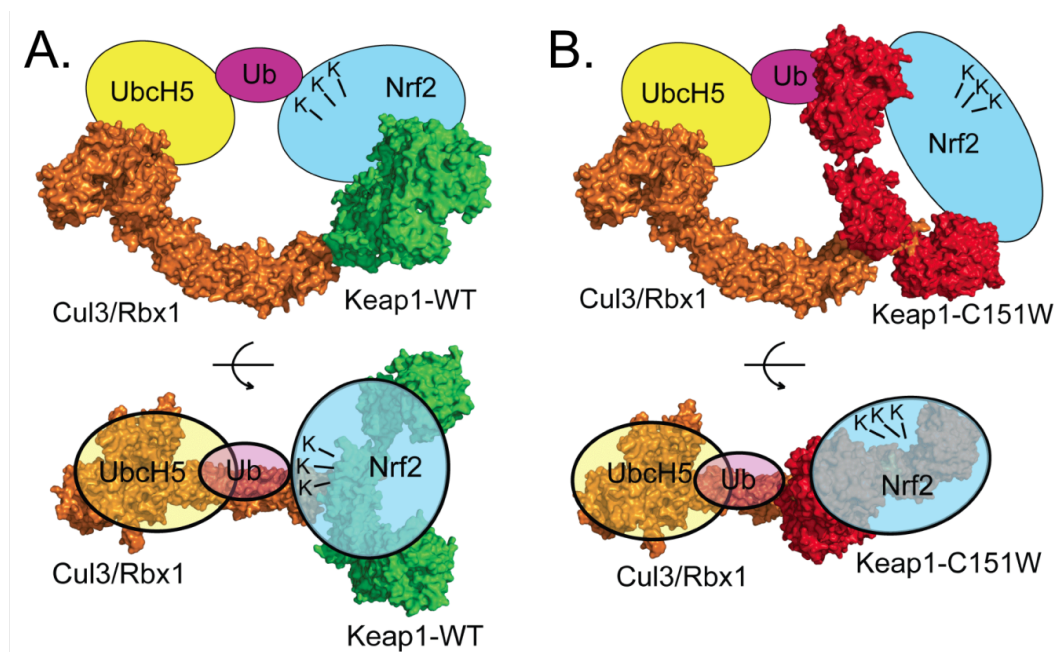


Figure 45. Conformational Change Model of Ubiquitination Impairment

Based on the results of the experiments in this chapter, a conformational change model was created where Nrf2-bound wild type Keap1 binds to Cul3 orienting Nrf2's lysines for ubiquitination by the ubiquitin-charged UbcH5 (A). When modification of Keap1 Cys151 occurs, an alteration, in binding, causes a realignment of Keap1's substrate binding domains. This realignment is hypothesized to cause Nrf2's lysines to be in a less optimal orientation, leading to a decreased rate of ubiquitination (B).



$$K_d^w > K_d^c > K_d^s$$

$$k_{cat}^w < k_{cat}^c < k_{cat}^s$$

Figure 46. Differential Rate Model Summarizing Cul3/Rbx1:Keap1 Complex Formation and Catalysis

Cited Literature

1. Hershko, A. (2005) The ubiquitin system for protein degradation and some of its roles in the control of the cell division cycle, *Cell Death Differ* 12, 1191-1197.
2. Ye, Y., and Rape, M. (2009) Building ubiquitin chains: E2 enzymes at work, *Nat Rev Mol Cell Biol* 10, 755-764.
3. Hershko, A., and Ciechanover, A. (1998) The ubiquitin system, *Annual review of biochemistry* 67, 425-479.
4. Willems, A. R., Schwab, M., and Tyers, M. (2004) A hitchhiker's guide to the cullin ubiquitin ligases: SCF and its kin, *Biochimica et biophysica acta* 1695, 133-170.
5. Zheng, N., Schulman, B. A., Song, L., Miller, J. J., Jeffrey, P. D., Wang, P., Chu, C., Koepf, D. M., Elledge, S. J., Pagano, M., Conaway, R. C., Conaway, J. W., Harper, J. W., and Pavletich, N. P. (2002) Structure of the Cul1-Rbx1-Skp1-F boxSkp2 SCF ubiquitin ligase complex, *Nature* 416, 703-709.
6. Pintard, L., Willems, A., and Peter, M. (2004) Cullin-based ubiquitin ligases: Cul3-BTB complexes join the family, *The EMBO journal* 23, 1681-1687.
7. Petroski, M. D., and Deshaies, R. J. (2005) Function and regulation of cullin-RING ubiquitin ligases, *Nature reviews. Molecular cell biology* 6, 9-20.
8. Woelk, T., Sigismund, S., Penengo, L., and Polo, S. (2007) The ubiquitination code: a signalling problem, *Cell division* 2, 11.
9. Copple, I. M., Goldring, C. E., Kitteringham, N. R., and Park, B. K. (2008) The Nrf2-Keap1 defence pathway: role in protection against drug-induced toxicity, *Toxicology* 246, 24-33.
10. Itoh, K., Wakabayashi, N., Katoh, Y., Ishii, T., O'Connor, T., and Yamamoto, M. (2003) Keap1 regulates both cytoplasmic-nuclear shuttling and degradation of Nrf2 in response to electrophiles, *Genes to cells : devoted to molecular & cellular mechanisms* 8, 379-391.
11. Sekhar, K. R., Yan, X. X., and Freeman, M. L. (2002) Nrf2 degradation by the ubiquitin proteasome pathway is inhibited by KIAA0132, the human homologue to INrf2, *Oncogene* 21, 6829-6834.
12. Itoh, K., Chiba, T., Takahashi, S., Ishii, T., Igarashi, K., Katoh, Y., Oyake, T., Hayashi, N., Satoh, K., Hatayama, I., Yamamoto, M., and Nabeshima, Y. (1997) An Nrf2/small Maf heterodimer mediates the induction of phase II detoxifying enzyme genes through antioxidant response elements, *Biochemical and biophysical research communications* 236, 313-322.
13. Tang, X., Orlicky, S., Lin, Z., Willems, A., Neculai, D., Ceccarelli, D., Mercurio, F., Shilton, B. H., Sicheri, F., and Tyers, M. (2007) Suprafacial orientation of the SCFCdc4 dimer accommodates multiple geometries for substrate ubiquitination, *Cell* 129, 1165-1176.
14. Kamura, T., Conrad, M. N., Yan, Q., Conaway, R. C., and Conaway, J. W. (1999) The Rbx1 subunit of SCF and VHL E3 ubiquitin ligase activates Rub1 modification of cullins Cdc53 and Cul2, *Genes & development* 13, 2928-2933.
15. Kamura, T., Koepf, D. M., Conrad, M. N., Skowyra, D., Moreland, R. J., Iliopoulos, O., Lane, W. S., Kaelin, W. G., Jr., Elledge, S. J., Conaway, R. C., Harper, J. W., and Conaway, J. W. (1999) Rbx1, a component of the VHL tumor suppressor complex and SCF ubiquitin ligase, *Science (New York, N.Y.)* 284, 657-661.
16. Xu, L., Wei, Y., Reboul, J., Vaglio, P., Shin, T. H., Vidal, M., Elledge, S. J., and Harper, J. W. (2003) BTB proteins are substrate-specific adaptors in an SCF-like modular ubiquitin ligase containing CUL-3, *Nature* 425, 316-321.
17. Pintard, L., Willis, J. H., Willems, A., Johnson, J. L., Srayko, M., Kurz, T., Glaser, S., Mains, P. E., Tyers, M., Bowerman, B., and Peter, M. (2003) The BTB protein MEL-26 is a substrate-specific adaptor of the CUL-3 ubiquitin-ligase, *Nature* 425, 311-316.
18. Welcker, M., and Clurman, B. E. (2007) Fbw7/hCDC4 dimerization regulates its substrate interactions, *Cell division* 2, 7.
19. Li, Y., and Hao, B. Structural basis of dimerization-dependent ubiquitination by the SCF(Fbx4) ubiquitin ligase, *J Biol Chem* 285, 13896-13906.
20. Sporn, M. B. (1993) Chemoprevention of cancer, *Lancet* 342, 1211-1213.
21. Sporn, M. B., and Suh, N. (2000) Chemoprevention of cancer, *Carcinogenesis* 21, 525-530.
22. Sporn, M. B., and Suh, N. (2002) Chemoprevention: an essential approach to controlling cancer, *Nature reviews. Cancer* 2, 537-543.

23. Furukawa, M., and Xiong, Y. (2005) BTB protein Keap1 targets antioxidant transcription factor Nrf2 for ubiquitination by the Cullin 3-Roc1 ligase, *Molecular and cellular biology* 25, 162-171.
24. Fahey, J. W., Zhang, Y., and Talalay, P. (1997) Broccoli sprouts: an exceptionally rich source of inducers of enzymes that protect against chemical carcinogens, *Proc Natl Acad Sci U S A* 94, 10367-10372.
25. Lee, C. K., Son, S. H., Park, K. K., Park, J. H., Lim, S. S., and Chung, W. Y. (2008) Isoliquiritigenin inhibits tumor growth and protects the kidney and liver against chemotherapy-induced toxicity in a mouse xenograft model of colon carcinoma, *Journal of pharmacological sciences* 106, 444-451.
26. Chauhan, D. P. (2002) Chemotherapeutic potential of curcumin for colorectal cancer, *Current pharmaceutical design* 8, 1695-1706.
27. Gafner, S., Lee, S. K., Cuendet, M., Barth el emy, S., Vergnes, L., Labidalle, S., Mehta, R. G., Boone, C. W., and Pezzuto, J. M. (2004) Biologic evaluation of curcumin and structural derivatives in cancer chemoprevention model systems, *Phytochemistry* 65, 2849-2859.
28. Huang, M. T., Ma, W., Yen, P., Xie, J. G., Han, J., Frenkel, K., Grunberger, D., and Conney, A. H. (1997) Inhibitory effects of topical application of low doses of curcumin on 12-O-tetradecanoylphorbol-13-acetate-induced tumor promotion and oxidized DNA bases in mouse epidermis, *Carcinogenesis* 18, 83-88.
29. Itoh, K., Wakabayashi, N., Katoh, Y., Ishii, T., Igarashi, K., Engel, J. D., and Yamamoto, M. (1999) Keap1 represses nuclear activation of antioxidant responsive elements by Nrf2 through binding to the amino-terminal Neh2 domain, *Genes & Development* 13, 76-86.
30. Dinkova-Kostova, A. T., Holtzclaw, W. D., Cole, R. N., Itoh, K., Wakabayashi, N., Katoh, Y., Yamamoto, M., and Talalay, P. (2002) Direct evidence that sulfhydryl groups of Keap1 are the sensors regulating induction of phase 2 enzymes that protect against carcinogens and oxidants, *Proceedings of the National Academy of Sciences of the United States of America* 99, 11908-11913.
31. Kang, M. I., Kobayashi, A., Wakabayashi, N., Kim, S. G., and Yamamoto, M. (2004) Scaffolding of Keap1 to the actin cytoskeleton controls the function of Nrf2 as key regulator of cytoprotective phase 2 genes, *Proceedings of the National Academy of Sciences of the United States of America* 101, 2046-2051.
32. Hayes, J. D., and McMahon, M. (2001) Molecular basis for the contribution of the antioxidant responsive element to cancer chemoprevention, *Cancer letters* 174, 103-113.
33. Motohashi, H., and Yamamoto, M. (2004) Nrf2-Keap1 defines a physiologically important stress response mechanism, *Trends in molecular medicine* 10, 549-557.
34. Kobayashi, A., Kang, M. I., Okawa, H., Ohtsuji, M., Zenke, Y., Chiba, T., Igarashi, K., and Yamamoto, M. (2004) Oxidative stress sensor Keap1 functions as an adaptor for Cul3-based E3 ligase to regulate proteasomal degradation of Nrf2, *Molecular and cellular biology* 24, 7130-7139.
35. Wakabayashi, N., Dinkova-Kostova, A. T., Holtzclaw, W. D., Kang, M. I., Kobayashi, A., Yamamoto, M., Kensler, T. W., and Talalay, P. (2004) Protection against electrophile and oxidant stress by induction of the phase 2 response: fate of cysteines of the Keap1 sensor modified by inducers, *Proceedings of the National Academy of Sciences of the United States of America* 101, 2040-2045.
36. Luo, Y., Egger, A. L., Liu, D., Liu, G., Mesecar, A. D., and van Breemen, R. B. (2007) Sites of alkylation of human Keap1 by natural chemoprevention agents, *Journal of the American Society for Mass Spectrometry* 18, 2226-2232.
37. Holland, R., Hawkins, A. E., Egger, A. L., Mesecar, A. D., Fabris, D., and Fishbein, J. C. (2008) Prospective Type 1 and Type 2 Disulfides of Keap1 Protein, *Manuscript to be submitted*.
38. Dinkova-Kostova, A. T., Holtzclaw, W. D., and Kensler, T. W. (2005) The role of Keap1 in cellular protective responses, *Chemical research in toxicology* 18, 1779-1791.
39. Li, X., Zhang, D., Hannink, M., and Beamer, L. J. (2004) Crystal structure of the Kelch domain of human Keap1, *The Journal of biological chemistry* 279, 54750-54758.
40. Stogios, P. J., Chen, L., and Prive, G. G. (2007) Crystal structure of the BTB domain from the LRF/ZBTB7 transcriptional regulator, *Protein Sci* 16, 336-342.
41. Stead, M. A., Trinh, C. H., Garnett, J. A., Carr, S. B., Baron, A. J., Edwards, T. A., and Wright, S. C. (2007) A beta-sheet interaction interface directs the tetramerisation of the Miz-1 POZ domain, *J Mol Biol* 373, 820-826.
42. Li, X., Peng, H., Schultz, D. C., Lopez-Guisa, J. M., Rauscher, F. J., 3rd, and Marmorstein, R. (1999) Structure-function studies of the BTB/POZ transcriptional repression domain from the promyelocytic leukemia zinc finger oncoprotein, *Cancer research* 59, 5275-5282.

43. Stogios, P. (2007) BTB Domain Overview.
44. Tong, K. I., Katoh, Y., Kusunoki, H., Itoh, K., Tanaka, T., and Yamamoto, M. (2006) Keap1 recruits Neh2 through binding to ETGE and DLG motifs: characterization of the two-site molecular recognition model, *Molecular and cellular biology* 26, 2887-2900.
45. Tong, K. I., Kobayashi, A., Katsuoka, F., and Yamamoto, M. (2006) Two-site substrate recognition model for the Keap1-Nrf2 system: a hinge and latch mechanism, *Biological chemistry* 387, 1311-1320.
46. Tong, K. I., Padmanabhan, B., Kobayashi, A., Shang, C., Hirotsu, Y., Yokoyama, S., and Yamamoto, M. (2007) Different electrostatic potentials define ETGE and DLG motifs as hinge and latch in oxidative stress response, *Molecular and cellular biology* 27, 7511-7521.
47. Padmanabhan, B., Tong, K. I., Kobayashi, A., Yamamoto, M., and Yokoyama, S. (2008) Structural insights into the similar modes of Nrf2 transcription factor recognition by the cytoplasmic repressor Keap1, *Journal of synchrotron radiation* 15, 273-276.
48. Egger, A. L., Luo, Y., van Breemen, R. B., and Mesecar, A. D. (2007) Identification of the highly reactive cysteine 151 in the chemopreventive agent-sensor Keap1 protein is method-dependent, *Chemical research in toxicology* 20, 1878-1884.
49. Zhang, D. D., and Hannink, M. (2003) Distinct cysteine residues in Keap1 are required for Keap1-dependent ubiquitination of Nrf2 and for stabilization of Nrf2 by chemopreventive agents and oxidative stress, *Molecular and cellular biology* 23, 8137-8151.
50. Egger, A. L., Small, E., Hannink, M., and Mesecar, A. D. (2009) Cul3-mediated Nrf2 ubiquitination and antioxidant response element (ARE) activation are dependent on the partial molar volume at position 151 of Keap1, *Biochem J* 422, 171-180.
51. Rachakonda, G., Xiong, Y., Sekhar, K. R., Stamer, S. L., Liebler, D. C., and Freeman, M. L. (2008) Covalent modification at Cys151 dissociates the electrophile sensor Keap1 from the ubiquitin ligase CUL3, *Chemical research in toxicology* 21, 705-710.
52. Zhang, D. D., Lo, S. C., Sun, Z., Habib, G. M., Lieberman, M. W., and Hannink, M. (2005) Ubiquitination of Keap1, a BTB-Kelch substrate adaptor protein for Cul3, targets Keap1 for degradation by a proteasome-independent pathway, *J Biol Chem* 280, 30091-30099.
53. Holland, R., Hawkins, A. E., Egger, A. L., Mesecar, A. D., Fabris, D., and Fishbein, J. C. (2008) Prospective type 1 and type 2 disulfides of Keap1 protein, *Chem Res Toxicol* 21, 2051-2060.
54. Li, T., Pavletich, N. P., Schulman, B. A., and Zheng, N. (2005) High-level expression and purification of recombinant SCF ubiquitin ligases, *Methods Enzymol* 398, 125-142.
55. Angers, S., Li, T., Yi, X., MacCoss, M. J., Moon, R. T., and Zheng, N. (2006) Molecular architecture and assembly of the DDB1-CUL4A ubiquitin ligase machinery, *Nature* 443, 590-593.
56. Huang, D. T., Ayrault, O., Hunt, H. W., Taherbhoy, A. M., Duda, D. M., Scott, D. C., Borg, L. A., Neale, G., Murray, P. J., Roussel, M. F., and Schulman, B. A. (2009) E2-RING expansion of the NEDD8 cascade confers specificity to cullin modification, *Molecular cell* 33, 483-495.
57. Small, E., Egger, A., and Mesecar, A. D. (2010) Development of an efficient E. coli expression and purification system for a catalytically active, human Cullin3-RINGBox1 protein complex and elucidation of its quaternary structure with Keap1, *Biochem Biophys Res Commun.* 400(4), 471-5.
58. Li, T., Pavletich, N. P., Schulman, B. A., and Zheng, N. (2005) High-level expression and purification of recombinant SCF ubiquitin ligases, *Methods in enzymology* 398, 125-142.
59. Tolia, N. H., and Joshua-Tor, L. (2006) Strategies for protein coexpression in Escherichia coli, *Nat Methods* 3, 55-64.
60. Hong, F., Sekhar, K. R., Freeman, M. L., and Liebler, D. C. (2005) Specific patterns of electrophile adduction trigger Keap1 ubiquitination and Nrf2 activation, *The Journal of biological chemistry* 280, 31768-31775.
61. Zhang, D. D., Lo, S. C., Cross, J. V., Templeton, D. J., and Hannink, M. (2004) Keap1 is a redox-regulated substrate adaptor protein for a Cul3-dependent ubiquitin ligase complex, *Molecular and cellular biology* 24, 10941-10953.
62. Altschul, S. F., Gish, W., Miller, W., Myers, E. W., and Lipman, D. J. (1990) Basic local alignment search tool, *Journal of molecular biology* 215, 403-410.
63. Arnold, K., Bordoli, L., Kopp, J., and Schwede, T. (2006) The SWISS-MODEL workspace: a web-based environment for protein structure homology modelling, *Bioinformatics (Oxford, England)* 22, 195-201.
64. Kiefer, F., Arnold, K., Künzli, M., Bordoli, L., and Schwede, T. (2009) The SWISS-MODEL Repository and associated resources, *Nucleic acids research* 37, D387-392.

65. Guex, N., and Peitsch, M. C. (1997) SWISS-MODEL and the Swiss-PdbViewer: an environment for comparative protein modeling, *Electrophoresis* 18, 2714-2723.
66. DeLano, W. L. (2002) *The PyMOL Molecular Graphics System.*, DeLano Scientific, San Carlos, CA, USA.
67. Smolle, M., Prior, A. E., Brown, A. E., Cooper, A., Byron, O., and Lindsay, J. G. (2006) A new level of architectural complexity in the human pyruvate dehydrogenase complex, *J Biol Chem* 281, 19772-19780.
68. Imai, M. (2007) Solution structure of the BACK domain Kelch repeat and BTB domain-containing protein 4.
69. Hao, B., Oehlmann, S., Sowa, M. E., Harper, J. W., and Pavletich, N. P. (2007) Structure of a Fbw7-Skp1-cyclin E complex: multisite-phosphorylated substrate recognition by SCF ubiquitin ligases, *Mol Cell* 26, 131-143.
70. Ogura, T., Tong, K. I., Mio, K., Maruyama, Y., Kurokawa, H., Sato, C., and Yamamoto, M. (2010) Keap1 is a forked-stem dimer structure with two large spheres enclosing the intervening, double glycine repeat, and C-terminal domains, *Proc Natl Acad Sci U S A* 107, 2842-2847.
71. Cole, J. L. a. H., J. C. . (1999) Analytical Ultracentrifugation as a Contemporary Biomolecular Research Tool.
72. Demeler, B. Methods for the design and analysis of sedimentation velocity and sedimentation equilibrium experiments with proteins, *Curr Protoc Protein Sci Chapter 7*, Unit 7 13.
73. Laue, T. M. (1996) Choosing which optical system of the Optima XL-I analytical ultracentrifuge to use., in *Beckman Publication*.
74. MacGregor, I. K., Anderson, A. L., and Laue, T. M. (2004) Fluorescence detection for the XLI analytical ultracentrifuge, *Biophys Chem* 108, 165-185.
75. Kingsbury, J. S., Laue, T. M., Klimtchuk, E. S., Theberge, R., Costello, C. E., and Connors, L. H. (2008) The modulation of transthyretin tetramer stability by cysteine 10 adducts and the drug diflunisal. Direct analysis by fluorescence-detected analytical ultracentrifugation, *J Biol Chem* 283, 11887-11896.
76. Kroe, R. R., and Laue, T. M. (2009) NUTS and BOLTS: applications of fluorescence-detected sedimentation, *Anal Biochem* 390, 1-13.
77. Karabudak, E., Wohlleben, W., and Colfen, H. Investigation of beta-carotene-gelatin composite particles with a multiwavelength UV/vis detector for the analytical ultracentrifuge, *Eur Biophys J* 39, 397-403.
78. Svergun, D. I., and Koch, M. H. (2002) Advances in structure analysis using small-angle scattering in solution, *Curr Opin Struct Biol* 12, 654-660.
79. Glatter, O. (1977) *J. Appl. Cryst.* 10, 415-421.
80. Moore, P. B. (1980) *J. Appl. Cryst.* 13, 168-175.
81. Provencher, S. W. (1982) *Computer Phys. Commun.* 27, 213-227, 229-242.
82. Svergun, D. I. a. S., A.V. . (1987) *Doklady AN SSSR* 297, 1373-1377.
83. Svergun, D. I., Semenyuk, A.V. and Feigin, L.A. (1988) *Acta Cryst.* A44, 244-250.
84. Svergun D.I. (1991). *J. Appl. Cryst.*, 485-492. (1991) *J. Appl. Cryst.* 24.
85. Svergun D.I. (1992). *J. Appl. Cryst.*, -. (1992) *J. Appl. Cryst.*, 495-503.
86. Tikhonov, A. N. a. A., V.Ya. (1977) *Solution of Ill-Posed Problems.* , Wiley, New York.
87. Svergun, D. I. (1999) Restoring low resolution structure of biological macromolecules from solution scattering using simulated annealing, *Biophys J* 76, 2879-2886.
88. Volkov, W. a. S., D.I. (2003) Uniqueness of ab initio shape determination in small-angle scattering., *J. Appl. Cryst.* 36, 860-864.
89. Konarev, P. V., Petoukho, M.V., Volkov, V.V., Svergun, D.I. (2006) ATSAS 2.1, a program package for small-angle scattering data analysis., *J. Appl. Cryst.* 39, 277-286.
90. Demeler. (2010) Discussion of 2DSA Noise-Fitting Procedures, (Small, E., Ed.), San Antonio, Texas.
91. Franke, D. a. S., D.I. (2009) DAMMIF, a program for rapid ab-initio shape determination in small-angle scattering., *J. Appl. Cryst.* 42, 342-346.
92. Ogura, T., Tong, K. I., Mio, K., Maruyama, Y., Kurokawa, H., Sato, C., and Yamamoto, M. Keap1 is a forked-stem dimer structure with two large spheres enclosing the intervening, double glycine repeat, and C-terminal domains, *Proc Natl Acad Sci U S A* 107, 2842-2847.
93. Heller, W. (2008) Discussion of Pair Distribution Function Shapes and Dmax Scouting Procedures, (Small, E., Ed.), Oak Ridge, Tennessee.

94. McMahon, M., Thomas, N., Itoh, K., Yamamoto, M., and Hayes, J. D. (2006) Dimerization of substrate adaptors can facilitate cullin-mediated ubiquitylation of proteins by a "tethering" mechanism: a two-site interaction model for the Nrf2-Keap1 complex, *The Journal of biological chemistry* 281, 24756-24768.
95. Balbo, A., and Schuck, P. (2005) Analytical Ultracentrifugation in the Study of Protein Self-association and Heterogeneous Protein-Protein Interactions, in *Protein-Protein Interactions: A Molecular Cloning Manual* (Golemis, E., and Adams, P. D., Eds.), p 262, Cold Spring Harbor Laboratory Press, New York.
96. Zhang, D. D., and Hannink, M. (2003) Distinct cysteine residues in Keap1 are required for Keap1-dependent ubiquitination of Nrf2 and for stabilization of Nrf2 by chemopreventive agents and oxidative stress, *Mol Cell Biol* 23, 8137-8151.
97. Satoh, T., Okamoto, S. I., Cui, J., Watanabe, Y., Furuta, K., Suzuki, M., Tohyama, K., and Lipton, S. A. (2006) Activation of the Keap1/Nrf2 pathway for neuroprotection by electrophilic [correction of electrophilic] phase II inducers, *Proc Natl Acad Sci U S A* 103, 768-773.
98. Sakurai, T., Kanayama, M., Shibata, T., Itoh, K., Kobayashi, A., Yamamoto, M., and Uchida, K. (2006) Ebselen, a seleno-organic antioxidant, as an electrophile, *Chem Res Toxicol* 19, 1196-1204.
99. Egger, A. L., Liu, G., Pezzuto, J. M., van Breemen, R. B., and Mesecar, A. D. (2005) Modifying specific cysteines of the electrophile-sensing human Keap1 protein is insufficient to disrupt binding to the Nrf2 domain Neh2, *Proceedings of the National Academy of Sciences of the United States of America* 102, 10070-10075.
100. Demeler, B. Methods for the design and analysis of sedimentation velocity and sedimentation equilibrium experiments with proteins, *Curr Protoc Protein Sci Chapter*, Unit 7.13.
101. Hu, C. (2010) Mass Spectrometry Analysis of Nrf2-Keap1 Chemoprevention Signaling Pathway, in *Doctoral Dissertation*, University of Illinois at Chicago.
102. Bilsel, O., and Matthews, C. R. (2006) Molecular dimensions and their distributions in early folding intermediates, *Curr Opin Struct Biol* 16, 86-93.
103. Receveur, V., Czjzek, M., Schulein, M., Panine, P., and Henrissat, B. (2002) Dimension, shape, and conformational flexibility of a two domain fungal cellulase in solution probed by small-angle X-ray scattering, *J Biol Chem* 277, 40887-40892.
104. Yu, E. W., and Koshland, D. E., Jr. (2001) Propagating conformational changes over long (and short) distances in proteins, *Proc Natl Acad Sci U S A* 98, 9517-9520.
105. Mesecar, A. D., Stoddard, B. L., and Koshland, D. E., Jr. (1997) Orbital steering in the catalytic power of enzymes: small structural changes with large catalytic consequences, *Science* 277, 202-206.

Appendix A – Codon-optimized Cul3 and Rbx1 Sequences

{Restriction enzyme and Thrombin cut sequences shown in black}

{Extra nucleotides for in-frame translation shown in red}

{Protein-of-interest sequences shown in blue}

Codon-optimized Rbx1 Sequence

GGATCC {BamH I cut sequence}
G {added for proper in frame reading}
 CTGGTGCCGCGCGGCAGC {Thrombin cut sequence}

ATGGCAGCCGCTATGGACGTAGATACCCCGAGCGGCACCAACTCCGGTGCCGGT
 AAGAAACGTTTCGAAGTGAAAAATGGAACGCTGTGGCACTGTGGGCGTGGGAT
 ATCGTTGTTGATAACTGCGCGATTTGTCGTAACCACATCATGGACCTGTGTATCGA
 ATGCCAGGCGAACCAAGCGTCTGCAACTTCCGAAGAATGTACCGTTGCTTGGGGC
 GTATGCAATCACGCTTTCATTTTCATTGCATTTCTCGCTGGCTGAAAACCTCGCCA
 GGTCTGCCCGCTGGACAACCGTGAGTGGGAATTCAGAAATACGGTCACTAA

AAGCTT {Hind III cut sequence}

Codon-optimized Cul3 Sequence

CAT {Nde I cut sequence}

ATGAGCAACCTCAGCAAAGGTACTGGCAGCCGTAAGGATACGAAAATGCGTATC
 CGTGCGTTTCCGATGACGATGGATGAAAAATATGTTAACAGCATCTGGGACCTCC
 TCAAGAACGCCATTCAGGAGATTCAGCGTAAAAACAACAGCGGCCTGTCCTTCGA
 AGAACTGTATCGCAACGCGTATACCATGGTTCTCCACAAACACGGTGAGAAACTG
 TATACCGGCCTGCGTGAAGTCGTTACCGAACATCTGATCAACAAAGTTCGTGAAG
 ACGTTCTGAACTCCCTGAACAACAACCTTCTGCAAACCTTGAACCAGGCGTGGAA
 CGATCACCAGACCGCAATGGTTATGATCCGTGATATCCTTATGTACATGGATCGC
 GTCTACGTGCAGCAGAACAACGTTGAGAACGTTTACAACCTGGGCCTGATTATTT
 TCCGTGATCAAGTAGTCCGTTATGGTTGCATCCGTGACCACCTGCGCCAGACCTT
 GCTGGACATGATTGCACGCGAACGTAAAGGTGAAGTCGTAGATCGTGGCGCGAT
 CCGCAATGCCTGCCAGATGCTGATGATTCTGGGTCTGGAAGGCCGCTCCGTTTAT
 GAAGAAGACTTCGAAGCGCCGTTCTGGAATGTCTGCTGAATTCTTCCAAATGG
 AATCTCAGAAGTTTCTGGCGGAAAACAGCGCATCTGTGTATATCAAGAAAGTTGA
 GGCACGCATCAATGAAGAGATCGAACGCGTGATGCACTGTCTGGACAAATCCAC
 CGAAGAACCGATTGTAAAAGTAGTGAACGTGAACTGATCTCAAACACATGAA
 GACGATTGTGGAATGGAGAACTCGGGCCTGGTCCACATGCTCAAAAACGGTAA
 GACTGAAGACCTGGGTTGTATGTACAAACTGTTCTCCCGTGTGCCAAACGGCCTG
 AAAACTATGTGCGAATGCATGAGCTCCTATCTGCGCGAGCAGGGCAAAGCTCTGG
 TTTCCGAAGAAGGTGAGGGTAAAAATCCGGTTGACTACATTCAGGGCCTGCTGGA

Appendix B – Homology Model – Keap1 Cysteine Residues

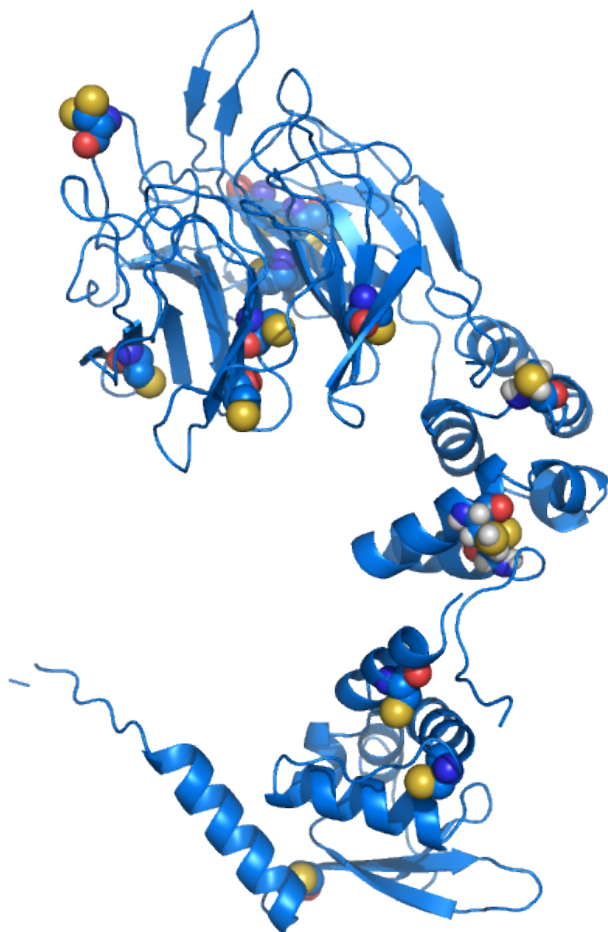


Figure 47 Keap1 Homology Model, shown with 16 cysteine residues distributed along the length of the protein. Cys151 is visible as the second cysteine from the bottom of the figure.

Appendix C – SEC – Proteins of Known Molecular Weight

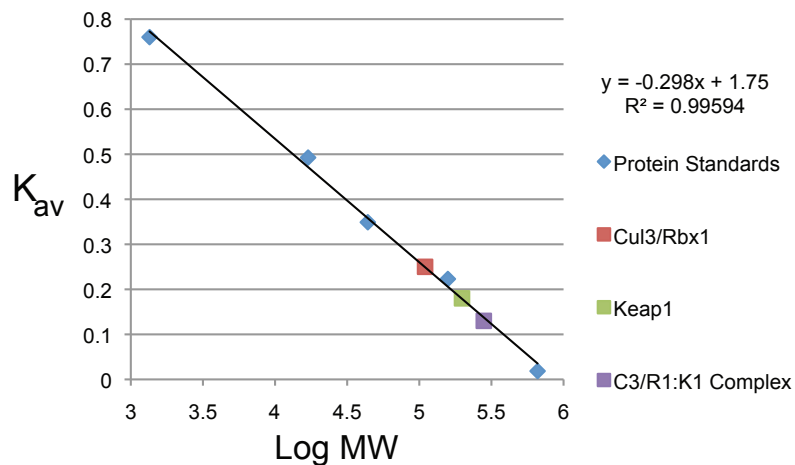


Figure 48. A standard curve derived from the analytical size exclusion data of Vitamin B12, myoglobin, ovalbumin, gamma globulin, and thyroglobulin. Also plotted are the K_{av} values calculated for the experimental samples.

Appendix D - AUC - Effect of DMSO on Keap1 Sedimentation Velocity

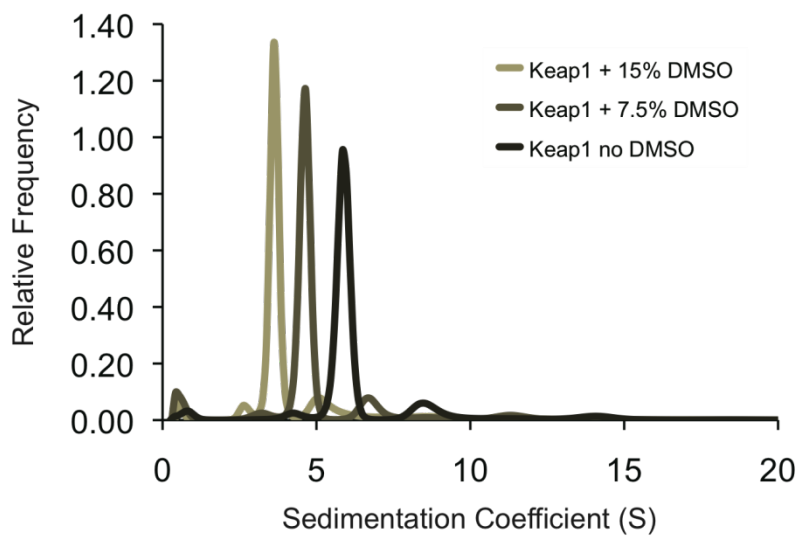


Figure 49. The Effect of DMSO on Keap1 Sedimentation Velocity

Appendix E – AUC – Cul3 and Keap1 vHW, 2DSA, GA, and GA-50 Analysis Reports

 * Enhanced van Holde - Weischet Analysis *

Data Report for Run "June10Chan1", Cell 1, Wavelength 1

Detailed Run Information:

Cell Description: Sample 4 Reference 1
 Raw Data Directory: /Users/seeyolater/ultrascan/data/June10Chan1/
 Rotor Speed: 42000 rpm
 Average Temperature: 25.1447 °C
 Temperature Variation: Within Tolerance
 Time Correction: 1 minute(s) 12 second(s)
 Run Duration: 5 hour(s) 40 minute(s)
 Wavelength: 280 nm
 Baseline Absorbance: -0.00970096 OD
 Meniscus Position: 5.79915 cm
 Edited Data starts at: 5.833 cm
 Edited Data stops at: 7.137 cm

Hydrodynamic Settings:

Viscosity correction: 1.02719
 Viscosity (absolute): 0.909858
 Density correction: 1.00585 g/ccm
 Density (absolute): 1.00464 g/ccm
 Vbar: 0.734629 ccm/g
 Vbar corrected for 20°C: 0.732442 ccm/g
 Buoyancy (Water, 20°C) : 0.268851
 Buoyancy (absolute) 0.261964
 Correction Factor: 0.931971

Data Analysis Settings:

Divisions: 50
 Smoothing Frame: 11
 Analyzed Boundary: 50 %
 Boundary Position: 25 %
 Selected Groups:

No groups were selected...

Average S: 4.73853
 Initial concentration from plateau fit: 0.129176 OD/fringes

Scan Information:

Scan: Corrected Time: Plateau Concentration:

1:	28 min 8 sec	0.124901 OD
2:	34 min 18 sec	0.123983 OD
3:	40 min 37 sec	0.12305 OD
4:	46 min 49 sec	0.122141 OD
5:	52 min 58 sec	0.121246 OD
6:	59 min 12 sec	0.120345 OD
7:	65 min 21 sec	0.119463 OD
8:	71 min 29 sec	0.11859 OD
9:	77 min 39 sec	0.117718 OD
10:	83 min 52 sec	0.116846 OD
11:	97 min 51 sec	0.114908 OD
12:	103 min 53 sec	0.114082 OD

13: 110 min 1 sec 0.113248 OD
 14: 116 min 8 sec 0.112422 OD
 15: 122 min 21 sec 0.111589 OD
 16: 128 min 25 sec 0.110783 OD
 17: 134 min 30 sec 0.109979 OD
 18: 140 min 35 sec 0.109182 OD
 19: 146 min 47 sec 0.108375 OD
 20: 152 min 48 sec 0.107598 OD
 21: 158 min 57 sec 0.106809 OD
 22: 164 min 59 sec 0.106041 OD
 23: 171 min 3 sec 0.105275 OD
 24: 177 min 10 sec 0.104507 OD
 25: 183 min 21 sec 0.103737 OD
 26: 189 min 38 sec 0.10296 OD
 27: 195 min 57 sec 0.102185 OD
 28: 202 min 2 sec 0.101445 OD
 29: 208 min 3 sec 0.100717 OD
 30: 214 min 3 sec 0.0999969 OD
 31: 220 min 7 sec 0.0992739 OD
 32: 226 min 10 sec 0.098558 OD
 33: 232 min 17 sec 0.0978396 OD
 34: 238 min 17 sec 0.0971399 OD
 35: 244 min 15 sec 0.0964491 OD
 36: 250 min 21 sec 0.0957479 OD
 37: 256 min 30 sec 0.0950462 OD
 38: 262 min 34 sec 0.0943589 OD
 39: 268 min 43 sec 0.0936673 OD
 40: 274 min 49 sec 0.0929864 OD
 41: 281 min 2 sec 0.0922975 OD
 42: 287 min 9 sec 0.0916247 OD
 43: 293 min 10 sec 0.0909676 OD
 44: 299 min 16 sec 0.0903063 OD
 45: 305 min 26 sec 0.0896426 OD
 46: 311 min 28 sec 0.088998 OD
 47: 317 min 42 sec 0.0883369 OD
 48: 323 min 50 sec 0.0876912 OD

Initial Concentration: 0.127325OD
 (Correlation. coeff.: -0.998892
 Standard Dev.: 0.00157834)

Initial Concentration from exponential fit: 0.129176OD

 * 2-dimensional Spectrum Analysis *

Data Report for Run "June10Chan1", Cell 1, Wavelength 1

Detailed Run Information:

Cell Description: Sample 4 Reference 1
 Raw Data Directory: /Users/seeyolater/ultrascan/data/June10Chan1/
 Rotor Speed: 42000 rpm
 Average Temperature: 25.1447 °C
 Temperature Variation: Within Tolerance
 Time Correction: 1 minute(s) 12 second(s)
 Run Duration: 5 hour(s) 40 minute(s)
 Wavelength: 280 nm
 Baseline Absorbance: 0.135835 OD
 Meniscus Position: 5.79915 cm
 Edited Data starts at: 5.833 cm
 Edited Data stops at: 7.137 cm

Hydrodynamic Settings:

Viscosity correction: 1.02719
 Viscosity (absolute): 0.909858
 Density correction: 1.00585 g/ccm
 Density (absolute): 1.00464 g/ccm
 Vbar: 0.734629 ccm/g
 Vbar corrected for 20°C: 0.732442 ccm/g
 Buoyancy (Water, 20°C) : 0.268851
 Buoyancy (absolute) 0.261963
 Correction Factor: 0.931974

Data Analysis Settings:

Number of Components: 12
 Residual Mean Square Deviation: 0.00448402
 Weight-Average sedimentation coefficient:

Weight Average S20,W: 5.1685e-13
 Weight Average D20,W: 6.4822e-07
 Weight Average Molecular Weight: 1.7648e+05
 Total concentration: 1.3256e-01

Distribution Information:

Molecular Weight:	S 20,W:	D 20,W:	concentration:	
1.5994e+05	2.6296e-13	1.4905e-07	1.4573e-03	(1.099 %)
7.7325e+05	7.5185e-13	8.8150e-08	3.6147e-03	(2.727 %)
5.6406e+05	6.0926e-13	9.7924e-08	5.2735e-03	(3.978 %)
4.6885e+03	1.0000e-13	1.9337e-06	2.3903e-02	(18.031 %)
3.7508e+04	1.0000e-13	2.4171e-07	2.6748e-04	(0.202 %)
1.9490e+05	1.2000e-12	5.5820e-07	1.3950e-02	(10.524 %)
9.1700e+04	4.6667e-13	4.6137e-07	4.8509e-02	(36.593 %)
7.9189e+05	8.3333e-13	9.5403e-08	2.4793e-03	(1.870 %)
6.5102e+05	6.7037e-13	9.3354e-08	4.7194e-03	(3.560 %)
1.6753e+05	5.2778e-13	2.8560e-07	1.8537e-02	(13.983 %)
1.9932e+05	5.4815e-13	2.4932e-07	9.8335e-03	(7.418 %)
9.6557e+04	2.0185e-13	1.8952e-07	2.0322e-05	(0.015 %)
1:	28 min 8 sec	0.255885 OD (3.259e+10, 3.259e+10)		
2:	34 min 18 sec	0.242617 OD (3.982e+10, 3.982e+10)		
3:	40 min 37 sec	0.235713 OD (4.715e+10, 4.715e+10)		
4:	46 min 49 sec	0.230196 OD (5.435e+10, 5.435e+10)		
5:	52 min 58 sec	0.232987 OD (6.15e+10, 6.15e+10)		
6:	59 min 12 sec	0.232069 OD (6.872e+10, 6.872e+10)		
7:	65 min 21 sec	0.230977 OD (7.587e+10, 7.587e+10)		
8:	71 min 29 sec	0.228831 OD (8.299e+10, 8.299e+10)		
9:	77 min 39 sec	0.231028 OD (9.015e+10, 9.015e+10)		
10:	83 min 52 sec	0.228672 OD (9.737e+10, 9.737e+10)		
11:	97 min 51 sec	0.229185 OD (1.135e+11, 1.135e+11)		
12:	103 min 53 sec	0.224768 OD (1.206e+11, 1.206e+11)		
13:	110 min 1 sec	0.225767 OD (1.277e+11, 1.277e+11)		
14:	116 min 8 sec	0.224083 OD (1.348e+11, 1.348e+11)		
15:	122 min 21 sec	0.22361 OD (1.42e+11, 1.42e+11)		
16:	128 min 25 sec	0.22357 OD (1.49e+11, 1.49e+11)		
17:	134 min 30 sec	0.2224 OD (1.561e+11, 1.561e+11)		
18:	140 min 35 sec	0.223154 OD (1.632e+11, 1.632e+11)		
19:	146 min 47 sec	0.220853 OD (1.703e+11, 1.703e+11)		
20:	152 min 48 sec	0.221083 OD (1.774e+11, 1.774e+11)		
21:	158 min 57 sec	0.218668 OD (1.845e+11, 1.845e+11)		
22:	164 min 59 sec	0.216767 OD (1.915e+11, 1.915e+11)		
23:	171 min 3 sec	0.217923 OD (1.985e+11, 1.985e+11)		
24:	177 min 10 sec	0.219642 OD (2.056e+11, 2.056e+11)		
25:	183 min 21 sec	0.218075 OD (2.128e+11, 2.128e+11)		
26:	189 min 38 sec	0.218207 OD (2.201e+11, 2.201e+11)		
27:	195 min 57 sec	0.215623 OD (2.274e+11, 2.274e+11)		
28:	202 min 2 sec	0.217515 OD (2.345e+11, 2.345e+11)		
29:	208 min 3 sec	0.210921 OD (2.415e+11, 2.415e+11)		
30:	214 min 3 sec	0.214601 OD (2.484e+11, 2.484e+11)		
31:	220 min 7 sec	0.214524 OD (2.555e+11, 2.555e+11)		

32:	226 min 10 sec	0.213529 OD (2.625e+11, 2.625e+11)
33:	232 min 17 sec	0.212762 OD (2.696e+11, 2.696e+11)
34:	238 min 17 sec	0.209504 OD (2.766e+11, 2.766e+11)
35:	244 min 15 sec	0.209385 OD (2.835e+11, 2.835e+11)
36:	250 min 21 sec	0.21209 OD (2.906e+11, 2.906e+11)
37:	256 min 30 sec	0.209266 OD (2.977e+11, 2.977e+11)
38:	262 min 34 sec	0.209436 OD (3.048e+11, 3.048e+11)
39:	268 min 43 sec	0.207175 OD (3.119e+11, 3.119e+11)
40:	274 min 49 sec	0.205789 OD (3.19e+11, 3.19e+11)
41:	281 min 2 sec	0.202078 OD (3.262e+11, 3.262e+11)
42:	287 min 9 sec	0.199076 OD (3.333e+11, 3.333e+11)
43:	293 min 10 sec	0.196703 OD (3.403e+11, 3.403e+11)
44:	299 min 16 sec	0.200225 OD (3.474e+11, 3.474e+11)
45:	305 min 26 sec	0.193165 OD (3.545e+11, 3.545e+11)
46:	311 min 28 sec	0.191592 OD (3.615e+11, 3.615e+11)
47:	317 min 42 sec	0.187398 OD (3.687e+11, 3.687e+11)
48:	323 min 50 sec	0.182753 OD (3.759e+11, 3.759e+11)

 * Genetic Algorithm Analysis *

Data Report for Run "June10Chan1", Cell 1, Wavelength 1

Detailed Run Information:

Cell Description: Sample 4 Reference 1
 Raw Data Directory: /Users/seejolater/ultrascan/data/June10Chan1/
 Rotor Speed: 42000 rpm
 Average Temperature: 25.1447 °C
 Temperature Variation: Within Tolerance
 Time Correction: 1 minute(s) 12 second(s)
 Run Duration: 5 hour(s) 40 minute(s)
 Wavelength: 280 nm
 Baseline Absorbance: -0.00970096 OD
 Meniscus Position: 5.79915 cm
 Edited Data starts at: 5.833 cm
 Edited Data stops at: 7.137 cm

Hydrodynamic Settings:

Viscosity correction: 1.02719
 Viscosity (absolute): 0.909858
 Density correction: 1.00585 g/ccm
 Density (absolute): 1.00464 g/ccm
 Vbar: 0.734629 ccm/g
 Vbar corrected for 20°C: 0.732442 ccm/g
 Buoyancy (Water, 20°C): 0.268851
 Buoyancy (absolute) 0.261964
 Correction Factor: 0.931971

Data Analysis Settings:

Number of Components: 4
 Residual Mean Square Deviation: 0.00393173
 Weight-Average sedimentation coefficient:

Weight Average S_{20,W}: 5.4811e-13
 Weight Average D_{20,W}: 6.7529e-07
 Weight Average Molecular Weight: 8.3939e+04
 Total concentration: 1.1703e-01

Distribution Information:

Molecular Weight: S_{20,W}: D_{20,W}: concentration:

1.6035e+04	2.2700e-13	1.2834e-06	1.1135e-02	(9.515 %)
7.0398e+04	5.0300e-13	6.4777e-07	8.5351e-02	(72.931 %)
1.6734e+05	6.2300e-13	3.3753e-07	9.6009e-03	(8.204 %)
1.8547e+05	1.1610e-12	5.6750e-07	1.0943e-02	(9.351 %)
1: 28 min 8 sec	0.112358 OD (3.259e+10, 3.259e+10)			
2: 34 min 18 sec	0.112921 OD (3.982e+10, 3.982e+10)			
3: 40 min 37 sec	0.112923 OD (4.715e+10, 4.715e+10)			
4: 46 min 49 sec	0.114988 OD (5.435e+10, 5.435e+10)			
5: 52 min 58 sec	0.113644 OD (6.15e+10, 6.15e+10)			
6: 59 min 12 sec	0.109204 OD (6.872e+10, 6.872e+10)			
7: 65 min 21 sec	0.108533 OD (7.587e+10, 7.587e+10)			
8: 71 min 29 sec	0.109683 OD (8.299e+10, 8.299e+10)			
9: 77 min 39 sec	0.109495 OD (9.015e+10, 9.015e+10)			
10: 83 min 52 sec	0.109244 OD (9.737e+10, 9.737e+10)			
11: 97 min 51 sec	0.105862 OD (1.135e+11, 1.135e+11)			
12: 103 min 53 sec	0.105169 OD (1.206e+11, 1.206e+11)			
13: 110 min 1 sec	0.103139 OD (1.277e+11, 1.277e+11)			
14: 116 min 8 sec	0.101355 OD (1.348e+11, 1.348e+11)			
15: 122 min 21 sec	0.104494 OD (1.42e+11, 1.42e+11)			
16: 128 min 25 sec	0.0988114 OD (1.49e+11, 1.49e+11)			
17: 134 min 30 sec	0.0987531 OD (1.561e+11, 1.561e+11)			
18: 140 min 35 sec	0.095823 OD (1.632e+11, 1.632e+11)			
19: 146 min 47 sec	0.0938875 OD (1.703e+11, 1.703e+11)			
20: 152 min 48 sec	0.0940323 OD (1.774e+11, 1.774e+11)			
21: 158 min 57 sec	0.0924857 OD (1.845e+11, 1.845e+11)			
22: 164 min 59 sec	0.093728 OD (1.915e+11, 1.915e+11)			
23: 171 min 3 sec	0.0938644 OD (1.985e+11, 1.985e+11)			
24: 177 min 10 sec	0.0906867 OD (2.056e+11, 2.056e+11)			
25: 183 min 21 sec	0.09112 OD (2.128e+11, 2.128e+11)			
26: 189 min 38 sec	0.0869429 OD (2.201e+11, 2.201e+11)			
27: 195 min 57 sec	0.0867278 OD (2.274e+11, 2.274e+11)			
28: 202 min 2 sec	0.0864424 OD (2.345e+11, 2.345e+11)			
29: 208 min 3 sec	0.0873009 OD (2.415e+11, 2.415e+11)			
30: 214 min 3 sec	0.0850864 OD (2.484e+11, 2.484e+11)			
31: 220 min 7 sec	0.0849725 OD (2.555e+11, 2.555e+11)			
32: 226 min 10 sec	0.0839218 OD (2.625e+11, 2.625e+11)			
33: 232 min 17 sec	0.0816689 OD (2.696e+11, 2.696e+11)			
34: 238 min 17 sec	0.0826696 OD (2.766e+11, 2.766e+11)			
35: 244 min 15 sec	0.0785491 OD (2.835e+11, 2.835e+11)			
36: 250 min 21 sec	0.0766401 OD (2.906e+11, 2.906e+11)			
37: 256 min 30 sec	0.0759027 OD (2.977e+11, 2.977e+11)			
38: 262 min 34 sec	0.0744067 OD (3.048e+11, 3.048e+11)			
39: 268 min 43 sec	0.0708483 OD (3.119e+11, 3.119e+11)			
40: 274 min 49 sec	0.0688247 OD (3.19e+11, 3.19e+11)			
41: 281 min 2 sec	0.0630085 OD (3.262e+11, 3.262e+11)			
42: 287 min 9 sec	0.0611069 OD (3.333e+11, 3.333e+11)			
43: 293 min 10 sec	0.057863 OD (3.403e+11, 3.403e+11)			
44: 299 min 16 sec	0.0549296 OD (3.474e+11, 3.474e+11)			
45: 305 min 26 sec	0.0499992 OD (3.545e+11, 3.545e+11)			
46: 311 min 28 sec	0.0467166 OD (3.615e+11, 3.615e+11)			
47: 317 min 42 sec	0.0434529 OD (3.687e+11, 3.687e+11)			
48: 323 min 50 sec	0.041341 OD (3.759e+11, 3.759e+11)			

 * 2-dimensional Spectrum Analysis *

Data Report for Run "June10Chan1", Cell 1, Wavelength 1

Detailed Run Information:

Cell Description: Sample 4 Reference 1
 Raw Data Directory: /Users/seeeyolater/ultrascan/data/June10Chan1/
 Rotor Speed: 42000 rpm
 Average Temperature: 25.1447 °C
 Temperature Variation: Within Tolerance
 Time Correction: 1 minute(s) 12 second(s)

Run Duration: 5 hour(s) 40 minute(s)
 Wavelength: 280 nm
 Baseline Absorbance: -0.00970096 OD
 Meniscus Position: 5.79915 cm
 Edited Data starts at: 5.833 cm
 Edited Data stops at: 7.137 cm

Hydrodynamic Settings:

Viscosity correction: 1.02719
 Viscosity (absolute): 0.909858
 Density correction: 1.00585 g/ccm
 Density (absolute): 1.00464 g/ccm
 Vbar: 0.734629 ccm/g
 Vbar corrected for 20°C: 0.732442 ccm/g
 Buoyancy (Water, 20°C): 0.268851
 Buoyancy (absolute) 0.261964
 Correction Factor: 0.931971

Data Analysis Settings:

Number of Components: 200
 Residual Mean Square Deviation: 0.00384583
 Weight-Average sedimentation coefficient:

Weight Average S_{20,W}: 5.5616e-13
 Weight Average D_{20,W}: 6.2719e-07
 Weight Average Molecular Weight: 9.3484e+04
 Total concentration: 1.1758e-01

Distribution Information:

Molecular Weight:	S _{20,W} :	D _{20,W} :	concentration:	
1.7432e+04	2.4000e-13	1.2482e-06	2.4612e-04	(0.209 %)
7.8865e+04	5.0500e-13	5.8052e-07	1.7382e-03	(1.478 %)
1.9625e+05	7.6300e-13	3.5248e-07	2.0951e-04	(0.178 %)
2.3101e+05	1.3440e-12	5.2745e-07	1.5828e-04	(0.135 %)
1.7541e+04	2.4100e-13	1.2456e-06	2.4568e-04	(0.209 %)
7.7957e+04	5.0500e-13	5.8729e-07	1.7401e-03	(1.480 %)
2.0590e+05	7.5900e-13	3.3419e-07	2.0415e-04	(0.174 %)
2.2587e+05	1.3240e-12	5.3142e-07	1.6082e-04	(0.137 %)
1.7760e+04	2.4300e-13	1.2404e-06	2.5096e-04	(0.213 %)
8.1368e+04	5.0400e-13	5.6155e-07	1.7174e-03	(1.461 %)
2.0266e+05	7.5100e-13	3.3596e-07	2.1944e-04	(0.187 %)
2.2357e+05	1.3150e-12	5.3323e-07	1.6248e-04	(0.138 %)
1.7323e+04	2.3900e-13	1.2508e-06	2.4263e-04	(0.206 %)
7.6377e+04	5.0600e-13	6.0062e-07	1.7592e-03	(1.496 %)
2.0082e+05	7.7800e-13	3.5123e-07	1.9548e-04	(0.166 %)
2.5783e+05	1.3390e-12	4.7082e-07	1.5368e-04	(0.131 %)
1.7432e+04	2.4000e-13	1.2482e-06	2.4511e-04	(0.208 %)
7.7281e+04	5.0600e-13	5.9359e-07	1.7540e-03	(1.492 %)
2.0624e+05	7.7400e-13	3.4023e-07	1.9282e-04	(0.164 %)
2.3415e+05	1.3040e-12	5.0488e-07	1.5666e-04	(0.133 %)
1.7323e+04	2.3900e-13	1.2508e-06	2.4466e-04	(0.208 %)
7.8865e+04	5.0500e-13	5.8052e-07	1.7427e-03	(1.482 %)
2.0766e+05	7.6800e-13	3.3529e-07	2.0625e-04	(0.175 %)
2.5085e+05	1.3270e-12	4.7959e-07	1.5672e-04	(0.133 %)
1.7323e+04	2.3900e-13	1.2508e-06	2.4364e-04	(0.207 %)
7.9540e+04	5.0400e-13	5.7446e-07	1.7340e-03	(1.475 %)
1.9702e+05	7.6500e-13	3.5202e-07	2.2037e-04	(0.187 %)
2.5496e+05	1.3670e-12	4.8609e-07	1.5537e-04	(0.132 %)
1.7541e+04	2.4100e-13	1.2456e-06	2.4408e-04	(0.208 %)
7.6377e+04	5.0600e-13	6.0062e-07	1.7596e-03	(1.497 %)
2.0830e+05	7.8400e-13	3.4123e-07	1.9771e-04	(0.168 %)
2.3775e+05	1.3700e-12	5.2242e-07	1.5210e-04	(0.129 %)
1.7215e+04	2.3800e-13	1.2534e-06	2.4269e-04	(0.206 %)

7.7281e+04	5.0600e-13	5.9359e-07	1.7600e-03	(1.497 %)
2.0870e+05	7.8500e-13	3.4101e-07	1.9581e-04	(0.167 %)
2.3318e+05	1.3390e-12	5.2060e-07	1.5264e-04	(0.130 %)
1.7760e+04	2.4300e-13	1.2404e-06	2.5170e-04	(0.214 %)
7.9099e+04	5.0600e-13	5.7995e-07	1.7382e-03	(1.478 %)
1.9702e+05	7.6500e-13	3.5202e-07	2.0359e-04	(0.173 %)
2.3691e+05	1.3400e-12	5.1278e-07	1.5818e-04	(0.135 %)
1.7215e+04	2.3800e-13	1.2534e-06	2.4266e-04	(0.206 %)
7.7957e+04	5.0500e-13	5.8729e-07	1.7451e-03	(1.484 %)
2.0753e+05	7.6300e-13	3.3331e-07	2.0350e-04	(0.173 %)
2.2664e+05	1.3270e-12	5.3082e-07	1.5962e-04	(0.136 %)
1.7215e+04	2.3800e-13	1.2534e-06	2.4169e-04	(0.206 %)
7.7052e+04	5.0500e-13	5.9418e-07	1.7452e-03	(1.484 %)
1.9274e+05	7.5700e-13	3.5607e-07	2.0173e-04	(0.172 %)
2.4576e+05	1.3090e-12	4.8288e-07	1.6053e-04	(0.137 %)
1.7106e+04	2.3700e-13	1.2561e-06	2.4067e-04	(0.205 %)
7.7052e+04	5.0500e-13	5.9418e-07	1.7472e-03	(1.486 %)
2.0509e+05	7.5700e-13	3.3463e-07	2.0002e-04	(0.170 %)
2.2332e+05	1.3140e-12	5.3344e-07	1.6217e-04	(0.138 %)
1.7541e+04	2.4100e-13	1.2456e-06	2.4681e-04	(0.210 %)
7.8865e+04	5.0500e-13	5.8052e-07	1.7388e-03	(1.479 %)
1.9592e+05	7.6700e-13	3.5492e-07	2.1109e-04	(0.180 %)
2.3789e+05	1.3570e-12	5.1714e-07	1.5625e-04	(0.133 %)
1.7541e+04	2.4100e-13	1.2456e-06	2.4917e-04	(0.212 %)
8.1368e+04	5.0400e-13	5.6155e-07	1.7188e-03	(1.462 %)
1.9202e+05	7.5200e-13	3.5505e-07	2.2183e-04	(0.189 %)
2.2664e+05	1.3270e-12	5.3082e-07	1.6128e-04	(0.137 %)
1.7323e+04	2.3900e-13	1.2508e-06	2.4456e-04	(0.208 %)
7.7281e+04	5.0600e-13	5.9359e-07	1.7528e-03	(1.491 %)
2.0696e+05	7.7100e-13	3.3774e-07	1.9816e-04	(0.169 %)
2.3632e+05	1.3510e-12	5.1829e-07	1.5692e-04	(0.133 %)
1.7541e+04	2.4100e-13	1.2456e-06	2.4535e-04	(0.209 %)
7.7957e+04	5.0500e-13	5.8729e-07	1.7423e-03	(1.482 %)
2.0794e+05	7.6400e-13	3.3310e-07	2.0527e-04	(0.175 %)
2.3585e+05	1.3360e-12	5.1354e-07	1.5850e-04	(0.135 %)
1.7760e+04	2.4300e-13	1.2404e-06	2.4611e-04	(0.209 %)
7.6377e+04	5.0600e-13	6.0062e-07	1.7563e-03	(1.494 %)
2.0323e+05	7.8100e-13	3.4839e-07	1.9688e-04	(0.167 %)
2.3359e+05	1.3540e-12	5.2550e-07	1.5312e-04	(0.130 %)
1.7323e+04	2.3900e-13	1.2508e-06	2.4290e-04	(0.207 %)
7.7957e+04	5.0500e-13	5.8729e-07	1.7484e-03	(1.487 %)
2.0777e+05	7.7300e-13	3.3730e-07	2.0459e-04	(0.174 %)
2.3638e+05	1.3380e-12	5.1316e-07	1.5542e-04	(0.132 %)
1.7541e+04	2.4100e-13	1.2456e-06	2.4685e-04	(0.210 %)
7.8865e+04	5.0500e-13	5.8052e-07	1.7384e-03	(1.479 %)
2.0038e+05	7.6400e-13	3.4566e-07	2.0705e-04	(0.176 %)
2.4275e+05	1.3230e-12	4.9410e-07	1.5795e-04	(0.134 %)
1.7323e+04	2.3900e-13	1.2508e-06	2.4353e-04	(0.207 %)
7.7957e+04	5.0500e-13	5.8729e-07	1.7443e-03	(1.484 %)
2.0604e+05	7.6400e-13	3.3616e-07	2.0441e-04	(0.174 %)
2.2792e+05	1.3320e-12	5.2982e-07	1.5896e-04	(0.135 %)
1.7106e+04	2.3700e-13	1.2561e-06	2.4262e-04	(0.206 %)
7.9540e+04	5.0400e-13	5.7446e-07	1.7308e-03	(1.472 %)
1.9607e+05	7.5300e-13	3.4818e-07	2.1639e-04	(0.184 %)
2.2741e+05	1.3300e-12	5.3022e-07	1.6152e-04	(0.137 %)
1.7432e+04	2.4000e-13	1.2482e-06	2.4339e-04	(0.207 %)
7.6377e+04	5.0600e-13	6.0062e-07	1.7592e-03	(1.496 %)
2.0198e+05	7.8100e-13	3.5055e-07	1.9705e-04	(0.168 %)
2.3489e+05	1.3590e-12	5.2453e-07	1.5315e-04	(0.130 %)
1.7432e+04	2.4000e-13	1.2482e-06	2.4344e-04	(0.207 %)
7.6377e+04	5.0600e-13	6.0062e-07	1.7589e-03	(1.496 %)
2.0159e+05	7.8000e-13	3.5078e-07	1.9631e-04	(0.167 %)
2.3308e+05	1.3520e-12	5.2589e-07	1.5367e-04	(0.131 %)
1.7541e+04	2.4100e-13	1.2456e-06	2.4599e-04	(0.209 %)
7.9540e+04	5.0400e-13	5.7446e-07	1.7286e-03	(1.470 %)
1.9248e+05	7.5800e-13	3.5702e-07	2.1912e-04	(0.186 %)
2.3153e+05	1.3460e-12	5.2706e-07	1.5867e-04	(0.135 %)
1.7541e+04	2.4100e-13	1.2456e-06	2.4732e-04	(0.210 %)
8.0452e+04	5.0400e-13	5.6794e-07	1.7256e-03	(1.468 %)
2.0885e+05	7.5700e-13	3.2860e-07	2.2122e-04	(0.188 %)

2.3567e+05	1.3620e-12	5.2395e-07	1.5954e-04	(0.136 %)
1.7215e+04	2.3800e-13	1.2534e-06	2.4407e-04	(0.208 %)
7.8865e+04	5.0500e-13	5.8052e-07	1.7417e-03	(1.481 %)
2.0835e+05	7.6500e-13	3.3288e-07	2.0971e-04	(0.178 %)
2.3567e+05	1.3620e-12	5.2395e-07	1.5791e-04	(0.134 %)
1.7760e+04	2.4300e-13	1.2404e-06	2.5018e-04	(0.213 %)
7.9777e+04	5.0500e-13	5.7389e-07	1.7326e-03	(1.474 %)
1.9515e+05	7.6500e-13	3.5539e-07	2.1119e-04	(0.180 %)
2.2869e+05	1.3350e-12	5.2922e-07	1.5741e-04	(0.134 %)
1.7432e+04	2.4000e-13	1.2482e-06	2.4643e-04	(0.210 %)
8.0452e+04	5.0400e-13	5.6794e-07	1.7263e-03	(1.468 %)
1.9724e+05	7.5600e-13	3.4749e-07	2.1647e-04	(0.184 %)
2.2590e+05	1.3110e-12	5.2614e-07	1.6053e-04	(0.137 %)
1.7650e+04	2.4200e-13	1.2430e-06	2.4813e-04	(0.211 %)
7.8865e+04	5.0500e-13	5.8052e-07	1.7350e-03	(1.476 %)
1.9881e+05	7.6000e-13	3.4657e-07	2.0919e-04	(0.178 %)
2.4606e+05	1.3350e-12	4.9188e-07	1.5891e-04	(0.135 %)
1.7541e+04	2.4100e-13	1.2456e-06	2.4752e-04	(0.211 %)
7.8865e+04	5.0500e-13	5.8052e-07	1.7340e-03	(1.475 %)
1.9210e+05	7.5700e-13	3.5726e-07	2.1040e-04	(0.179 %)
2.3370e+05	1.3410e-12	5.2022e-07	1.6008e-04	(0.136 %)
1.7760e+04	2.4300e-13	1.2404e-06	2.5237e-04	(0.215 %)
8.2288e+04	5.0400e-13	5.5527e-07	1.7135e-03	(1.457 %)
1.9045e+05	7.5100e-13	3.5749e-07	2.1995e-04	(0.187 %)
2.1723e+05	1.2900e-12	5.3838e-07	1.6234e-04	(0.138 %)
1.7760e+04	2.4300e-13	1.2404e-06	2.5225e-04	(0.215 %)
8.0692e+04	5.0500e-13	5.6738e-07	1.7247e-03	(1.467 %)
1.9210e+05	7.5700e-13	3.5726e-07	2.1550e-04	(0.183 %)
2.3101e+05	1.3440e-12	5.2745e-07	1.5985e-04	(0.136 %)
1.7215e+04	2.3800e-13	1.2534e-06	2.4182e-04	(0.206 %)
7.8631e+04	5.0400e-13	5.8110e-07	1.7353e-03	(1.476 %)
1.9578e+05	7.5700e-13	3.5054e-07	2.1453e-04	(0.182 %)
2.2844e+05	1.3340e-12	5.2942e-07	1.5988e-04	(0.136 %)
1.7432e+04	2.4000e-13	1.2482e-06	2.4509e-04	(0.208 %)
7.7281e+04	5.0600e-13	5.9359e-07	1.7543e-03	(1.492 %)
2.1481e+05	7.7600e-13	3.2751e-07	1.9782e-04	(0.168 %)
2.3411e+05	1.3560e-12	5.2511e-07	1.5551e-04	(0.132 %)
1.7215e+04	2.3800e-13	1.2534e-06	2.4295e-04	(0.207 %)
7.9540e+04	5.0400e-13	5.7446e-07	1.7337e-03	(1.475 %)
2.1496e+05	7.5800e-13	3.1968e-07	2.1460e-04	(0.183 %)
2.2895e+05	1.3360e-12	5.2903e-07	1.6050e-04	(0.137 %)
1.7760e+04	2.4300e-13	1.2404e-06	2.5105e-04	(0.214 %)
7.9099e+04	5.0600e-13	5.7995e-07	1.7425e-03	(1.482 %)
1.9899e+05	7.7500e-13	3.5309e-07	2.0474e-04	(0.174 %)
2.3789e+05	1.3570e-12	5.1714e-07	1.5443e-04	(0.131 %)
1.7323e+04	2.3900e-13	1.2508e-06	2.4537e-04	(0.209 %)
7.8865e+04	5.0500e-13	5.8052e-07	1.7381e-03	(1.478 %)
2.0697e+05	7.5700e-13	3.3159e-07	2.0409e-04	(0.174 %)
2.2205e+05	1.3090e-12	5.3445e-07	1.6215e-04	(0.138 %)
1.7323e+04	2.3900e-13	1.2508e-06	2.4377e-04	(0.207 %)
7.7281e+04	5.0600e-13	5.9359e-07	1.7579e-03	(1.495 %)
2.2283e+05	7.8100e-13	3.1775e-07	1.9687e-04	(0.167 %)
2.3789e+05	1.3570e-12	5.1714e-07	1.5411e-04	(0.131 %)
1.7323e+04	2.3900e-13	1.2508e-06	2.4316e-04	(0.207 %)
7.7957e+04	5.0500e-13	5.8729e-07	1.7468e-03	(1.486 %)
2.0696e+05	7.7100e-13	3.3774e-07	2.0847e-04	(0.177 %)
2.3801e+05	1.3710e-12	5.2223e-07	1.5546e-04	(0.132 %)
1.7541e+04	2.4100e-13	1.2456e-06	2.5028e-04	(0.213 %)
8.0692e+04	5.0500e-13	5.6738e-07	1.7273e-03	(1.469 %)
1.9578e+05	7.5700e-13	3.5054e-07	2.1362e-04	(0.182 %)
2.3213e+05	1.3350e-12	5.2138e-07	1.6035e-04	(0.136 %)
1.6890e+04	2.3500e-13	1.2614e-06	2.4104e-04	(0.205 %)
7.8865e+04	5.0500e-13	5.8052e-07	1.7469e-03	(1.486 %)
2.2466e+05	7.6700e-13	3.0952e-07	2.0646e-04	(0.176 %)
2.3711e+05	1.3540e-12	5.1771e-07	1.5835e-04	(0.135 %)
1.7215e+04	2.3800e-13	1.2534e-06	2.4392e-04	(0.207 %)
7.8865e+04	5.0500e-13	5.8052e-07	1.7427e-03	(1.482 %)
2.0835e+05	7.6500e-13	3.3288e-07	2.0463e-04	(0.174 %)
2.2485e+05	1.3200e-12	5.3222e-07	1.5908e-04	(0.135 %)
1.7980e+04	2.4500e-13	1.2354e-06	2.5413e-04	(0.216 %)

8.0692e+04	5.0500e-13	5.6738e-07	1.7228e-03	(1.465 %)
1.9172e+05	7.5600e-13	3.5749e-07	2.1205e-04	(0.180 %)
2.2281e+05	1.3120e-12	5.3384e-07	1.6090e-04	(0.137 %)
1.7432e+04	2.4000e-13	1.2482e-06	2.4547e-04	(0.209 %)
7.7281e+04	5.0600e-13	5.9359e-07	1.7518e-03	(1.490 %)
2.0012e+05	7.7300e-13	3.5019e-07	2.0079e-04	(0.171 %)
2.3697e+05	1.3670e-12	5.2299e-07	1.5546e-04	(0.132 %)
1.7106e+04	2.3700e-13	1.2561e-06	2.3976e-04	(0.204 %)
7.7052e+04	5.0500e-13	5.9418e-07	1.7532e-03	(1.491 %)
2.1274e+05	7.7100e-13	3.2857e-07	2.0298e-04	(0.173 %)
2.5626e+05	1.3460e-12	4.7619e-07	1.5575e-04	(0.132 %)
1.7541e+04	2.4100e-13	1.2456e-06	2.4769e-04	(0.211 %)
7.8865e+04	5.0500e-13	5.8052e-07	1.7327e-03	(1.474 %)
1.9058e+05	7.5300e-13	3.5821e-07	2.0696e-04	(0.176 %)
2.2874e+05	1.3090e-12	5.1881e-07	1.6222e-04	(0.138 %)
1.7106e+04	2.3700e-13	1.2561e-06	2.3841e-04	(0.203 %)
7.6151e+04	5.0500e-13	6.0121e-07	1.7559e-03	(1.493 %)
2.0124e+05	7.7100e-13	3.4734e-07	2.0285e-04	(0.173 %)
2.5161e+05	1.3550e-12	4.8823e-07	1.5523e-04	(0.132 %)
1.7541e+04	2.4100e-13	1.2456e-06	2.4770e-04	(0.211 %)
8.0452e+04	5.0400e-13	5.6794e-07	1.7230e-03	(1.465 %)
1.9058e+05	7.5300e-13	3.5821e-07	2.1862e-04	(0.186 %)
2.2434e+05	1.3180e-12	5.3263e-07	1.6111e-04	(0.137 %)
1.7215e+04	2.3800e-13	1.2534e-06	2.4178e-04	(0.206 %)
7.6377e+04	5.0600e-13	6.0062e-07	1.7599e-03	(1.497 %)
2.0167e+05	7.7700e-13	3.4929e-07	1.9450e-04	(0.165 %)
2.2972e+05	1.3390e-12	5.2843e-07	1.5521e-04	(0.132 %)
1: 28 min 8 sec	0.112358 OD (3.259e+10, 3.259e+10)			
2: 34 min 18 sec	0.112921 OD (3.982e+10, 3.982e+10)			
3: 40 min 37 sec	0.112923 OD (4.715e+10, 4.715e+10)			
4: 46 min 49 sec	0.114988 OD (5.435e+10, 5.435e+10)			
5: 52 min 58 sec	0.113644 OD (6.15e+10, 6.15e+10)			
6: 59 min 12 sec	0.109204 OD (6.872e+10, 6.872e+10)			
7: 65 min 21 sec	0.108533 OD (7.587e+10, 7.587e+10)			
8: 71 min 29 sec	0.109683 OD (8.299e+10, 8.299e+10)			
9: 77 min 39 sec	0.109495 OD (9.015e+10, 9.015e+10)			
10: 83 min 52 sec	0.109244 OD (9.737e+10, 9.737e+10)			
11: 97 min 51 sec	0.105862 OD (1.135e+11, 1.135e+11)			
12: 103 min 53 sec	0.105169 OD (1.206e+11, 1.206e+11)			
13: 110 min 1 sec	0.103139 OD (1.277e+11, 1.277e+11)			
14: 116 min 8 sec	0.101355 OD (1.348e+11, 1.348e+11)			
15: 122 min 21 sec	0.104494 OD (1.42e+11, 1.42e+11)			
16: 128 min 25 sec	0.0988114 OD (1.49e+11, 1.49e+11)			
17: 134 min 30 sec	0.0987531 OD (1.561e+11, 1.561e+11)			
18: 140 min 35 sec	0.095823 OD (1.632e+11, 1.632e+11)			
19: 146 min 47 sec	0.0938875 OD (1.703e+11, 1.703e+11)			
20: 152 min 48 sec	0.0940323 OD (1.774e+11, 1.774e+11)			
21: 158 min 57 sec	0.0924857 OD (1.845e+11, 1.845e+11)			
22: 164 min 59 sec	0.093728 OD (1.915e+11, 1.915e+11)			
23: 171 min 3 sec	0.0938644 OD (1.985e+11, 1.985e+11)			
24: 177 min 10 sec	0.0906867 OD (2.056e+11, 2.056e+11)			
25: 183 min 21 sec	0.09112 OD (2.128e+11, 2.128e+11)			
26: 189 min 38 sec	0.0869429 OD (2.201e+11, 2.201e+11)			
27: 195 min 57 sec	0.0867278 OD (2.274e+11, 2.274e+11)			
28: 202 min 2 sec	0.0864424 OD (2.345e+11, 2.345e+11)			
29: 208 min 3 sec	0.0873009 OD (2.415e+11, 2.415e+11)			
30: 214 min 3 sec	0.0850864 OD (2.484e+11, 2.484e+11)			
31: 220 min 7 sec	0.0849725 OD (2.555e+11, 2.555e+11)			
32: 226 min 10 sec	0.0839218 OD (2.625e+11, 2.625e+11)			
33: 232 min 17 sec	0.0816689 OD (2.696e+11, 2.696e+11)			
34: 238 min 17 sec	0.0826696 OD (2.766e+11, 2.766e+11)			
35: 244 min 15 sec	0.0785491 OD (2.835e+11, 2.835e+11)			
36: 250 min 21 sec	0.0766401 OD (2.906e+11, 2.906e+11)			
37: 256 min 30 sec	0.0759027 OD (2.977e+11, 2.977e+11)			
38: 262 min 34 sec	0.0744067 OD (3.048e+11, 3.048e+11)			
39: 268 min 43 sec	0.0708483 OD (3.119e+11, 3.119e+11)			
40: 274 min 49 sec	0.0688247 OD (3.19e+11, 3.19e+11)			
41: 281 min 2 sec	0.0630085 OD (3.262e+11, 3.262e+11)			
42: 287 min 9 sec	0.0611069 OD (3.333e+11, 3.333e+11)			
43: 293 min 10 sec	0.057863 OD (3.403e+11, 3.403e+11)			

44: 299 min 16 sec 0.0549296 OD (3.474e+11, 3.474e+11)
 45: 305 min 26 sec 0.0499992 OD (3.545e+11, 3.545e+11)
 46: 311 min 28 sec 0.0467166 OD (3.615e+11, 3.615e+11)
 47: 317 min 42 sec 0.0434529 OD (3.687e+11, 3.687e+11)
 48: 323 min 50 sec 0.041341 OD (3.759e+11, 3.759e+11)

 * Enhanced van Holde - Weischet Analysis *

Data Report for Run "June10Chan1", Cell 2, Wavelength 1

Detailed Run Information:

Cell Description: Sample 5 Reference 2
 Raw Data Directory: /Users/seeyolater/ultrascan/data/June10Chan1/
 Rotor Speed: 42000 rpm
 Average Temperature: 25.1447 °C
 Temperature Variation: Within Tolerance
 Time Correction: 1 minute(s) 12 second(s)
 Run Duration: 5 hour(s) 40 minute(s)
 Wavelength: 280 nm
 Baseline Absorbance: -0.0244332 OD
 Meniscus Position: 5.81698 cm
 Edited Data starts at: 5.848 cm
 Edited Data stops at: 7.149 cm

Hydrodynamic Settings:

Viscosity correction: 1.02719
 Viscosity (absolute): 0.909858
 Density correction: 1.00585 g/ccm
 Density (absolute): 1.00464 g/ccm
 Vbar: 0.726349 ccm/g
 Vbar corrected for 20°C: 0.724163 ccm/g
 Buoyancy (Water, 20°C): 0.277116
 Buoyancy (absolute) 0.270282
 Correction Factor: 0.931059

Data Analysis Settings:

Divisions: 50
 Smoothing Frame: 11
 Analyzed Boundary: 50 %
 Boundary Position: 37 %
 Selected Groups:

No groups were selected...

Average S: 5.68609
 Initial concentration from plateau fit: 0.247231 OD/fringes

Scan Information:

Scan: Corrected Time: Plateau Concentration:

1: 17 min 53 sec 0.241068 OD
 2: 24 min 2 sec 0.238985 OD
 3: 30 min 13 sec 0.236908 OD
 4: 36 min 23 sec 0.234855 OD
 5: 42 min 40 sec 0.232782 OD
 6: 48 min 52 sec 0.230753 OD
 7: 55 min 3 sec 0.228748 OD
 8: 61 min 14 sec 0.226761 OD

9:	67 min 20 sec	0.224817 OD
10:	73 min 28 sec	0.222879 OD
11:	79 min 40 sec	0.220937 OD
12:	85 min 53 sec	0.219007 OD
13:	93 min 38 sec	0.216624 OD
14:	99 min 50 sec	0.214737 OD
15:	105 min 50 sec	0.212926 OD
16:	111 min 59 sec	0.211086 OD
17:	118 min 14 sec	0.209232 OD
18:	124 min 18 sec	0.207448 OD
19:	130 min 23 sec	0.205674 OD
20:	136 min 26 sec	0.203926 OD
21:	142 min 37 sec	0.202154 OD
22:	148 min 47 sec	0.200402 OD
23:	154 min 53 sec	0.198684 OD
24:	160 min 56 sec	0.196994 OD
25:	166 min 58 sec	0.195324 OD
26:	173 min 2 sec	0.193659 OD
27:	179 min 16 sec	0.191962 OD
28:	185 min 24 sec	0.190308 OD
29:	191 min 40 sec	0.188632 OD
30:	197 min 58 sec	0.186962 OD
31:	204 min 2 sec	0.185368 OD
32:	210 min 5 sec	0.183792 OD
33:	216 min 8 sec	0.182229 OD
34:	222 min 11 sec	0.180679 OD
35:	228 min 13 sec	0.179147 OD
36:	234 min 16 sec	0.177624 OD
37:	240 min 15 sec	0.17613 OD
38:	246 min 18 sec	0.174633 OD
39:	252 min 21 sec	0.173148 OD
40:	258 min 28 sec	0.17166 OD
41:	264 min 38 sec	0.170172 OD
42:	270 min 44 sec	0.168713 OD
43:	276 min 48 sec	0.167275 OD
44:	283 min 2 sec	0.165809 OD
45:	289 min 6 sec	0.164396 OD
46:	295 min 13 sec	0.162983 OD
47:	301 min 17 sec	0.161593 OD

Initial Concentration: 0.243384OD
 (Correlation. coeff.: -0.998622
 Standard Dev.: 0.00341425)

Initial Concentration from exponential fit: 0.247231OD

 * 2-dimensional Spectrum Analysis *

Data Report for Run "June10Chan1", Cell 2, Wavelength 1

Detailed Run Information:

Cell Description: Sample 5 Reference 2
 Raw Data Directory: /Users/seeyolater/ultrascan/data/June10Chan1/
 Rotor Speed: 42000 rpm
 Average Temperature: 25.1447 °C
 Temperature Variation: Within Tolerance
 Time Correction: 1 minute(s) 12 second(s)
 Run Duration: 5 hour(s) 40 minute(s)
 Wavelength: 280 nm
 Baseline Absorbance: 0.00527071 OD
 Meniscus Position: 5.81698 cm
 Edited Data starts at: 5.848 cm
 Edited Data stops at: 7.149 cm

Hydrodynamic Settings:

Viscosity correction: 1.02719
 Viscosity (absolute): 0.909858
 Density correction: 1.00585 g/ccm
 Density (absolute): 1.00464 g/ccm
 Vbar: 0.726349 ccm/g
 Vbar corrected for 20°C: 0.724163 ccm/g
 Buoyancy (Water, 20°C): 0.277116
 Buoyancy (absolute) 0.270282
 Correction Factor: 0.931059

Data Analysis Settings:

Number of Components: 8
 Residual Mean Square Deviation: 0.0062355
 Weight-Average sedimentation coefficient:

Weight Average S20,W: 6.0885e-13
 Weight Average D20,W: 4.9857e-07
 Weight Average Molecular Weight: 1.6518e+05
 Total concentration: 2.1823e-01

Distribution Information:

Molecular Weight	S 20,W:	D 20,W:	concentration:	
3.8650e+04	4.0000e-13	9.1027e-07	4.4374e-02	(20.333 %)
1.3854e+05	9.8889e-13	6.2784e-07	2.0320e-02	(9.311 %)
4.5102e+05	5.6667e-13	1.1051e-07	5.8706e-03	(2.690 %)
6.4440e+05	6.8889e-13	9.4028e-08	3.5068e-03	(1.607 %)
7.4017e+05	7.5556e-13	8.9784e-08	4.7407e-03	(2.172 %)
1.9035e+05	6.1111e-13	2.8237e-07	1.0506e-01	(48.141 %)
7.4986e+04	6.2222e-13	7.2984e-07	3.3591e-02	(15.392 %)
7.5701e+05	7.7778e-13	9.0369e-08	7.7078e-04	(0.353 %)
1:	17 min 53 sec	0.240728 OD (2.075e+10, 2.075e+10)		
2:	24 min 2 sec	0.238712 OD (2.787e+10, 2.787e+10)		
3:	30 min 13 sec	0.249275 OD (3.507e+10, 3.507e+10)		
4:	36 min 23 sec	0.235328 OD (4.223e+10, 4.223e+10)		
5:	42 min 40 sec	0.235491 OD (4.953e+10, 4.953e+10)		
6:	48 min 52 sec	0.235978 OD (5.674e+10, 5.674e+10)		
7:	55 min 3 sec	0.231494 OD (6.392e+10, 6.392e+10)		
8:	61 min 14 sec	0.23082 OD (7.11e+10, 7.11e+10)		
9:	67 min 20 sec	0.232129 OD (7.817e+10, 7.817e+10)		
10:	73 min 28 sec	0.230677 OD (8.53e+10, 8.53e+10)		
11:	79 min 40 sec	0.223787 OD (9.246e+10, 9.246e+10)		
12:	85 min 53 sec	0.225125 OD (9.971e+10, 9.971e+10)		
13:	93 min 38 sec	0.227543 OD (1.087e+11, 1.087e+11)		
14:	99 min 50 sec	0.221694 OD (1.159e+11, 1.159e+11)		
15:	105 min 50 sec	0.224352 OD (1.228e+11, 1.228e+11)		
16:	111 min 59 sec	0.222036 OD (1.3e+11, 1.3e+11)		
17:	118 min 14 sec	0.220121 OD (1.372e+11, 1.372e+11)		
18:	124 min 18 sec	0.199301 OD (1.443e+11, 1.443e+11)		
19:	130 min 23 sec	0.195924 OD (1.513e+11, 1.513e+11)		
20:	136 min 26 sec	0.196905 OD (1.583e+11, 1.583e+11)		
21:	142 min 37 sec	0.198201 OD (1.655e+11, 1.655e+11)		
22:	148 min 47 sec	0.193392 OD (1.727e+11, 1.727e+11)		
23:	154 min 53 sec	0.191171 OD (1.798e+11, 1.798e+11)		
24:	160 min 56 sec	0.188968 OD (1.868e+11, 1.868e+11)		
25:	166 min 58 sec	0.189223 OD (1.938e+11, 1.938e+11)		
26:	173 min 2 sec	0.186881 OD (2.008e+11, 2.008e+11)		
27:	179 min 16 sec	0.180094 OD (2.081e+11, 2.081e+11)		
28:	185 min 24 sec	0.180469 OD (2.152e+11, 2.152e+11)		
29:	191 min 40 sec	0.179184 OD (2.225e+11, 2.225e+11)		
30:	197 min 58 sec	0.177988 OD (2.297e+11, 2.297e+11)		
31:	204 min 2 sec	0.180753 OD (2.367e+11, 2.367e+11)		
32:	210 min 5 sec	0.170773 OD (2.438e+11, 2.438e+11)		
33:	216 min 8 sec	0.171294 OD (2.509e+11, 2.509e+11)		
34:	222 min 11 sec	0.166026 OD (2.579e+11, 2.579e+11)		

35: 228 min 13 sec 0.161188 OD (2.649e+11, 2.649e+11)
 36: 234 min 16 sec 0.153521 OD (2.719e+11, 2.719e+11)
 37: 240 min 15 sec 0.142516 OD (2.788e+11, 2.788e+11)
 38: 246 min 18 sec 0.131543 OD (2.859e+11, 2.859e+11)
 39: 252 min 21 sec 0.121242 OD (2.929e+11, 2.929e+11)
 40: 258 min 28 sec 0.109898 OD (3e+11, 3e+11)
 41: 264 min 38 sec 0.0982556 OD (3.072e+11, 3.072e+11)
 42: 270 min 44 sec 0.0922412 OD (3.143e+11, 3.143e+11)
 43: 276 min 48 sec 0.0835928 OD (3.213e+11, 3.213e+11)
 44: 283 min 2 sec 0.079636 OD (3.285e+11, 3.285e+11)
 45: 289 min 6 sec 0.0755418 OD (3.356e+11, 3.356e+11)
 46: 295 min 13 sec 0.0738167 OD (3.427e+11, 3.427e+11)
 47: 301 min 17 sec 0.0693019 OD (3.496e+11, 3.496e+11)

 * Genetic Algorithm Analysis *

Data Report for Run "June10Chan1", Cell 2, Wavelength 1

Detailed Run Information:

Cell Description: Sample 5 Reference 2
 Raw Data Directory: /Users/seeyolater/ultrascan/data/June10Chan1/
 Rotor Speed: 42000 rpm
 Average Temperature: 25.1447 °C
 Temperature Variation: Within Tolerance
 Time Correction: 1 minute(s) 12 second(s)
 Run Duration: 5 hour(s) 40 minute(s)
 Wavelength: 280 nm
 Baseline Absorbance: -0.0244332 OD
 Meniscus Position: 5.81698 cm
 Edited Data starts at: 5.848 cm
 Edited Data stops at: 7.149 cm

Hydrodynamic Settings:

Viscosity correction: 1.02719
 Viscosity (absolute): 0.909858
 Density correction: 1.00585 g/ccm
 Density (absolute): 1.00464 g/ccm
 Vbar: 0.726349 ccm/g
 Vbar corrected for 20°C: 0.724163 ccm/g
 Buoyancy (Water, 20°C): 0.277116
 Buoyancy (absolute) 0.270282
 Correction Factor: 0.931059

Data Analysis Settings:

Number of Components: 4
 Residual Mean Square Deviation: 0.00569131
 Weight-Average sedimentation coefficient:

Weight Average S_{20,W}: 6.0794e-13
 Weight Average D_{20,W}: 5.3099e-07
 Weight Average Molecular Weight: 1.1379e+05
 Total concentration: 2.1844e-01

Distribution Information:

Molecular Weight	S _{20,W} :	D _{20,W} :	concentration:	
2.9775e+04	3.1400e-13	9.2756e-07	2.8754e-02	(13.163 %)
1.0033e+05	6.3800e-13	5.5931e-07	9.0236e-02	(41.309 %)
1.5105e+05	5.8200e-13	3.3889e-07	8.0839e-02	(37.008 %)

	1.4705e+05	1.0290e-12	6.1548e-07	1.8610e-02	(8.520 %)
1:	17 min 53 sec	0.207821 OD (2.075e+10, 2.075e+10)			
2:	24 min 2 sec	0.2089 OD (2.787e+10, 2.787e+10)			
3:	30 min 13 sec	0.216682 OD (3.507e+10, 3.507e+10)			
4:	36 min 23 sec	0.208099 OD (4.223e+10, 4.223e+10)			
5:	42 min 40 sec	0.209689 OD (4.953e+10, 4.953e+10)			
6:	48 min 52 sec	0.210434 OD (5.674e+10, 5.674e+10)			
7:	55 min 3 sec	0.205185 OD (6.392e+10, 6.392e+10)			
8:	61 min 14 sec	0.204149 OD (7.11e+10, 7.11e+10)			
9:	67 min 20 sec	0.20315 OD (7.817e+10, 7.817e+10)			
10:	73 min 28 sec	0.202823 OD (8.53e+10, 8.53e+10)			
11:	79 min 40 sec	0.194946 OD (9.246e+10, 9.246e+10)			
12:	85 min 53 sec	0.194426 OD (9.971e+10, 9.971e+10)			
13:	93 min 38 sec	0.196336 OD (1.087e+11, 1.087e+11)			
14:	99 min 50 sec	0.189942 OD (1.159e+11, 1.159e+11)			
15:	105 min 50 sec	0.19187 OD (1.228e+11, 1.228e+11)			
16:	111 min 59 sec	0.188465 OD (1.3e+11, 1.3e+11)			
17:	118 min 14 sec	0.185458 OD (1.372e+11, 1.372e+11)			
18:	124 min 18 sec	0.180771 OD (1.443e+11, 1.443e+11)			
19:	130 min 23 sec	0.180549 OD (1.513e+11, 1.513e+11)			
20:	136 min 26 sec	0.176672 OD (1.583e+11, 1.583e+11)			
21:	142 min 37 sec	0.177106 OD (1.655e+11, 1.655e+11)			
22:	148 min 47 sec	0.172176 OD (1.727e+11, 1.727e+11)			
23:	154 min 53 sec	0.169185 OD (1.798e+11, 1.798e+11)			
24:	160 min 56 sec	0.166394 OD (1.868e+11, 1.868e+11)			
25:	166 min 58 sec	0.165891 OD (1.938e+11, 1.938e+11)			
26:	173 min 2 sec	0.162694 OD (2.008e+11, 2.008e+11)			
27:	179 min 16 sec	0.157501 OD (2.081e+11, 2.081e+11)			
28:	185 min 24 sec	0.155398 OD (2.152e+11, 2.152e+11)			
29:	191 min 40 sec	0.15389 OD (2.225e+11, 2.225e+11)			
30:	197 min 58 sec	0.152511 OD (2.297e+11, 2.297e+11)			
31:	204 min 2 sec	0.154455 OD (2.367e+11, 2.367e+11)			
32:	210 min 5 sec	0.146105 OD (2.438e+11, 2.438e+11)			
33:	216 min 8 sec	0.144395 OD (2.509e+11, 2.509e+11)			
34:	222 min 11 sec	0.14045 OD (2.579e+11, 2.579e+11)			
35:	228 min 13 sec	0.133477 OD (2.649e+11, 2.649e+11)			
36:	234 min 16 sec	0.125526 OD (2.719e+11, 2.719e+11)			
37:	240 min 15 sec	0.114283 OD (2.788e+11, 2.788e+11)			
38:	246 min 18 sec	0.105179 OD (2.859e+11, 2.859e+11)			
39:	252 min 21 sec	0.0945587 OD (2.929e+11, 2.929e+11)			
40:	258 min 28 sec	0.0824206 OD (3e+11, 3e+11)			
41:	264 min 38 sec	0.0703066 OD (3.072e+11, 3.072e+11)			
42:	270 min 44 sec	0.0642822 OD (3.143e+11, 3.143e+11)			
43:	276 min 48 sec	0.0546695 OD (3.213e+11, 3.213e+11)			
44:	283 min 2 sec	0.050724 OD (3.285e+11, 3.285e+11)			
45:	289 min 6 sec	0.0448657 OD (3.356e+11, 3.356e+11)			
46:	295 min 13 sec	0.0422934 OD (3.427e+11, 3.427e+11)			
47:	301 min 17 sec	0.0395981 OD (3.496e+11, 3.496e+11)			

 * 2-dimensional Spectrum Analysis *

Data Report for Run "June10Chan1", Cell 2, Wavelength 1

Detailed Run Information:

Cell Description: Sample 5 Reference 2
 Raw Data Directory: /Users/seeyolater/ultrascan/data/June10Chan1/
 Rotor Speed: 42000 rpm
 Average Temperature: 25.1447 °C
 Temperature Variation: Within Tolerance
 Time Correction: 1 minute(s) 12 second(s)
 Run Duration: 5 hour(s) 40 minute(s)
 Wavelength: 280 nm
 Baseline Absorbance: -0.0244332 OD
 Meniscus Position: 5.81698 cm
 Edited Data starts at: 5.848 cm

Edited Data stops at: 7.149 cm

Hydrodynamic Settings:

Viscosity correction: 1.02719
 Viscosity (absolute): 0.909858
 Density correction: 1.00585 g/ccm
 Density (absolute): 1.00464 g/ccm
 Vbar: 0.726349 ccm/g
 Vbar corrected for 20°C: 0.724163 ccm/g
 Buoyancy (Water, 20°C): 0.277116
 Buoyancy (absolute) 0.270282
 Correction Factor: 0.931059

Data Analysis Settings:

Number of Components: 150
 Residual Mean Square Deviation: 0.00562487
 Weight-Average sedimentation coefficient:

Weight Average S20,W: 6.1001e-13
 Weight Average D20,W: 5.8864e-07
 Weight Average Molecular Weight: 9.5566e+04
 Total concentration: 2.1886e-01

Distribution Information:

Molecular Weight:	S 20,W:	D 20,W:	concentration:	
2.6611e+04	2.7900e-13	9.2214e-07	4.8104e-04	(0.220 %)
9.8506e+04	6.0600e-13	5.4109e-07	3.5224e-03	(1.609 %)
1.5592e+05	1.0700e-12	6.0358e-07	3.7285e-04	(0.170 %)
2.6611e+04	2.7900e-13	9.2214e-07	4.8046e-04	(0.220 %)
9.8506e+04	6.0600e-13	5.4109e-07	3.5271e-03	(1.612 %)
1.5856e+05	1.0820e-12	6.0022e-07	3.7078e-04	(0.169 %)
2.6586e+04	2.8200e-13	9.3295e-07	4.8862e-04	(0.223 %)
9.8750e+04	6.0700e-13	5.4065e-07	3.5249e-03	(1.611 %)
1.5921e+05	1.0850e-12	5.9939e-07	3.6464e-04	(0.167 %)
2.6755e+04	2.8000e-13	9.2050e-07	4.8281e-04	(0.221 %)
9.8506e+04	6.0600e-13	5.4109e-07	3.5189e-03	(1.608 %)
1.5483e+05	1.0650e-12	6.0499e-07	3.7385e-04	(0.171 %)
2.6611e+04	2.7900e-13	9.2214e-07	4.8124e-04	(0.220 %)
9.8506e+04	6.0600e-13	5.4109e-07	3.5208e-03	(1.609 %)
1.5505e+05	1.0660e-12	6.0471e-07	3.7355e-04	(0.171 %)
2.6586e+04	2.8200e-13	9.3295e-07	4.8862e-04	(0.223 %)
9.8750e+04	6.0700e-13	5.4065e-07	3.5249e-03	(1.611 %)
1.5921e+05	1.0850e-12	5.9939e-07	3.6464e-04	(0.167 %)
2.6755e+04	2.8000e-13	9.2050e-07	4.8267e-04	(0.221 %)
9.8506e+04	6.0600e-13	5.4109e-07	3.5200e-03	(1.608 %)
1.5549e+05	1.0680e-12	6.0414e-07	3.7332e-04	(0.171 %)
2.6183e+04	2.7600e-13	9.2714e-07	4.7410e-04	(0.217 %)
9.7371e+04	6.0600e-13	5.4740e-07	3.5339e-03	(1.615 %)
1.5702e+05	1.0750e-12	6.0217e-07	3.6881e-04	(0.169 %)
2.6468e+04	2.7800e-13	9.2380e-07	4.7933e-04	(0.219 %)
9.8506e+04	6.0600e-13	5.4109e-07	3.5256e-03	(1.611 %)
1.5680e+05	1.0740e-12	6.0245e-07	3.7204e-04	(0.170 %)
2.6326e+04	2.7700e-13	9.2547e-07	4.7546e-04	(0.217 %)
9.7371e+04	6.0600e-13	5.4740e-07	3.5335e-03	(1.614 %)
1.5768e+05	1.0780e-12	6.0133e-07	3.6843e-04	(0.168 %)
2.6468e+04	2.7800e-13	9.2380e-07	4.7943e-04	(0.219 %)
9.8506e+04	6.0600e-13	5.4109e-07	3.5248e-03	(1.611 %)
1.5636e+05	1.0720e-12	6.0301e-07	3.7238e-04	(0.170 %)
2.6611e+04	2.7900e-13	9.2214e-07	4.8100e-04	(0.220 %)
9.8506e+04	6.0600e-13	5.4109e-07	3.5228e-03	(1.610 %)
1.5614e+05	1.0710e-12	6.0329e-07	3.7267e-04	(0.170 %)
2.6755e+04	2.8000e-13	9.2050e-07	4.8512e-04	(0.222 %)
9.9645e+04	6.0600e-13	5.3491e-07	3.5128e-03	(1.605 %)

1.5418e+05	1.0620e-12	6.0584e-07	3.7722e-04	(0.172 %)
2.6586e+04	2.8200e-13	9.3295e-07	4.8871e-04	(0.223 %)
9.8750e+04	6.0700e-13	5.4065e-07	3.5242e-03	(1.610 %)
1.5877e+05	1.0830e-12	5.9994e-07	3.6496e-04	(0.167 %)
2.6611e+04	2.7900e-13	9.2214e-07	4.8066e-04	(0.220 %)
9.8506e+04	6.0600e-13	5.4109e-07	3.5256e-03	(1.611 %)
1.5768e+05	1.0780e-12	6.0133e-07	3.7147e-04	(0.170 %)
2.6326e+04	2.7700e-13	9.2547e-07	4.7532e-04	(0.217 %)
9.7371e+04	6.0600e-13	5.4740e-07	3.5346e-03	(1.615 %)
1.5834e+05	1.0810e-12	6.0050e-07	3.6793e-04	(0.168 %)
2.6586e+04	2.8200e-13	9.3295e-07	4.9076e-04	(0.224 %)
9.9892e+04	6.0700e-13	5.3447e-07	3.5202e-03	(1.608 %)
1.5921e+05	1.0850e-12	5.9939e-07	3.6739e-04	(0.168 %)
2.6468e+04	2.7800e-13	9.2380e-07	4.7933e-04	(0.219 %)
9.8506e+04	6.0600e-13	5.4109e-07	3.5256e-03	(1.611 %)
1.5680e+05	1.0740e-12	6.0245e-07	3.7204e-04	(0.170 %)
2.6304e+04	2.8000e-13	9.3628e-07	4.8579e-04	(0.222 %)
9.8750e+04	6.0700e-13	5.4065e-07	3.5259e-03	(1.611 %)
1.5790e+05	1.0790e-12	6.0105e-07	3.6536e-04	(0.167 %)
2.6183e+04	2.7600e-13	9.2714e-07	4.7373e-04	(0.216 %)
9.7371e+04	6.0600e-13	5.4740e-07	3.5369e-03	(1.616 %)
1.5877e+05	1.0830e-12	5.9994e-07	3.6749e-04	(0.168 %)
2.6274e+04	2.7900e-13	9.3399e-07	4.7954e-04	(0.219 %)
9.8506e+04	6.0600e-13	5.4109e-07	3.5260e-03	(1.611 %)
1.5768e+05	1.0780e-12	6.0133e-07	3.7195e-04	(0.170 %)
2.6326e+04	2.7700e-13	9.2547e-07	4.7527e-04	(0.217 %)
9.7371e+04	6.0600e-13	5.4740e-07	3.5350e-03	(1.615 %)
1.5856e+05	1.0820e-12	6.0022e-07	3.6776e-04	(0.168 %)
2.6661e+04	2.7700e-13	9.1383e-07	4.7922e-04	(0.219 %)
9.8506e+04	6.0600e-13	5.4109e-07	3.5240e-03	(1.610 %)
1.5527e+05	1.0670e-12	6.0442e-07	3.7264e-04	(0.170 %)
2.6611e+04	2.7900e-13	9.2214e-07	4.8066e-04	(0.220 %)
9.8506e+04	6.0600e-13	5.4109e-07	3.5256e-03	(1.611 %)
1.5768e+05	1.0780e-12	6.0133e-07	3.7147e-04	(0.170 %)
2.6586e+04	2.8200e-13	9.3295e-07	4.8862e-04	(0.223 %)
9.8750e+04	6.0700e-13	5.4065e-07	3.5249e-03	(1.611 %)
1.5921e+05	1.0850e-12	5.9939e-07	3.6464e-04	(0.167 %)
2.6611e+04	2.7900e-13	9.2214e-07	4.8037e-04	(0.219 %)
9.8506e+04	6.0600e-13	5.4109e-07	3.5279e-03	(1.612 %)
1.5899e+05	1.0840e-12	5.9967e-07	3.7044e-04	(0.169 %)
2.6727e+04	2.8300e-13	9.3130e-07	4.9018e-04	(0.224 %)
9.8750e+04	6.0700e-13	5.4065e-07	3.5233e-03	(1.610 %)
1.5921e+05	1.0850e-12	5.9939e-07	3.6475e-04	(0.167 %)
2.6274e+04	2.7900e-13	9.3399e-07	4.7920e-04	(0.219 %)
9.8506e+04	6.0600e-13	5.4109e-07	3.5287e-03	(1.612 %)
1.5921e+05	1.0850e-12	5.9939e-07	3.7076e-04	(0.169 %)
2.6898e+04	2.8100e-13	9.1886e-07	4.8661e-04	(0.222 %)
9.9645e+04	6.0600e-13	5.3491e-07	3.5116e-03	(1.605 %)
1.5440e+05	1.0630e-12	6.0556e-07	3.7715e-04	(0.172 %)
2.6468e+04	2.7800e-13	9.2380e-07	4.7880e-04	(0.219 %)
9.8506e+04	6.0600e-13	5.4109e-07	3.5298e-03	(1.613 %)
1.5921e+05	1.0850e-12	5.9939e-07	3.7017e-04	(0.169 %)
2.6183e+04	2.7600e-13	9.2714e-07	4.7612e-04	(0.218 %)
9.8506e+04	6.0600e-13	5.4109e-07	3.5302e-03	(1.613 %)
1.5768e+05	1.0780e-12	6.0133e-07	3.7113e-04	(0.170 %)
2.6950e+04	2.7900e-13	9.1054e-07	4.8224e-04	(0.220 %)
9.8506e+04	6.0600e-13	5.4109e-07	3.5208e-03	(1.609 %)
1.5527e+05	1.0670e-12	6.0442e-07	3.7288e-04	(0.170 %)
2.6133e+04	2.7800e-13	9.3567e-07	4.7807e-04	(0.218 %)
9.8506e+04	6.0600e-13	5.4109e-07	3.5272e-03	(1.612 %)
1.5746e+05	1.0770e-12	6.0161e-07	3.7201e-04	(0.170 %)
2.6468e+04	2.7800e-13	9.2380e-07	4.7909e-04	(0.219 %)
9.8506e+04	6.0600e-13	5.4109e-07	3.5275e-03	(1.612 %)
1.5790e+05	1.0790e-12	6.0105e-07	3.7118e-04	(0.170 %)
2.6755e+04	2.8000e-13	9.2050e-07	4.8287e-04	(0.221 %)
9.8506e+04	6.0600e-13	5.4109e-07	3.5185e-03	(1.608 %)
1.5461e+05	1.0640e-12	6.0527e-07	3.7402e-04	(0.171 %)
2.6755e+04	2.8000e-13	9.2050e-07	4.8272e-04	(0.221 %)
9.8506e+04	6.0600e-13	5.4109e-07	3.5197e-03	(1.608 %)
1.5527e+05	1.0670e-12	6.0442e-07	3.7349e-04	(0.171 %)

2.6274e+04	2.7900e-13	9.3399e-07	4.7934e-04	(0.219 %)
9.8506e+04	6.0600e-13	5.4109e-07	3.5276e-03	(1.612 %)
1.5856e+05	1.0820e-12	6.0022e-07	3.7127e-04	(0.170 %)
2.6586e+04	2.8200e-13	9.3295e-07	4.8862e-04	(0.223 %)
9.8750e+04	6.0700e-13	5.4065e-07	3.5249e-03	(1.611 %)
1.5921e+05	1.0850e-12	5.9939e-07	3.6464e-04	(0.167 %)
2.6326e+04	2.7700e-13	9.2547e-07	4.7518e-04	(0.217 %)
9.7371e+04	6.0600e-13	5.4740e-07	3.5358e-03	(1.616 %)
1.5899e+05	1.0840e-12	5.9967e-07	3.6743e-04	(0.168 %)
2.6755e+04	2.8000e-13	9.2050e-07	4.8237e-04	(0.220 %)
9.8506e+04	6.0600e-13	5.4109e-07	3.5224e-03	(1.609 %)
1.5680e+05	1.0740e-12	6.0245e-07	3.7227e-04	(0.170 %)
2.6415e+04	2.8000e-13	9.3232e-07	4.8325e-04	(0.221 %)
9.9645e+04	6.0600e-13	5.3491e-07	3.5193e-03	(1.608 %)
1.5746e+05	1.0770e-12	6.0161e-07	3.7502e-04	(0.171 %)
2.6611e+04	2.7900e-13	9.2214e-07	4.8114e-04	(0.220 %)
9.8506e+04	6.0600e-13	5.4109e-07	3.5216e-03	(1.609 %)
1.5549e+05	1.0680e-12	6.0414e-07	3.7320e-04	(0.171 %)
2.6274e+04	2.7900e-13	9.3399e-07	4.7930e-04	(0.219 %)
9.8506e+04	6.0600e-13	5.4109e-07	3.5280e-03	(1.612 %)
1.5877e+05	1.0830e-12	5.9994e-07	3.7110e-04	(0.170 %)
2.6468e+04	2.7800e-13	9.2380e-07	4.7928e-04	(0.219 %)
9.8506e+04	6.0600e-13	5.4109e-07	3.5260e-03	(1.611 %)
1.5702e+05	1.0750e-12	6.0217e-07	3.7187e-04	(0.170 %)
2.6898e+04	2.8100e-13	9.1886e-07	4.8341e-04	(0.221 %)
9.8506e+04	6.0600e-13	5.4109e-07	3.5247e-03	(1.610 %)
1.5899e+05	1.0840e-12	5.9967e-07	3.7066e-04	(0.169 %)
2.6326e+04	2.7700e-13	9.2547e-07	4.7806e-04	(0.218 %)
9.8506e+04	6.0600e-13	5.4109e-07	3.5252e-03	(1.611 %)
1.5571e+05	1.0690e-12	6.0386e-07	3.7279e-04	(0.170 %)
2.6806e+04	2.7800e-13	9.1218e-07	4.8048e-04	(0.220 %)
9.8506e+04	6.0600e-13	5.4109e-07	3.5244e-03	(1.610 %)
1.5636e+05	1.0720e-12	6.0301e-07	3.7189e-04	(0.170 %)
2.6611e+04	2.7900e-13	9.2214e-07	4.8139e-04	(0.220 %)
9.8506e+04	6.0600e-13	5.4109e-07	3.5196e-03	(1.608 %)
1.5440e+05	1.0630e-12	6.0556e-07	3.7408e-04	(0.171 %)
2.6586e+04	2.8200e-13	9.3295e-07	4.8862e-04	(0.223 %)
9.8750e+04	6.0700e-13	5.4065e-07	3.5249e-03	(1.611 %)
1.5921e+05	1.0850e-12	5.9939e-07	3.6464e-04	(0.167 %)
2.6806e+04	2.7800e-13	9.1218e-07	4.8039e-04	(0.219 %)
9.8506e+04	6.0600e-13	5.4109e-07	3.5252e-03	(1.611 %)
1.5680e+05	1.0740e-12	6.0245e-07	3.7154e-04	(0.170 %)
1: 17 min 53 sec	0.207821 OD (2.075e+10, 2.075e+10)			
2: 24 min 2 sec	0.2089 OD (2.787e+10, 2.787e+10)			
3: 30 min 13 sec	0.216682 OD (3.507e+10, 3.507e+10)			
4: 36 min 23 sec	0.208099 OD (4.223e+10, 4.223e+10)			
5: 42 min 40 sec	0.209689 OD (4.953e+10, 4.953e+10)			
6: 48 min 52 sec	0.210434 OD (5.674e+10, 5.674e+10)			
7: 55 min 3 sec	0.205185 OD (6.392e+10, 6.392e+10)			
8: 61 min 14 sec	0.204149 OD (7.11e+10, 7.11e+10)			
9: 67 min 20 sec	0.20315 OD (7.817e+10, 7.817e+10)			
10: 73 min 28 sec	0.202823 OD (8.53e+10, 8.53e+10)			
11: 79 min 40 sec	0.194946 OD (9.246e+10, 9.246e+10)			
12: 85 min 53 sec	0.194426 OD (9.971e+10, 9.971e+10)			
13: 93 min 38 sec	0.196336 OD (1.087e+11, 1.087e+11)			
14: 99 min 50 sec	0.189942 OD (1.159e+11, 1.159e+11)			
15: 105 min 50 sec	0.19187 OD (1.228e+11, 1.228e+11)			
16: 111 min 59 sec	0.188465 OD (1.3e+11, 1.3e+11)			
17: 118 min 14 sec	0.185458 OD (1.372e+11, 1.372e+11)			
18: 124 min 18 sec	0.180771 OD (1.443e+11, 1.443e+11)			
19: 130 min 23 sec	0.180549 OD (1.513e+11, 1.513e+11)			
20: 136 min 26 sec	0.176672 OD (1.583e+11, 1.583e+11)			
21: 142 min 37 sec	0.177106 OD (1.655e+11, 1.655e+11)			
22: 148 min 47 sec	0.172176 OD (1.727e+11, 1.727e+11)			
23: 154 min 53 sec	0.169185 OD (1.798e+11, 1.798e+11)			
24: 160 min 56 sec	0.166394 OD (1.868e+11, 1.868e+11)			
25: 166 min 58 sec	0.165891 OD (1.938e+11, 1.938e+11)			
26: 173 min 2 sec	0.162694 OD (2.008e+11, 2.008e+11)			
27: 179 min 16 sec	0.157501 OD (2.081e+11, 2.081e+11)			
28: 185 min 24 sec	0.155398 OD (2.152e+11, 2.152e+11)			

29:	191 min 40 sec	0.15389 OD (2.225e+11, 2.225e+11)
30:	197 min 58 sec	0.152511 OD (2.297e+11, 2.297e+11)
31:	204 min 2 sec	0.154455 OD (2.367e+11, 2.367e+11)
32:	210 min 5 sec	0.146105 OD (2.438e+11, 2.438e+11)
33:	216 min 8 sec	0.144395 OD (2.509e+11, 2.509e+11)
34:	222 min 11 sec	0.14045 OD (2.579e+11, 2.579e+11)
35:	228 min 13 sec	0.133477 OD (2.649e+11, 2.649e+11)
36:	234 min 16 sec	0.125526 OD (2.719e+11, 2.719e+11)
37:	240 min 15 sec	0.114283 OD (2.788e+11, 2.788e+11)
38:	246 min 18 sec	0.105179 OD (2.859e+11, 2.859e+11)
39:	252 min 21 sec	0.0945587 OD (2.929e+11, 2.929e+11)
40:	258 min 28 sec	0.0824206 OD (3e+11, 3e+11)
41:	264 min 38 sec	0.0703066 OD (3.072e+11, 3.072e+11)
42:	270 min 44 sec	0.0642822 OD (3.143e+11, 3.143e+11)
43:	276 min 48 sec	0.0546695 OD (3.213e+11, 3.213e+11)
44:	283 min 2 sec	0.050724 OD (3.285e+11, 3.285e+11)
45:	289 min 6 sec	0.0448657 OD (3.356e+11, 3.356e+11)
46:	295 min 13 sec	0.0422934 OD (3.427e+11, 3.427e+11)
47:	301 min 17 sec	0.0395981 OD (3.496e+11, 3.496e+11)

Appendix F – AUC - Wild type Complex vHW Analysis

Van Holde-Weischet Results file for 2:1, 1:1, & 1:2 ratio experiments.

```
*****
* Enhanced van Holde - Weischet Analysis *
*****
```

Data Report for Run "WTRatios", Cell 1, Wavelength 1

Detailed Run Information:

Cell Description: Sample 1
 Raw Data Directory: /Users/seejolater/ultrascan/data/WTRatios/
 Rotor Speed: 60000 rpm
 Average Temperature: 25.3542 °C
 Temperature Variation: Within Tolerance
 Time Correction: 1 minute(s) 49 second(s)
 Run Duration: 2 hour(s) 55 minute(s)
 Wavelength: 280 nm
 Baseline Absorbance: -0.00174973 OD
 Meniscus Position: 5.89972 cm
 Edited Data starts at: 5.942 cm
 Edited Data stops at: 7.137 cm

Hydrodynamic Settings:

Viscosity correction: 1.0363
 Viscosity (absolute): 0.913569
 Density correction: 1.00994 g/ccm
 Density (absolute): 1.00868 g/ccm
 Vbar: 0.734718 ccm/g
 Vbar corrected for 20°C: 0.732442 ccm/g
 Buoyancy (Water, 20°C): 0.268851
 Buoyancy (absolute) 0.258907
 Correction Factor: 0.946822

Data Analysis Settings:

Divisions: 50
 Smoothing Frame: 2
 Analyzed Boundary: 70 %
 Boundary Position: 15 %
 Selected Groups:

No groups were selected...

Average S: 7.39015
 Initial concentration from plateau fit: 0.827074 OD/fringes

Scan Information:

Scan: Corrected Time: Plateau Concentration:

1:	12 min 41 sec	0.788949 OD
2:	30 min 47 sec	0.737565 OD
3:	39 min 13 sec	0.71478 OD
4:	47 min 39 sec	0.692699 OD
5:	56 min 21 sec	0.670634 OD
6:	64 min 55 sec	0.649595 OD
7:	73 min 23 sec	0.62945 OD
8:	81 min 54 sec	0.609815 OD
9:	90 min 28 sec	0.590684 OD
10:	99 min 1 sec	0.572188 OD
11:	107 min 44 sec	0.553928 OD
12:	116 min 12 sec	0.536749 OD
13:	124 min 40 sec	0.520104 OD
14:	133 min 3 sec	0.50413 OD
15:	141 min 30 sec	0.488526 OD
16:	149 min 59 sec	0.473347 OD

17: 158 min 27 sec 0.458667 OD
 18: 166 min 53 sec 0.444498 OD
 19: 175 min 25 sec 0.430606 OD

Initial Concentration: 0.795806OD
 (Correlation. coeff.: -0.996582
 Standard Dev.: 0.0237042)

Initial Concentration from exponential fit: 0.827074OD

 --END OF FILE--

 * 2-dimensional Spectrum Analysis *

Data Report for Run "WTRatios", Cell 1, Wavelength 1

Detailed Run Information:

Cell Description: Sample 1
 Raw Data Directory: /Users/seejolater/ultrascan/data/WTRatios/
 Rotor Speed: 60000 rpm
 Average Temperature: 25.3542 °C
 Temperature Variation: Within Tolerance
 Time Correction: 1 minute(s) 49 second(s)
 Run Duration: 2 hour(s) 55 minute(s)
 Wavelength: 280 nm
 Baseline Absorbance: 0.00369551 OD
 Meniscus Position: 5.89972 cm
 Edited Data starts at: 5.942 cm
 Edited Data stops at: 7.137 cm

Hydrodynamic Settings:

Viscosity correction: 1.0363
 Viscosity (absolute): 0.913569
 Density correction: 1.00994 g/ccm
 Density (absolute): 1.00868 g/ccm
 Vbar: 0.734718 ccm/g
 Vbar corrected for 20°C: 0.732442 ccm/g
 Buoyancy (Water, 20°C): 0.268851
 Buoyancy (absolute) 0.258907
 Correction Factor: 0.946822

Data Analysis Settings:

Number of Components: 16
 Residual Mean Square Deviation: 0.00628274
 Weight-Average sedimentation coefficient:
 Weight Average S_{20,W}: 7.8500e-13
 Weight Average D_{20,W}: 3.9870e-07
 Weight Average Molecular Weight: 2.7682e+05
 Total concentration: 8.4129e-01

Distribution Information:

Molecular Weight:	S _{20,W} :	D _{20,W} :	concentration:	
1.0905e+05	4.8889e-13	4.0645e-07	1.6325e-01	(19.404 %)
2.3442e+05	3.5926e-13	1.3894e-07	2.1626e-03	(0.257 %)
1.6885e+05	9.8148e-13	5.2699e-07	1.3549e-01	(16.105 %)
2.0000e+06	1.5000e-12	6.7995e-08	7.6114e-03	(0.905 %)
1.4260e+06	1.1630e-12	7.3936e-08	9.8529e-03	(1.171 %)
3.2422e+05	1.3185e-12	3.6868e-07	1.5789e-03	(0.188 %)
1.0625e+05	5.1481e-13	4.3927e-07	7.8624e-02	(9.346 %)
8.7181e+05	8.2593e-13	8.5888e-08	2.1484e-02	(2.554 %)

1.0631e+06	9.2963e-13	7.9275e-08	1.5321e-02	(1.821 %)
2.6534e+05	1.4741e-12	5.0364e-07	1.7108e-02	(2.033 %)
4.2226e+05	1.0333e-12	2.2185e-07	1.6089e-01	(19.124 %)
1.2555e+05	6.4444e-13	4.6536e-07	3.8983e-02	(4.634 %)
1.2909e+06	1.1370e-12	7.9853e-08	1.0942e-02	(1.301 %)
2.6485e+05	9.8148e-13	3.3597e-07	6.8914e-02	(8.191 %)
3.1265e+05	4.1111e-13	1.1921e-07	7.3646e-03	(0.875 %)
6.3866e+04	4.8889e-13	6.9399e-07	1.0172e-01	(12.091 %)

1:	12 min 41 sec	0.780688 OD (2.998e+10, 2.998e+10)
2:	30 min 47 sec	0.746364 OD (7.299e+10, 7.299e+10)
3:	39 min 13 sec	0.723543 OD (9.299e+10, 9.299e+10)
4:	47 min 39 sec	0.685587 OD (1.128e+11, 1.128e+11)
5:	56 min 21 sec	0.657788 OD (1.335e+11, 1.335e+11)
6:	64 min 55 sec	0.601374 OD (1.538e+11, 1.538e+11)
7:	73 min 23 sec	0.40377 OD (1.739e+11, 1.739e+11)
8:	81 min 54 sec	0.334561 OD (1.941e+11, 1.941e+11)
9:	90 min 28 sec	0.309745 OD (2.143e+11, 2.143e+11)
10:	99 min 1 sec	0.303651 OD (2.346e+11, 2.346e+11)
11:	107 min 44 sec	0.288513 OD (2.551e+11, 2.551e+11)
12:	116 min 12 sec	0.270687 OD (2.751e+11, 2.751e+11)
13:	124 min 40 sec	0.248611 OD (2.951e+11, 2.951e+11)
14:	133 min 3 sec	0.204528 OD (3.152e+11, 3.152e+11)
15:	141 min 30 sec	0.145143 OD (3.351e+11, 3.351e+11)
16:	149 min 59 sec	0.082281 OD (3.552e+11, 3.552e+11)
17:	158 min 27 sec	0.041731 OD (3.753e+11, 3.753e+11)
18:	166 min 53 sec	0.022861 OD (3.954e+11, 3.954e+11)
19:	175 min 25 sec	0.0171419 OD (4.156e+11, 4.156e+11)
		(3.351e+11, 3.351e+11)
16:	149 min 59 sec	0.0812759 OD (3.552e+11, 3.552e+11)
17:	158 min 27 sec	0.0378521 OD (3.753e+11, 3.753e+11)
18:	166 min 53 sec	0.0187431 OD (3.954e+11, 3.954e+11)
19:	175 min 25 sec	0.0116967 OD (4.156e+11, 4.156e+11)

 * Genetic Algorithm Analysis *

Data Report for Run "WTRatios", Cell 1, Wavelength 1

Detailed Run Information:

Cell Description: Sample 1
 Raw Data Directory: /Users/seejolater/ultrascan/data/WTRatios/
 Rotor Speed: 60000 rpm
 Average Temperature: 25.3542 °C
 Temperature Variation: Within Tolerance
 Time Correction: 1 minute(s) 49 second(s)
 Run Duration: 2 hour(s) 55 minute(s)
 Wavelength: 280 nm
 Baseline Absorbance: -0.00174973 OD
 Meniscus Position: 5.89972 cm
 Edited Data starts at: 5.942 cm
 Edited Data stops at: 7.137 cm

Hydrodynamic Settings:

Viscosity correction: 1.0363
 Viscosity (absolute): 0.913569
 Density correction: 1.00994 g/ccm
 Density (absolute): 1.00868 g/ccm
 Vbar: 0.734718 ccm/g
 Vbar corrected for 20°C: 0.732442 ccm/g
 Buoyancy (Water, 20°C) : 0.268851
 Buoyancy (absolute) 0.258907
 Correction Factor: 0.946822

Data Analysis Settings:

Number of Components: 5
 Residual Mean Square Deviation: 0.00682745
 Weight-Average sedimentation coefficient:

Weight Average S20,W: 7.7405e-13
 Weight Average D20,W: 4.9323e-07
 Weight Average Molecular Weight: 1.9226e+05
 Total concentration: 8.3532e-01

Distribution Information:

Molecular Weight:	S 20,W:	D 20,W:	concentration:	
8.5525e+04	4.8800e-13	5.1729e-07	3.1254e-01	(37.416 %)
6.4140e+04	5.7200e-13	8.0850e-07	7.4755e-02	(8.949 %)
4.4953e+05	1.0120e-12	2.0410e-07	2.0696e-01	(24.776 %)
1.7292e+05	1.1080e-12	5.8091e-07	1.0823e-01	(12.957 %)
1.3041e+05	9.1800e-13	6.3820e-07	1.3283e-01	(15.902 %)
1: 12 min 41 sec	0.777182 OD (2.998e+10, 2.998e+10)			
2: 30 min 47 sec	0.746351 OD (7.299e+10, 7.299e+10)			
3: 39 min 13 sec	0.722892 OD (9.299e+10, 9.299e+10)			
4: 47 min 39 sec	0.687817 OD (1.128e+11, 1.128e+11)			
5: 56 min 21 sec	0.66183 OD (1.335e+11, 1.335e+11)			
6: 64 min 55 sec	0.605518 OD (1.538e+11, 1.538e+11)			
7: 73 min 23 sec	0.408724 OD (1.739e+11, 1.739e+11)			
8: 81 min 54 sec	0.336498 OD (1.941e+11, 1.941e+11)			
9: 90 min 28 sec	0.313399 OD (2.143e+11, 2.143e+11)			
10: 99 min 1 sec	0.305689 OD (2.346e+11, 2.346e+11)			
11: 107 min 44 sec	0.290504 OD (2.551e+11, 2.551e+11)			
12: 116 min 12 sec	0.272568 OD (2.751e+11, 2.751e+11)			
13: 124 min 40 sec	0.249721 OD (2.951e+11, 2.951e+11)			
14: 133 min 3 sec	0.208597 OD (3.152e+11, 3.152e+11)			
15: 141 min 30 sec	0.145687 OD (3.351e+11, 3.351e+11)			
16: 149 min 59 sec	0.0812759 OD (3.552e+11, 3.552e+11)			
17: 158 min 27 sec	0.0378521 OD (3.753e+11, 3.753e+11)			
18: 166 min 53 sec	0.0187431 OD (3.954e+11, 3.954e+11)			
19: 175 min 25 sec	0.0116967 OD (4.156e+11, 4.156e+11)			

--END OF FILE--

 * 2-dimensional Spectrum Analysis *

Data Report for Run "WTRatios", Cell 1, Wavelength 1

Detailed Run Information:

Cell Description: Sample 1
 Raw Data Directory: /Users/seeyolater/ultrascan/data/WTRatios/
 Rotor Speed: 60000 rpm
 Average Temperature: 25.3542 °C
 Temperature Variation: Within Tolerance
 Time Correction: 1 minute(s) 49 second(s)
 Run Duration: 2 hour(s) 55 minute(s)
 Wavelength: 280 nm
 Baseline Absorbance: -0.00174973 OD
 Meniscus Position: 5.89972 cm
 Edited Data starts at: 5.942 cm
 Edited Data stops at: 7.137 cm

Hydrodynamic Settings:

Viscosity correction: 1.0363
 Viscosity (absolute): 0.913569
 Density correction: 1.00994 g/ccm
 Density (absolute): 1.00868 g/ccm
 Vbar: 0.734718 ccm/g
 Vbar corrected for 20°C: 0.732442 ccm/g
 Buoyancy (Water, 20°C): 0.268851
 Buoyancy (absolute): 0.258907
 Correction Factor: 0.946822

Data Analysis Settings:

Number of Components: 49
 Residual Mean Square Deviation: 0.00659856
 Weight-Average sedimentation coefficient:

Weight Average S_{20,W}: 7.7678e-13
 Weight Average D_{20,W}: 5.0425e-07
 Weight Average Molecular Weight: 1.7457e+05
 Total concentration: 8.3715e-01

Distribution Information:

Molecular Weight:	S _{20,W} :	D _{20,W} :	concentration:
7.8070e+04	4.9400e-13	5.7366e-07	3.5982e-02 (4.298 %)
8.3137e+04	6.8000e-13	7.4152e-07	3.9306e-03 (0.470 %)
1.3924e+05	9.5900e-13	6.2441e-07	1.8155e-02 (2.169 %)
3.9287e+05	1.0240e-12	2.3630e-07	2.1039e-02 (2.513 %)
2.0003e+05	1.2210e-12	5.5338e-07	4.6122e-03 (0.551 %)
7.8070e+04	4.9400e-13	5.7366e-07	3.5993e-02 (4.299 %)
8.3688e+04	6.8300e-13	7.3989e-07	4.0599e-03 (0.485 %)
1.5821e+05	9.5800e-13	5.4898e-07	1.8034e-02 (2.154 %)
3.9086e+05	1.0260e-12	2.3798e-07	2.0952e-02 (2.503 %)
2.0028e+05	1.2220e-12	5.5315e-07	4.6834e-03 (0.559 %)
7.8070e+04	4.9400e-13	5.7366e-07	3.5968e-02 (4.296 %)
8.2954e+04	6.7900e-13	7.4207e-07	3.9530e-03 (0.472 %)
1.4177e+05	9.6100e-13	6.1452e-07	1.8894e-02 (2.257 %)
3.9660e+05	1.0250e-12	2.3431e-07	2.0328e-02 (2.428 %)
2.0003e+05	1.2210e-12	5.5338e-07	4.5738e-03 (0.546 %)
7.8959e+04	4.9400e-13	5.6720e-07	3.5889e-02 (4.287 %)
8.3798e+04	6.8360e-13	7.3957e-07	4.5318e-03 (0.541 %)
1.8101e+05	1.0020e-12	5.0187e-07	3.9695e-02 (4.742 %)
1.9969e+05	1.2196e-12	5.5370e-07	3.5756e-03 (0.427 %)
7.8070e+04	4.9400e-13	5.7366e-07	3.5952e-02 (4.295 %)
8.2588e+04	6.7700e-13	7.4317e-07	3.9334e-03 (0.470 %)
1.4321e+05	9.5800e-13	6.0645e-07	1.8191e-02 (2.173 %)
3.9029e+05	1.0250e-12	2.3809e-07	2.1059e-02 (2.516 %)
2.0028e+05	1.2220e-12	5.5315e-07	4.5847e-03 (0.548 %)
7.8959e+04	4.9400e-13	5.6720e-07	3.5946e-02 (4.294 %)
8.2954e+04	6.7900e-13	7.4207e-07	3.9796e-03 (0.475 %)
1.5433e+05	9.5100e-13	5.5867e-07	1.6677e-02 (1.992 %)
3.9660e+05	1.0250e-12	2.3431e-07	2.2309e-02 (2.665 %)
1.9969e+05	1.2196e-12	5.5370e-07	4.8094e-03 (0.574 %)
7.8959e+04	4.9400e-13	5.6720e-07	3.5951e-02 (4.294 %)
8.2954e+04	6.7900e-13	7.4207e-07	3.9394e-03 (0.471 %)
1.4276e+05	9.5600e-13	6.0709e-07	1.7771e-02 (2.123 %)
3.9344e+05	1.0250e-12	2.3619e-07	2.1420e-02 (2.559 %)
1.9979e+05	1.2200e-12	5.5361e-07	4.6362e-03 (0.554 %)
7.8959e+04	4.9400e-13	5.6720e-07	3.5952e-02 (4.294 %)
8.5266e+04	6.7800e-13	7.2088e-07	3.9171e-03 (0.468 %)
1.4321e+05	9.5800e-13	6.0645e-07	1.8533e-02 (2.214 %)
3.9718e+05	1.0260e-12	2.3419e-07	2.0733e-02 (2.477 %)
1.9969e+05	1.2196e-12	5.5370e-07	4.5793e-03 (0.547 %)
7.8959e+04	4.9400e-13	5.6720e-07	3.5951e-02 (4.294 %)
8.2954e+04	6.7900e-13	7.4207e-07	3.9370e-03 (0.470 %)
1.4133e+05	9.5900e-13	6.1516e-07	1.8716e-02 (2.236 %)
3.9718e+05	1.0260e-12	2.3419e-07	2.0567e-02 (2.457 %)
1.9969e+05	1.2196e-12	5.5370e-07	4.5419e-03 (0.543 %)
7.8959e+04	4.9400e-13	5.6720e-07	3.5952e-02 (4.294 %)
8.3137e+04	6.8000e-13	7.4152e-07	3.9893e-03 (0.477 %)
1.4155e+05	9.6000e-13	6.1484e-07	1.8386e-02 (2.196 %)
3.9602e+05	1.0240e-12	2.3442e-07	2.0727e-02 (2.476 %)
1.9969e+05	1.2196e-12	5.5370e-07	4.6639e-03 (0.557 %)
1: 12 min 41 sec	0.777182 OD (2.998e+10, 2.998e+10)		
2: 30 min 47 sec	0.746351 OD (7.299e+10, 7.299e+10)		
3: 39 min 13 sec	0.722892 OD (9.299e+10, 9.299e+10)		
4: 47 min 39 sec	0.687817 OD (1.128e+11, 1.128e+11)		
5: 56 min 21 sec	0.66183 OD (1.335e+11, 1.335e+11)		
6: 64 min 55 sec	0.605518 OD (1.538e+11, 1.538e+11)		
7: 73 min 23 sec	0.408724 OD (1.739e+11, 1.739e+11)		
8: 81 min 54 sec	0.336498 OD (1.941e+11, 1.941e+11)		
9: 90 min 28 sec	0.313399 OD (2.143e+11, 2.143e+11)		
10: 99 min 1 sec	0.305689 OD (2.346e+11, 2.346e+11)		

11: 107 min 44 sec 0.290504 OD (2.551e+11, 2.551e+11)
 12: 116 min 12 sec 0.272568 OD (2.751e+11, 2.751e+11)
 13: 124 min 40 sec 0.249721 OD (2.951e+11, 2.951e+11)
 14: 133 min 3 sec 0.208597 OD (3.152e+11, 3.152e+11)
 15: 141 min 30 sec 0.145687 OD (3.351e+11, 3.351e+11)
 16: 149 min 59 sec 0.0812759 OD (3.552e+11, 3.552e+11)
 17: 158 min 27 sec 0.0378521 OD (3.753e+11, 3.753e+11)
 18: 166 min 53 sec 0.0187431 OD (3.954e+11, 3.954e+11)
 19: 175 min 25 sec 0.0116967 OD (4.156e+11, 4.156e+11)

--END OF FILE--

 * Enhanced van Holde - Weischet Analysis *

Data Report for Run "WTRatios", Cell 2, Wavelength 1

Detailed Run Information:

Cell Description: Sample 2
 Raw Data Directory: /Users/seejolater/ultrascan/data/WTRatios/
 Rotor Speed: 60000 rpm
 Average Temperature: 25.3542 °C
 Temperature Variation: Within Tolerance
 Time Correction: 1 minute(s) 49 second(s)
 Run Duration: 2 hour(s) 55 minute(s)
 Wavelength: 280 nm
 Baseline Absorbance: 0.00736853 OD
 Meniscus Position: 5.86932 cm
 Edited Data starts at: 5.913 cm
 Edited Data stops at: 7.137 cm

Hydrodynamic Settings:

Viscosity correction: 1.0363
 Viscosity (absolute): 0.913569
 Density correction: 1.00994 g/ccm
 Density (absolute): 1.00868 g/ccm
 Vbar: 0.734718 ccm/g
 Vbar corrected for 20°C: 0.732442 ccm/g
 Buoyancy (Water, 20°C) : 0.268851
 Buoyancy (absolute) 0.258907
 Correction Factor: 0.946822

Data Analysis Settings:

Divisions: 50
 Smoothing Frame: 2
 Analyzed Boundary: 70 %
 Boundary Position: 15 %
 Selected Groups:

No groups were selected...

Average S: 8.27726
 Initial concentration from plateau fit: 0.629836 OD/fringes

Scan Information:

Scan: Corrected Time: Plateau Concentration:

1: 6 min 53 sec 0.599351 OD
 2: 15 min 29 sec 0.563328 OD
 3: 25 min 7 sec 0.525542 OD
 4: 33 min 33 sec 0.494549 OD
 5: 42 min 0 sec 0.465328 OD
 6: 50 min 38 sec 0.437255 OD

7: 59 min 15 sec 0.410925 OD
 8: 67 min 45 sec 0.386506 OD
 9: 76 min 12 sec 0.363669 OD
 10: 84 min 46 sec 0.341893 OD
 11: 93 min 16 sec 0.321576 OD
 12: 102 min 0 sec 0.301958 OD
 13: 110 min 31 sec 0.28398 OD
 14: 118 min 58 sec 0.267201 OD
 15: 127 min 22 sec 0.251503 OD
 16: 135 min 49 sec 0.236643 OD

Initial Concentration: 0.59023OD
 (Correlation. coeff.: -0.992025
 Standard Dev.: 0.0276687)

Initial Concentration from exponential fit: 0.629836OD

 --END OF FILE--

 * 2-dimensional Spectrum Analysis *

Data Report for Run "WTRatios", Cell 2, Wavelength 1

Detailed Run Information:

Cell Description: Sample 2
 Raw Data Directory: /Users/seejolater/ultrascan/data/WTRatios/
 Rotor Speed: 60000 rpm
 Average Temperature: 25.3542 °C
 Temperature Variation: Within Tolerance
 Time Correction: 1 minute(s) 49 second(s)
 Run Duration: 2 hour(s) 55 minute(s)
 Wavelength: 280 nm
 Baseline Absorbance: 0.013465 OD
 Meniscus Position: 5.86932 cm
 Edited Data starts at: 5.913 cm
 Edited Data stops at: 7.137 cm

Hydrodynamic Settings:

Viscosity correction: 1.0363
 Viscosity (absolute): 0.913569
 Density correction: 1.00994 g/ccm
 Density (absolute): 1.00868 g/ccm
 Vbar: 0.734718 ccm/g
 Vbar corrected for 20°C: 0.732442 ccm/g
 Buoyancy (Water, 20°C) : 0.268851
 Buoyancy (absolute) 0.258907
 Correction Factor: 0.946822

Data Analysis Settings:

Number of Components: 16
 Residual Mean Square Deviation: 0.00603558
 Weight-Average sedimentation coefficient:

Weight Average S20,W: 8.3438e-13
 Weight Average D20,W: 3.8403e-07
 Weight Average Molecular Weight: 3.6385e+05
 Total concentration: 6.0007e-01

Distribution Information:

Molecular Weight:	S 20,W:	D 20,W:	concentration:	
3.4269e+05	4.3704e-13	1.1562e-07	8.4462e-03	(1.408 %)

1.1455e+05	4.8889e-13	3.8694e-07	3.4315e-02	(5.719 %)
2.5442e+05	9.5556e-13	3.4050e-07	4.4492e-02	(7.414 %)
6.3750e+05	6.7037e-13	9.5333e-08	1.4935e-02	(2.489 %)
2.9481e+05	9.8148e-13	3.0182e-07	1.7100e-01	(28.497 %)
7.5161e+05	7.4815e-13	9.0242e-08	1.3222e-02	(2.203 %)
1.0456e+06	1.0852e-12	9.4090e-08	1.6753e-02	(2.792 %)
2.7558e+05	8.7778e-13	2.8877e-07	1.2773e-01	(21.286 %)
4.6885e+03	1.0000e-13	1.9337e-06	3.0209e-02	(5.034 %)
3.1265e+05	4.1111e-13	1.1921e-07	6.7521e-03	(1.125 %)
2.1790e+06	1.5000e-12	6.2409e-08	7.0293e-03	(1.171 %)
3.0006e+05	8.0000e-13	2.4171e-07	2.5970e-02	(4.328 %)
1.3892e+06	1.1111e-12	7.2512e-08	8.8167e-03	(1.469 %)
1.6909e+06	1.2667e-12	6.7914e-08	1.2615e-02	(2.102 %)
8.1391e+05	1.4741e-12	1.6419e-07	1.7440e-02	(2.906 %)
7.4000e+04	5.1481e-13	6.3071e-07	6.0340e-02	(10.056 %)
1: 6 min 53 sec	0.561066 OD (1.638e+10, 1.638e+10)			
2: 15 min 29 sec	0.543182 OD (3.675e+10, 3.675e+10)			
3: 25 min 7 sec	0.532909 OD (5.957e+10, 5.957e+10)			
4: 33 min 33 sec	0.523146 OD (7.941e+10, 7.941e+10)			
5: 42 min 0 sec	0.500415 OD (9.947e+10, 9.947e+10)			
6: 50 min 38 sec	0.472011 OD (1.2e+11, 1.2e+11)			
7: 59 min 15 sec	0.452329 OD (1.403e+11, 1.403e+11)			
8: 67 min 45 sec	0.418687 OD (1.605e+11, 1.605e+11)			
9: 76 min 12 sec	0.301652 OD (1.805e+11, 1.805e+11)			
10: 84 min 46 sec	0.18889 OD (2.008e+11, 2.008e+11)			
11: 93 min 16 sec	0.149748 OD (2.21e+11, 2.21e+11)			
12: 102 min 0 sec	0.133028 OD (2.416e+11, 2.416e+11)			
13: 110 min 31 sec	0.126423 OD (2.618e+11, 2.618e+11)			
14: 118 min 58 sec	0.118024 OD (2.818e+11, 2.818e+11)			
15: 127 min 22 sec	0.11486 OD (3.017e+11, 3.017e+11)			
16: 135 min 49 sec	0.104778 OD (3.218e+11, 3.218e+11)			
135 min 49 sec	0.098681 OD (3.218e+11, 3.218e+11)			

--END OF FILE--

* Genetic Algorithm Analysis *

Data Report for Run "WTRatios", Cell 2, Wavelength 1

Detailed Run Information:

Cell Description: Sample 2
Raw Data Directory: /Users/seeyoulater/ultrascan/data/WTRatios/
Rotor Speed: 60000 rpm
Average Temperature: 25.3542 °C
Temperature Variation: Within Tolerance
Time Correction: 1 minute(s) 49 second(s)
Run Duration: 2 hour(s) 55 minute(s)
Wavelength: 280 nm
Baseline Absorbance: 0.00736853 OD
Meniscus Position: 5.86932 cm
Edited Data starts at: 5.913 cm
Edited Data stops at: 7.137 cm

Hydrodynamic Settings:

Viscosity correction: 1.0363
Viscosity (absolute): 0.913569
Density correction: 1.00994 g/ccm
Density (absolute): 1.00868 g/ccm
Vbar: 0.734718 ccm/g
Vbar corrected for 20°C: 0.732442 ccm/g
Buoyancy (Water, 20°C): 0.268851
Buoyancy (absolute): 0.258907
Correction Factor: 0.946822

Data Analysis Settings:

Number of Components: 5
 Residual Mean Square Deviation: 0.0110727
 Weight-Average sedimentation coefficient:

Weight Average S_{20,W}: 8.2141e-13
 Weight Average D_{20,W}: 5.3619e-07
 Weight Average Molecular Weight: 2.1061e+05
 Total concentration: 5.9640e-01

Distribution Information:

Molecular Weight:	S _{20,W} :	D _{20,W} :	concentration:
1.3361e+04	2.0100e-13	1.3639e-06	4.7243e-02 (7.921 %)
6.3574e+04	5.6300e-13	8.0287e-07	1.2371e-01 (20.743 %)
1.7198e+05	1.1040e-12	5.8196e-07	1.3231e-01 (22.186 %)
1.8975e+05	8.4200e-13	4.0228e-07	6.4270e-02 (10.776 %)
3.5900e+05	9.2000e-13	2.3233e-07	2.2886e-01 (38.374 %)
1: 6 min 53 sec	0.56433 OD (1.638e+10, 1.638e+10)		
2: 15 min 29 sec	0.545133 OD (3.675e+10, 3.675e+10)		
3: 25 min 7 sec	0.534616 OD (5.957e+10, 5.957e+10)		
4: 33 min 33 sec	0.524529 OD (7.941e+10, 7.941e+10)		
5: 42 min 0 sec	0.50439 OD (9.947e+10, 9.947e+10)		
6: 50 min 38 sec	0.473327 OD (1.2e+11, 1.2e+11)		
7: 59 min 15 sec	0.45344 OD (1.403e+11, 1.403e+11)		
8: 67 min 45 sec	0.420448 OD (1.605e+11, 1.605e+11)		
9: 76 min 12 sec	0.303279 OD (1.805e+11, 1.805e+11)		
10: 84 min 46 sec	0.192721 OD (2.008e+11, 2.008e+11)		
11: 93 min 16 sec	0.148832 OD (2.21e+11, 2.21e+11)		
12: 102 min 0 sec	0.13111 OD (2.416e+11, 2.416e+11)		
13: 110 min 31 sec	0.123778 OD (2.618e+11, 2.618e+11)		
14: 118 min 58 sec	0.11731 OD (2.818e+11, 2.818e+11)		
15: 127 min 22 sec	0.109598 OD (3.017e+11, 3.017e+11)		
16: 135 min 49 sec	0.098681 OD (3.218e+11, 3.218e+11)		

--END OF FILE--

 * 2-dimensional Spectrum Analysis *

Data Report for Run "WTRatios", Cell 2, Wavelength 1

Detailed Run Information:

Cell Description: Sample 2
 Raw Data Directory: /Users/seeolater/ultrascan/data/WTRatios/
 Rotor Speed: 60000 rpm
 Average Temperature: 25.3542 °C
 Temperature Variation: Within Tolerance
 Time Correction: 1 minute(s) 49 second(s)
 Run Duration: 2 hour(s) 55 minute(s)
 Wavelength: 280 nm
 Baseline Absorbance: 0.00736853 OD
 Meniscus Position: 5.86932 cm
 Edited Data starts at: 5.913 cm
 Edited Data stops at: 7.137 cm

Hydrodynamic Settings:

Viscosity correction: 1.0363
 Viscosity (absolute): 0.913569
 Density correction: 1.00994 g/ccm
 Density (absolute): 1.00868 g/ccm
 Vbar: 0.734718 ccm/g
 Vbar corrected for 20°C: 0.732442 ccm/g
 Buoyancy (Water, 20°C): 0.268851
 Buoyancy (absolute): 0.258907

Correction Factor: 0.946822

Data Analysis Settings:

Number of Components: 50
 Residual Mean Square Deviation: 0.00658929
 Weight-Average sedimentation coefficient:

Weight Average S_{20,W}: 8.2641e-13
 Weight Average D_{20,W}: 6.4052e-07
 Weight Average Molecular Weight: 1.4664e+05
 Total concentration: 5.9816e-01

Distribution Information:

Molecular Weight:	S _{20,W} :	D _{20,W} :	concentration:
3.8046e+03	8.7000e-14	2.0731e-06	2.8250e-03 (0.472 %)
5.2105e+04	4.9800e-13	8.6649e-07	1.1909e-02 (1.991 %)
1.6427e+05	9.5600e-13	5.2762e-07	3.2546e-02 (5.441 %)
1.7772e+05	8.0600e-13	4.1117e-07	8.3624e-03 (1.398 %)
2.2205e+05	1.3090e-12	5.3445e-07	4.2203e-03 (0.706 %)
4.0031e+03	9.0000e-14	2.0383e-06	2.8595e-03 (0.478 %)
5.2419e+04	5.0000e-13	8.6476e-07	1.1998e-02 (2.006 %)
1.6948e+05	9.5900e-13	5.1300e-07	3.2080e-02 (5.363 %)
2.2988e+05	8.0700e-13	3.1826e-07	8.6169e-03 (1.441 %)
2.1471e+05	1.2800e-12	5.4048e-07	4.2575e-03 (0.712 %)
4.0700e+03	9.1000e-14	2.0270e-06	2.8717e-03 (0.480 %)
5.2576e+04	5.0100e-13	8.6390e-07	1.2068e-02 (2.018 %)
1.6673e+05	9.5700e-13	5.2036e-07	3.2160e-02 (5.377 %)
2.4169e+05	8.1000e-13	3.0384e-07	8.3246e-03 (1.392 %)
2.1345e+05	1.2750e-12	5.4153e-07	4.3831e-03 (0.733 %)
4.0700e+03	9.1000e-14	2.0270e-06	2.8766e-03 (0.481 %)
5.3999e+04	5.0000e-13	8.3945e-07	1.1967e-02 (2.001 %)
1.6647e+05	9.5600e-13	5.2063e-07	3.2586e-02 (5.448 %)
2.4321e+05	8.0400e-13	2.9970e-07	7.9899e-03 (1.336 %)
2.1345e+05	1.2750e-12	5.4153e-07	4.3895e-03 (0.734 %)
4.0031e+03	9.0000e-14	2.0383e-06	2.8699e-03 (0.480 %)
5.2576e+04	5.0100e-13	8.6390e-07	1.2037e-02 (2.012 %)
1.6699e+05	9.5800e-13	5.2009e-07	3.2251e-02 (5.392 %)
2.4035e+05	8.0700e-13	3.0440e-07	8.3421e-03 (1.395 %)
2.1320e+05	1.2740e-12	5.4175e-07	4.3027e-03 (0.719 %)
3.9366e+03	8.9000e-14	2.0497e-06	2.8622e-03 (0.479 %)
5.2576e+04	5.0100e-13	8.6390e-07	1.2061e-02 (2.016 %)
1.6452e+05	9.5700e-13	5.2735e-07	3.2360e-02 (5.410 %)
2.4079e+05	8.0800e-13	3.0421e-07	8.1882e-03 (1.369 %)
2.1320e+05	1.2740e-12	5.4175e-07	4.3326e-03 (0.724 %)
3.9366e+03	8.9000e-14	2.0497e-06	2.8749e-03 (0.481 %)
5.2734e+04	5.0200e-13	8.6304e-07	1.2084e-02 (2.020 %)
1.6182e+05	9.5500e-13	5.3505e-07	3.2599e-02 (5.450 %)
2.2658e+05	8.0900e-13	3.2370e-07	7.8853e-03 (1.318 %)
2.1521e+05	1.2820e-12	5.4005e-07	4.3777e-03 (0.732 %)
4.0031e+03	9.0000e-14	2.0383e-06	2.8971e-03 (0.484 %)
5.2891e+04	5.0300e-13	8.6218e-07	1.2066e-02 (2.017 %)
1.6039e+05	9.5800e-13	5.4151e-07	3.2509e-02 (5.435 %)
2.3031e+05	8.0800e-13	3.1806e-07	8.1747e-03 (1.367 %)
2.1496e+05	1.2810e-12	5.4026e-07	4.1643e-03 (0.696 %)
4.0031e+03	9.0000e-14	2.0383e-06	2.8564e-03 (0.478 %)
5.2419e+04	5.0000e-13	8.6476e-07	1.2027e-02 (2.011 %)
1.6673e+05	9.5700e-13	5.2036e-07	3.2269e-02 (5.395 %)
2.3239e+05	8.0800e-13	3.1521e-07	8.3141e-03 (1.390 %)
2.1446e+05	1.2790e-12	5.4069e-07	4.3486e-03 (0.727 %)
4.0700e+03	9.1000e-14	2.0270e-06	2.8768e-03 (0.481 %)
5.2576e+04	5.0100e-13	8.6390e-07	1.2025e-02 (2.010 %)
1.5530e+05	9.5500e-13	5.5750e-07	3.3015e-02 (5.519 %)
2.2738e+05	8.0600e-13	3.2136e-07	7.6482e-03 (1.279 %)
2.1471e+05	1.2800e-12	5.4048e-07	4.2481e-03 (0.710 %)
1: 6 min 53 sec	0.56433 OD (1.638e+10, 1.638e+10)		
2: 15 min 29 sec	0.545133 OD (3.675e+10, 3.675e+10)		
3: 25 min 7 sec	0.534616 OD (5.957e+10, 5.957e+10)		
4: 33 min 33 sec	0.524529 OD (7.941e+10, 7.941e+10)		
5: 42 min 0 sec	0.50439 OD (9.947e+10, 9.947e+10)		
6: 50 min 38 sec	0.473327 OD (1.2e+11, 1.2e+11)		

7: 59 min 15 sec 0.45344 OD (1.403e+11, 1.403e+11)
 8: 67 min 45 sec 0.420448 OD (1.605e+11, 1.605e+11)
 9: 76 min 12 sec 0.303279 OD (1.805e+11, 1.805e+11)
 10: 84 min 46 sec 0.192721 OD (2.008e+11, 2.008e+11)
 11: 93 min 16 sec 0.148832 OD (2.21e+11, 2.21e+11)
 12: 102 min 0 sec 0.13111 OD (2.416e+11, 2.416e+11)
 13: 110 min 31 sec 0.123778 OD (2.618e+11, 2.618e+11)
 14: 118 min 58 sec 0.11731 OD (2.818e+11, 2.818e+11)
 15: 127 min 22 sec 0.109598 OD (3.017e+11, 3.017e+11)
 16: 135 min 49 sec 0.098681 OD (3.218e+11, 3.218e+11)

--END OF FILE--

* Enhanced van Holde - Weischet Analysis *

Data Report for Run "WTRatios", Cell 3, Wavelength 1

Detailed Run Information:

Cell Description: Sample 3
 Raw Data Directory: /Users/seejolater/ultrascan/data/WTRatios/
 Rotor Speed: 60000 rpm
 Average Temperature: 25.3542 °C
 Temperature Variation: Within Tolerance
 Time Correction: 1 minute(s) 49 second(s)
 Run Duration: 2 hour(s) 55 minute(s)
 Wavelength: 280 nm
 Baseline Absorbance: 0.00959725 OD
 Meniscus Position: 5.877 cm
 Edited Data starts at: 5.933 cm
 Edited Data stops at: 7.131 cm

Hydrodynamic Settings:

Viscosity correction: 1.0363
 Viscosity (absolute): 0.913569
 Density correction: 1.00994 g/ccm
 Density (absolute): 1.00868 g/ccm
 Vbar: 0.734718 ccm/g
 Vbar corrected for 20°C: 0.732442 ccm/g
 Buoyancy (Water, 20°C) : 0.268851
 Buoyancy (absolute) 0.258907
 Correction Factor: 0.946822

Data Analysis Settings:

Divisions: 50
 Smoothing Frame: 2
 Analyzed Boundary: 60 %
 Boundary Position: 20 %
 Selected Groups:

No groups were selected...

Average S: 8.6427
 Initial concentration from plateau fit: 0.896865 OD/fringes

Scan Information:

Scan: Corrected Time: Plateau Concentration:

1: 9 min 45 sec 0.851667 OD
 2: 18 min 17 sec 0.813982 OD
 3: 27 min 56 sec 0.77337 OD
 4: 36 min 21 sec 0.739607 OD

5: 44 min 48 sec 0.707193 OD
 6: 53 min 26 sec 0.675543 OD
 7: 62 min 5 sec 0.645252 OD
 8: 70 min 33 sec 0.616918 OD
 9: 79 min 0 sec 0.589881 OD
 10: 87 min 32 sec 0.56378 OD
 11: 96 min 8 sec 0.538643 OD
 12: 104 min 53 sec 0.514218 OD
 13: 113 min 18 sec 0.491769 OD

Initial Concentration: 0.869573OD
 (Correlation. coeff.: -0.997101
 Standard Dev.: 0.0309968)

Initial Concentration from exponential fit: 0.896865OD

 --END OF FILE--

 * 2-dimensional Spectrum Analysis *

Data Report for Run "WTRatios", Cell 3, Wavelength 1

Detailed Run Information:

Cell Description: Sample 3
 Raw Data Directory: /Users/seejolater/ultrascan/data/WTRatios/
 Rotor Speed: 60000 rpm
 Average Temperature: 25.3542 °C
 Temperature Variation: Within Tolerance
 Time Correction: 1 minute(s) 49 second(s)
 Run Duration: 2 hour(s) 55 minute(s)
 Wavelength: 280 nm
 Baseline Absorbance: 0.00959725 OD
 Meniscus Position: 5.877 cm
 Edited Data starts at: 5.933 cm
 Edited Data stops at: 7.131 cm

Hydrodynamic Settings:

Viscosity correction: 1.0363
 Viscosity (absolute): 0.913569
 Density correction: 1.00994 g/ccm
 Density (absolute): 1.00868 g/ccm
 Vbar: 0.734718 ccm/g
 Vbar corrected for 20°C: 0.732442 ccm/g
 Buoyancy (Water, 20°C) : 0.268851
 Buoyancy (absolute) 0.258907
 Correction Factor: 0.946822

Data Analysis Settings:

Number of Components: 19
 Residual Mean Square Deviation: 0.00660052
 Weight-Average sedimentation coefficient:
 Weight Average S20,W: 8.7546e-13
 Weight Average D20,W: 5.8805e-07
 Weight Average Molecular Weight: 1.5938e+05
 Total concentration: 8.9334e-01

Distribution Information:

Molecular Weight:	S 20,W:	D 20,W:	concentration:	
1.1754e+05	6.7037e-13	5.1706e-07	2.8531e-02	(3.194 %)

3.4354e+05	1.3704e-12	3.6164e-07	1.1464e-02	(1.283 %)
2.0216e+05	3.0741e-13	1.3786e-07	8.8827e-04	(0.099 %)
5.7697e+05	6.1852e-13	9.7188e-08	6.6890e-03	(0.749 %)
2.0491e+05	1.2407e-12	5.4896e-07	3.2780e-02	(3.669 %)
2.4484e+05	3.5926e-13	1.3303e-07	2.4806e-03	(0.278 %)
1.4991e+05	1.0074e-12	6.0922e-07	1.3343e-01	(14.936 %)
1.7713e+05	2.8148e-13	1.4407e-07	1.4587e-03	(0.163 %)
3.4323e+05	1.5000e-12	3.9620e-07	3.6052e-02	(4.036 %)
1.2581e+05	4.8889e-13	3.5230e-07	1.8889e-02	(2.114 %)
5.9392e+04	5.1481e-13	7.8584e-07	1.4533e-02	(1.627 %)
2.0848e+05	9.0370e-13	3.9298e-07	1.6579e-01	(18.559 %)
1.1608e+06	1.0593e-12	8.2732e-08	1.0476e-03	(0.117 %)
7.6703e+04	6.4444e-13	7.6171e-07	5.9495e-02	(6.660 %)
2.1322e+05	9.5556e-13	4.0630e-07	7.6843e-02	(8.602 %)
4.6885e+03	1.0000e-13	1.9337e-06	2.1238e-02	(2.377 %)
1.5574e+05	1.0333e-12	6.0153e-07	6.5873e-03	(0.737 %)
8.1377e+04	6.7037e-13	7.4683e-07	2.0796e-02	(2.328 %)
1.1129e+05	8.2593e-13	6.7284e-07	2.5435e-01	(28.471 %)
1: 9 min 45 sec	0.845954 OD (2.303e+10, 2.303e+10)			
2: 18 min 17 sec	0.818618 OD (4.325e+10, 4.325e+10)			
3: 27 min 56 sec	0.790779 OD (6.607e+10, 6.607e+10)			
4: 36 min 21 sec	0.76507 OD (8.605e+10, 8.605e+10)			
5: 44 min 48 sec	0.732708 OD (1.061e+11, 1.061e+11)			
6: 53 min 26 sec	0.680705 OD (1.265e+11, 1.265e+11)			
7: 62 min 5 sec	0.640372 OD (1.471e+11, 1.471e+11)			
8: 70 min 33 sec	0.558976 OD (1.672e+11, 1.672e+11)			
9: 79 min 0 sec	0.390391 OD (1.872e+11, 1.872e+11)			
10: 87 min 32 sec	0.232125 OD (2.074e+11, 2.074e+11)			
11: 96 min 8 sec	0.153967 OD (2.276e+11, 2.276e+11)			
12: 104 min 53 sec	0.11248 OD (2.485e+11, 2.485e+11)			
13: 113 min 18 sec	0.0838791 OD (2.684e+11, 2.684e+11)			

--END OF FILE--

 * Genetic Algorithm Analysis *

Data Report for Run "WTRatios", Cell 3, Wavelength 1

Detailed Run Information:

Cell Description: Sample 3
 Raw Data Directory: /Users/seejolater/ultrascan/data/WTRatios/
 Rotor Speed: 60000 rpm
 Average Temperature: 25.3542 °C
 Temperature Variation: Within Tolerance
 Time Correction: 1 minute(s) 49 second(s)
 Run Duration: 2 hour(s) 55 minute(s)
 Wavelength: 280 nm
 Baseline Absorbance: 0.00959725 OD
 Meniscus Position: 5.877 cm
 Edited Data starts at: 5.933 cm
 Edited Data stops at: 7.131 cm

Hydrodynamic Settings:

Viscosity correction: 1.0363
 Viscosity (absolute): 0.913569
 Density correction: 1.00994 g/ccm
 Density (absolute): 1.00868 g/ccm
 Vbar: 0.734718 ccm/g
 Vbar corrected for 20°C: 0.732442 ccm/g
 Buoyancy (Water, 20°C) : 0.268851
 Buoyancy (absolute) 0.258907
 Correction Factor: 0.946822

Data Analysis Settings:

Number of Components: 3
 Residual Mean Square Deviation: 0.0170161
 Weight-Average sedimentation coefficient:

Weight Average S_{20,W}: 8.6311e-13
 Weight Average D_{20,W}: 6.6898e-07
 Weight Average Molecular Weight: 1.2061e+05
 Total concentration: 8.8406e-01

Distribution Information:

Molecular Weight:	S _{20,W} :	D _{20,W} :	concentration:	
1.2011e+05	8.6900e-13	6.5595e-07	5.4651e-01	(61.818 %)
1.7268e+05	1.1070e-12	5.8117e-07	1.8031e-01	(20.396 %)
6.2632e+04	5.6300e-13	8.1494e-07	1.5725e-01	(17.787 %)
1: 9 min 45 sec	0.845954 OD (2.303e+10, 2.303e+10)			
2: 18 min 17 sec	0.818618 OD (4.325e+10, 4.325e+10)			
3: 27 min 56 sec	0.790779 OD (6.607e+10, 6.607e+10)			
4: 36 min 21 sec	0.76507 OD (8.605e+10, 8.605e+10)			
5: 44 min 48 sec	0.732708 OD (1.061e+11, 1.061e+11)			
6: 53 min 26 sec	0.680705 OD (1.265e+11, 1.265e+11)			
7: 62 min 5 sec	0.640372 OD (1.471e+11, 1.471e+11)			
8: 70 min 33 sec	0.558976 OD (1.672e+11, 1.672e+11)			
9: 79 min 0 sec	0.390391 OD (1.872e+11, 1.872e+11)			
10: 87 min 32 sec	0.232125 OD (2.074e+11, 2.074e+11)			
11: 96 min 8 sec	0.153967 OD (2.276e+11, 2.276e+11)			
12: 104 min 53 sec	0.11248 OD (2.485e+11, 2.485e+11)			
13: 113 min 18 sec	0.0838791 OD (2.684e+11, 2.684e+11)			

Appendix G - AUC – Wild type and Mutant Keap1 vHW Analysis Reports

 * Enhanced van Holde - Weischet Analysis *

Data Report for Run "Keap1Mutants", Cell 1, Wavelength 1

Detailed Run Information:

Cell Description: Keap1
 Raw Data Directory: /Users/seejolater/ultrascan/data/Keap1Mutants/
 Rotor Speed: 50000 rpm
 Average Temperature: 20.0393 °C
 Temperature Variation: Within Tolerance
 Time Correction: 1 minute(s) 45 second(s)
 Run Duration: 3 hour(s) 13 minute(s)
 Wavelength: 281 nm
 Baseline Absorbance: 0.00427273 OD
 Meniscus Position: 6.05936 cm
 Edited Data starts at: 6.085 cm
 Edited Data stops at: 7.151 cm

Hydrodynamic Settings:

Viscosity correction: 1.0363
 Viscosity (absolute): 1.03531
 Density correction: 1.00994 g/ccm
 Density (absolute): 1.00993 g/ccm
 Vbar: 0.724173 ccm/g
 Vbar corrected for 20°C: 0.724163 ccm/g
 Buoyancy (Water, 20°C) : 0.277116
 Buoyancy (absolute) 0.268632
 Correction Factor: 1.06594

Data Analysis Settings:

Divisions: 50
 Smoothing Frame: 7
 Analyzed Boundary: 50 %
 Boundary Position: 25 %
 Selected Groups:

No groups were selected...

Average S: 6.0555
 Initial concentration from plateau fit: 0.211544 OD/fringes

Scan Information:

Scan: Corrected Time: Plateau Concentration:

1:	2 min 41 sec	0.20997 OD
2:	6 min 50 sec	0.207559 OD
3:	11 min 52 sec	0.204671 OD
4:	16 min 49 sec	0.20187 OD
5:	21 min 48 sec	0.199089 OD
6:	26 min 44 sec	0.196374 OD
7:	31 min 43 sec	0.193669 OD
8:	36 min 43 sec	0.190992 OD
9:	41 min 47 sec	0.188317 OD
10:	46 min 42 sec	0.185757 OD
11:	51 min 41 sec	0.183198 OD
12:	56 min 39 sec	0.180683 OD
13:	61 min 37 sec	0.178202 OD
14:	66 min 35 sec	0.175756 OD
15:	71 min 33 sec	0.173343 OD
16:	76 min 32 sec	0.170955 OD
17:	81 min 32 sec	0.168592 OD

18: 86 min 33 sec 0.166254 OD
 19: 91 min 28 sec 0.163994 OD
 20: 96 min 27 sec 0.161735 OD
 21: 101 min 26 sec 0.159507 OD
 22: 106 min 24 sec 0.157317 OD
 23: 111 min 28 sec 0.155114 OD
 24: 116 min 22 sec 0.153012 OD
 25: 121 min 21 sec 0.150905 OD
 26: 126 min 21 sec 0.148819 OD
 27: 131 min 19 sec 0.146776 OD
 28: 136 min 21 sec 0.144733 OD
 29: 141 min 17 sec 0.142759 OD
 30: 146 min 15 sec 0.140799 OD
 31: 151 min 12 sec 0.138873 OD
 32: 156 min 14 sec 0.136941 OD
 33: 161 min 10 sec 0.135073 OD
 34: 166 min 12 sec 0.133194 OD
 35: 171 min 9 sec 0.131371 OD
 36: 176 min 4 sec 0.129585 OD
 37: 181 min 2 sec 0.127806 OD
 38: 186 min 2 sec 0.12604 OD
 39: 191 min 6 sec 0.124274 OD

Initial Concentration: 0.207434OD
 (Correlation. coeff.: -0.997605
 Standard Dev.: 0.00407467)

Initial Concentration from exponential fit: 0.211544OD

 * Enhanced van Holde - Weischet Analysis *

Data Report for Run "Keap1Mutants", Cell 2, Wavelength 1

Detailed Run Information:

Cell Description: Keap 1-C151S
 Raw Data Directory: /Users/seejolater/ultrascan/data/Keap1Mutants/
 Rotor Speed: 50000 rpm
 Average Temperature: 20.0393 °C
 Temperature Variation: Within Tolerance
 Time Correction: 1 minute(s) 45 second(s)
 Run Duration: 3 hour(s) 13 minute(s)
 Wavelength: 281 nm
 Baseline Absorbance: -0.000561684 OD
 Meniscus Position: 6.04907 cm
 Edited Data starts at: 6.088 cm
 Edited Data stops at: 7.149 cm

Hydrodynamic Settings:

Viscosity correction: 1.0363
 Viscosity (absolute): 1.03531
 Density correction: 1.00994 g/ccm
 Density (absolute): 1.00993 g/ccm
 Vbar: 0.720017 ccm/g
 Vbar corrected for 20°C: 0.72 ccm/g
 Buoyancy (Water, 20°C) : 0.281271
 Buoyancy (absolute) 0.27283
 Correction Factor: 1.06527

Data Analysis Settings:

Divisions: 50
 Smoothing Frame: 15
 Analyzed Boundary: 50 %
 Boundary Position: 25 %
 Selected Groups:

No groups were selected...

Average S: 6.0944
Initial concentration from plateau fit: 0.118924 OD/fringes

Scan Information:

Scan: Corrected Time: Plateau Concentration:

1:	3 min 40 sec	0.117717 OD
2:	7 min 50 sec	0.116361 OD
3:	12 min 52 sec	0.114743 OD
4:	17 min 48 sec	0.11318 OD
5:	22 min 48 sec	0.111617 OD
6:	27 min 41 sec	0.110111 OD
7:	32 min 41 sec	0.108591 OD
8:	37 min 45 sec	0.107071 OD
9:	42 min 48 sec	0.105578 OD
10:	47 min 41 sec	0.104154 OD
11:	52 min 39 sec	0.102725 OD
12:	57 min 35 sec	0.101325 OD
13:	62 min 37 sec	0.0999167 OD
14:	67 min 33 sec	0.0985553 OD
15:	72 min 34 sec	0.0971898 OD
16:	77 min 30 sec	0.0958654 OD
17:	82 min 37 sec	0.0945109 OD
18:	87 min 31 sec	0.0932317 OD
19:	92 min 30 sec	0.0919485 OD
20:	97 min 25 sec	0.0906998 OD
21:	102 min 25 sec	0.0894473 OD
22:	107 min 20 sec	0.0882325 OD
23:	112 min 27 sec	0.0869859 OD
24:	117 min 19 sec	0.0858165 OD
25:	122 min 21 sec	0.0846236 OD
26:	127 min 22 sec	0.0834511 OD
27:	132 min 21 sec	0.0823025 OD
28:	137 min 22 sec	0.0811622 OD
29:	142 min 14 sec	0.0800712 OD
30:	147 min 13 sec	0.0789691 OD
31:	152 min 11 sec	0.0778858 OD
32:	157 min 13 sec	0.0768031 OD
33:	162 min 8 sec	0.0757601 OD
34:	167 min 11 sec	0.0747035 OD
35:	172 min 6 sec	0.073689 OD
36:	177 min 2 sec	0.0726849 OD
37:	182 min 2 sec	0.0716811 OD
38:	187 min 1 sec	0.0706946 OD
39:	192 min 6 sec	0.0697022 OD

Initial Concentration: 0.116547OD
(Correlation. coeff.: -0.997598
Standard Dev.: 0.00228274)

Initial Concentration from exponential fit: 0.118924OD

* Enhanced van Holde - Weischet Analysis *

Data Report for Run "Keap1Mutants", Cell 3, Wavelength 1

Detailed Run Information:

Cell Description: Keap 1-C151°
Raw Data Directory: /Users/seejolater/ultrascan/data/Keap1Mutants/
Rotor Speed: 50000 rpm
Average Temperature: 20.0393 °C
Temperature Variation: Within Tolerance
Time Correction: 1 minute(s) 45 second(s)
Run Duration: 3 hour(s) 13 minute(s)
Wavelength: 281 nm

Baseline Absorbance: 0.00408182 OD
 Meniscus Position: 6.06063 cm
 Edited Data starts at: 6.091 cm
 Edited Data stops at: 7.141 cm

Hydrodynamic Settings:

Viscosity correction: 1.0363
 Viscosity (absolute): 1.03531
 Density correction: 1.00994 g/ccm
 Density (absolute): 1.00993 g/ccm
 Vbar: 0.724173 ccm/g
 Vbar corrected for 20°C: 0.724163 ccm/g
 Buoyancy (Water, 20°C): 0.277116
 Buoyancy (absolute) 0.268632
 Correction Factor: 1.06594

Data Analysis Settings:

Divisions: 50
 Smoothing Frame: 11
 Analyzed Boundary: 50 %
 Boundary Position: 25 %
 Selected Groups:

No groups were selected...

Average S: 6.07024
 Initial concentration from plateau fit: 0.266523 OD/fringes

Scan Information:

Scan: Corrected Time: Plateau Concentration:

1:	4 min 42 sec	0.263788 OD
2:	8 min 55 sec	0.261358 OD
3:	13 min 51 sec	0.258543 OD
4:	18 min 50 sec	0.255731 OD
5:	23 min 48 sec	0.252959 OD
6:	28 min 40 sec	0.250271 OD
7:	33 min 40 sec	0.24754 OD
8:	38 min 47 sec	0.244776 OD
9:	43 min 49 sec	0.242087 OD
10:	48 min 42 sec	0.239507 OD
11:	53 min 38 sec	0.236927 OD
12:	58 min 33 sec	0.234385 OD
13:	63 min 35 sec	0.23181 OD
14:	68 min 31 sec	0.229314 OD
15:	73 min 37 sec	0.226761 OD
16:	78 min 28 sec	0.22436 OD
17:	83 min 35 sec	0.221855 OD
18:	88 min 30 sec	0.219474 OD
19:	93 min 28 sec	0.217095 OD
20:	98 min 25 sec	0.214749 OD
21:	103 min 23 sec	0.212421 OD
22:	108 min 23 sec	0.210103 OD
23:	113 min 25 sec	0.207795 OD
24:	118 min 16 sec	0.205595 OD
25:	123 min 20 sec	0.203322 OD
26:	128 min 21 sec	0.201095 OD
27:	133 min 23 sec	0.198886 OD
28:	138 min 21 sec	0.19673 OD
29:	143 min 15 sec	0.194626 OD
30:	148 min 13 sec	0.192516 OD
31:	153 min 10 sec	0.190436 OD
32:	158 min 15 sec	0.188323 OD
33:	163 min 10 sec	0.186302 OD
34:	168 min 10 sec	0.184269 OD
35:	173 min 4 sec	0.182298 OD
36:	178 min 1 sec	0.180328 OD
37:	183 min 0 sec	0.178367 OD

38: 188 min 5 sec 0.176388 OD
39: 193 min 7 sec 0.17445 OD

Initial Concentration: 0.262954OD
(Correlation. coeff.: -0.998509
Standard Dev.: 0.00424947)

Initial Concentration from exponential fit: 0.266523OD

Appendix H - SAXS - Moore's Auto Correlation of C3/R1:K1 Complex SAXS Results

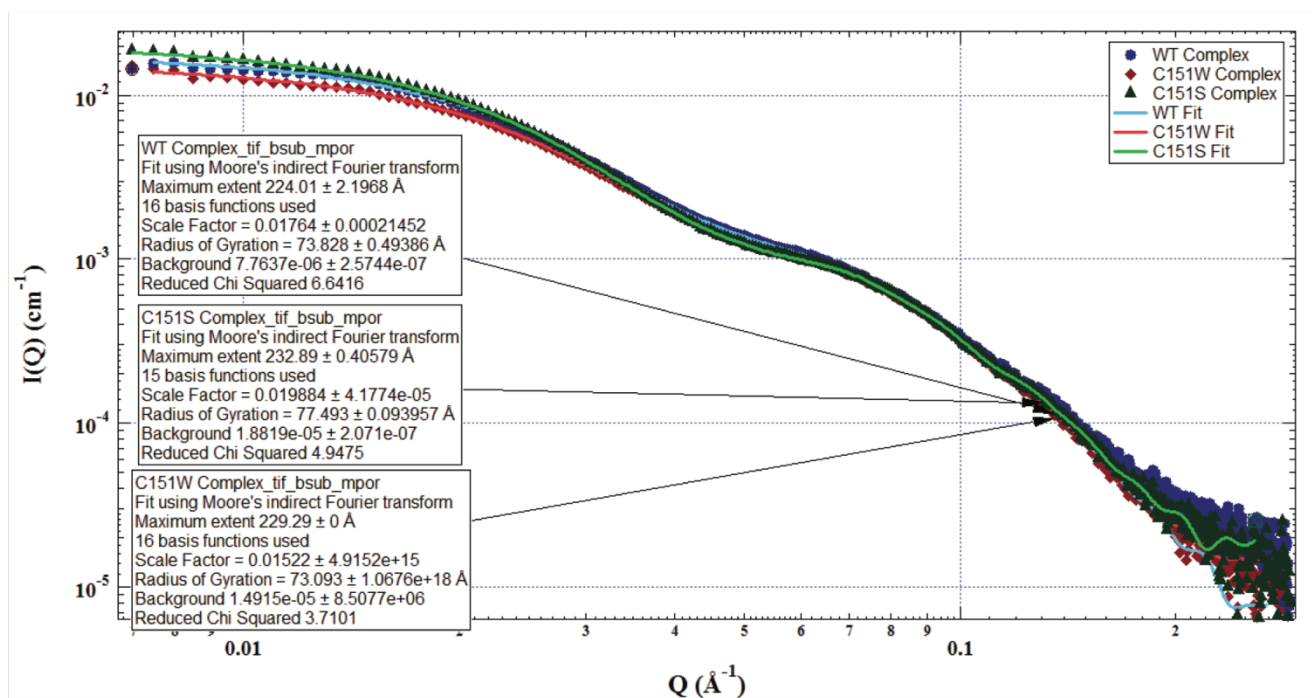


Figure 50. Wild type and mutant complex SAXS fitting results using Moore's indirect Fourier transform

Appendix I – SAXS - Batch File Programming Codes

Batch (.bat) Command Files

The following programming commands were put together to make it easier to keep files organized and create automatically repeating iterations of scattering programs. The files can be easily recreated, if a new notepad document is opened on any Windows PC and the command lines (shown below in italics) are copied into the file as saved as a .bat file. When the resulting .bat file is double-clicked on, the file will run the commands, provided all the needed files are located within the same directory.

1. MAKEdirCOPYall.bat

{This program will create a folder within the current directory named with the current date. It will also copy all .exe, .dat, .out, and .bat files from within that directory into the newly created one.}

```
@echo OFF
for /F "tokens=2-4 delims=/- " %%A in ('date/T') do set var= %%A%%B%%C
md %var%
copy *.exe %var%
copy *.dat %var%
copy *.out %var%
copy *.bat %var%
ECHO Files Copied
Pause
End
```

2. 20ModelAVGFilename.bat

{This is an example of a program that will run 20 iterations of the *ab initio* simulated annealing program DAMMIF using a previously and separately produced GNOM .out result file. Following the completion of all the iterations, the unneeded filename-0.pdb files are automatically deleted and the DAMAVER suite of programs are initiated for averaging of the 20 models. The resulting averaged model file (damfilt.pdb) is then automatically renamed to the current model set with the suffix, *-damfilt.pdb}

```
@ECHO OFF
dammif --mode slow --prefix C1 Filename.out
dammif --mode slow --prefix C2 Filename.out
dammif --mode slow --prefix C3 Filename.out
dammif --mode slow --prefix C4 Filename.out
dammif --mode slow --prefix C5 Filename.out
dammif --mode slow --prefix C6 Filename.out
dammif --mode slow --prefix C7 Filename.out
dammif --mode slow --prefix C8 Filename.out
dammif --mode slow --prefix C9 Filename.out
dammif --mode slow --prefix C10 Filename.out
dammif --mode slow --prefix C11 Filename.out
dammif --mode slow --prefix C12 Filename.out
dammif --mode slow --prefix C13 Filename.out
```

```
dammif --mode slow --prefix C14 Filename.out  
dammif --mode slow --prefix C15 Filename.out  
dammif --mode slow --prefix C16 Filename.out  
dammif --mode slow --prefix C17 Filename.out  
dammif --mode slow --prefix C18 Filename.out  
dammif --mode slow --prefix C19 Filename.out  
dammif --mode slow --prefix C20 Filename.out  
del *-0.pdb  
damaver /a  
rename damfilt.pdb Filename-avg.pdb  
Pause  
End
```